



May 23, 2008
E-26486

U. S. Nuclear Regulatory Commission
Attn: Document Control Desk
One White Flint North
11555 Rockville Pike
Rockville, MD 20852

Subject: Revision 3 to Transnuclear, Inc. (TN) Application for Amendment 10 to the Standardized NUHOMS[®] System (Docket No. 72-1004; TAC NO. L24052)

Reference: Letter from B. Jennifer Davis (NRC) to Donis Shaw (TN), "SECOND REQUEST FOR ADDITIONAL INFORMATION FOR REVIEW OF AMENDMENT 10 TO THE STANDARDIZED NUHOMS[®] SYSTEM (TAC NO. L24052), INCLUDING UPDATED REVIEW SCHEDULE," April 23, 2008

Gentlemen:

This submittal provides responses to the request for additional information (RAI) forwarded by the referenced letter. Enclosure 4 herein provides each of the NRC staff RAI followed by a TN response. Enclosure 6 provides Amendment 10 Revision 3 proposed changes to the NUHOMS[®] CoC 1004 Technical Specifications (TS) and the Standardized NUHOMS[®] System UFSAR, Revision 10.

Enclosure 2 provides a list of TS and UFSAR pages that changed and are included herein. Enclosure 3 provides additional changes to the TS and UFSAR that are not directly related to specific RAI questions. In the Technical Specifications, the Amendment 10 Revision 3 changes are shown as blue italicized font to distinguish them from the Amendment 10 Revisions 0 and 1 changes. For the UFSAR, replacement and new Amendment 10 SAR pages are provided, annotated as Revision 3, with changes indicated by italicized text and revision bars.

This submittal includes proprietary information which may not be used for any purpose other than to support your staff's review of the application. In accordance with 10 CFR 2.390, I am providing an affidavit (Enclosure 1) specifically requesting that you withhold this proprietary information from public disclosure. Enclosure 5 provides a non-proprietary version of the RAI responses and Enclosure 7 provides a non-proprietary version of the proposed changes to the Technical Specifications and the UFSAR.

Should the NRC staff require additional information to support review of this application, please do not hesitate to contact Mr. Don Shaw at 410-910-6878 or me at 410-910-6930.

Sincerely,

Robert Grubb
Senior Vice President - Engineering

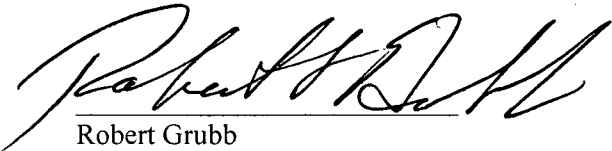
cc: B. Jennifer Davis (NRC SFST) (11 paper copies of this cover letter, Enclosures 1 through 4, and Enclosure 6, provided in a separate mailing)

Enclosures:

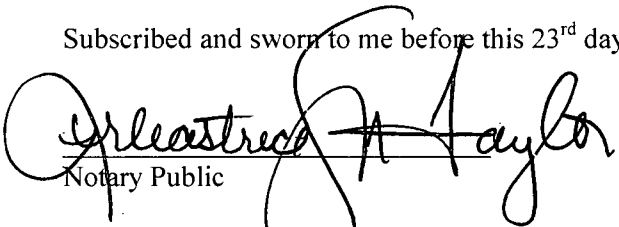
1. Affidavit
2. List of Changed Pages for Amendment 10 Revision 3
3. Additional Changes to the Amendment 10 SAR and Technical Specifications that are not Directly Related to Specific RAI Questions
4. RAI Responses (Proprietary version)
5. RAI Responses (Non-proprietary version)
6. Amendment 10 Revision 3 Proposed changes to the NUHOMS® CoC 1004 Amendment 9 Technical Specifications, and the UFSAR, Revision 10 (Proprietary version)
7. Amendment 10 Revision 3 Proposed changes to the NUHOMS® CoC 1004 Amendment 9 Technical Specifications, and the UFSAR, Revision 10 (Non-proprietary version)

- b) Development of this information by Transnuclear, Inc. required expenditure of considerable resources. To the best of my knowledge and belief, a competitor would have to undergo similar expense in generating equivalent information.
- c) In order to acquire such information, a competitor would also require considerable time and inconvenience related to the development of a design and analysis of a dry spent fuel storage system.
- d) The information required significant effort and expense to obtain the licensing approvals necessary for application of the information. Avoidance of this expense would decrease a competitor's cost in applying the information and marketing the product to which the information is applicable.
- e) The information consists of descriptions of the design and analysis of dry spent fuel storage systems, the application of which provide a competitive economic advantage. The availability of such information to competitors would enable them to modify their product to better compete with Transnuclear, Inc., take marketing or other actions to improve their product's position or impair the position of Transnuclear, Inc.'s product, and avoid developing similar data and analyses in support of their processes, methods or apparatus.
- f) In pricing Transnuclear, Inc.'s products and services, significant research, development, engineering, analytical, licensing, quality assurance and other costs and expenses must be included. The ability of Transnuclear, Inc.'s competitors to utilize such information without similar expenditure of resources may enable them to sell at prices reflecting significantly lower costs.

Further the deponent sayeth not.


 Robert Grubb
 Senior Vice President, Transnuclear, Inc.

Subscribed and sworn to me before this 23rd day of May, 2008.


 Notary Public

My Commission Expires 10 / 14 / 2008



List of Replacement or New Pages
for CoC 1004 Amendment 10 Application Revision 3

| Page | Reason for Change |
|---------------------|--|
| TS 1 and 2 | RAI 8-1 |
| TS A-23 | Please see Enclosure 3 |
| TS A-38 | Please see Enclosure 3 |
| TS A-117 | RAI 9-1 |
| SAR P.4-62 | RAI 4-4 |
| SAR P.4-63 | RAI 4-4 |
| SAR T.3.6-28 (new) | RAI 3-2 |
| SAR T.3.6-89 (new) | RAI 3-2 |
| SAR T.8-5 | RAI 4-7 and RAI 4-8 |
| SAR T.8-8 | RAI 7-1 |
| SAR T.8-9 to -12 | Information shifted due to changes made to page T.8-8 |
| SAR U.2-17 | Please see Enclosure 3 |
| SAR U.4-20 | RAI 4-6 |
| SAR U.4-21 to 25 | Information shifted due to changes made to page U.4-20 (including the page associated with RAI 4-9) |
| SAR U.4-26 | RAI 4-5 |
| SAR U.4-26A to -26B | Information shifted due to changes made to page U.4-26 |
| SAR U.4-44 | RAI 4-1 |
| SAR U.4-46 | RAI 4-3 |
| SAR U.4-50 | RAI 4-5 |
| SAR U.4-65 | RAI 4-10 |
| SAR U.4-66 | RAI 4-10 |
| SAR U.4-67 | RAI 4-10 |
| SAR U.4-70 | RAI 4-10 |
| SAR U.4-71 | RAI 4-10 |
| SAR U.4-72 | RAI 4-10 |
| SAR U.4-74 | RAI 4-10 |
| SAR U.4-75 | RAI 4-10 |
| SAR U.4-76 | RAI 4-10 |
| SAR U.4-96 | RAI 4-12 |
| SAR U.4-97 | RAI 4-12 |
| SAR U.4-98 | RAI 4-12 |
| SAR U.4-99 | RAI 4-12 |
| SAR U.8-5 | RAI 4-7 and RAI 4-8 |
| SAR U.8-7 | RAI 7-1 |
| SAR U.8-8 | RAI 7-1 |
| SAR U.8-9 to -12 | Information shifted due to changes made to page U.8-7 and -8 |

Additional Changes to the Amendment 10 SAR and Technical Specifications
that are not Directly Related to Specific RAI Questions

1. On Technical Specifications Page A-23, the word "case" is changed to "core" as an editorial correction.
2. Technical Specifications Page A-38 (Table 1-1bb) and Amendment 10 SAR Page U.2-17 (Table U.2-3) both show PWR fuel assembly design characteristics for the 32PTH1 DSC. In order to be consistent with the 32PTH1 DSC minimum cavity lengths shown on Amendment 10 SAR Chapter U.1 drawing NUH32PTH1-1001-SAR, Schedule 1 Dimension A, the maximum unirradiated fuel assembly length values for the 32PTH1-S and 32PTH1-M in these tables are changed to 162.6 and 170.0, respectively.

Enclosure 5 to TN E-26486

RAI Responses

(Non-proprietary version)

CHAPTER 3 Structural Evaluation

3-1: *With respect to your response to RAI 3-4 (Round 1), please provide justification for the assumption that the mechanical properties of unirradiated Zircaloy with radial hydrides represent the behavior of high burn-up irradiated Zircaloy-2 with radial hydrides.*

This information is required by the staff to verify the compliance with 10 CFR 72.236.

Response to 3-1

The following discussion provides TN's justification for the assumption that the mechanical properties of unirradiated Zircaloy with radial hydrides can be used to predict the behavior of high burn-up irradiated Zircaloy with radial hydrides.

Proprietary Information Withheld
Pursuant to 10 CFR 2.390

**Proprietary Information Withheld
Pursuant to 10 CFR 2.390**

**Proprietary Information Withheld
Pursuant to 10 CFR 2.390**

In addition, it is also important to point out that based on the results shown on the response to RAI # 1, Question 3-4 [3-1-4] the maximum calculated hoop stress is 24,312 psi. This calculated stress, when compared with the reduced cladding yield strength (20% reduction), still shows a factor of safety of 2.43. The uncertainty of the yield strength of the cladding due to the effect of radial hydrides can be easily accommodated with this large margin of safety.

References:

- 3-1-1 K. J. Geelhood and C. E. Beyer, "Mechanical Properties for irradiated Zircaloy", Transactions of ANS Conference (Vol. 93, pp 707-708), November 2005.
- 3-1-2 Sylvie Arsene, Jinbo Bai, and Philippe Bompard, "Hydride Embrittlement and Irradiation Effects on the Hoop Mechanical Properties of Pressurized Water Reactor (PWR) and Boiling-Water Reactor (BWR) Zircaloy Cladding Tubes, Part III. Mechanical Behavior of Hydride in Stress-Relieved Annealed and Recrystallized Zircaloy's at 20 °C and 300 °C", Metallurgical and Materials Transaction A, Volume 34A, March 2003.
- 3-1-3 S. B. Wisner and R. B. Adamson, "Combined Effect of Radiation Damage and Hydrides on the Ductility of Zircaloy-2", Nuclear Engineering and Design, 185, 1998, page 33-39.
- 3-1-4 Letter from Robert Grubb (TN) to NRC Document Control Desk, "Revision 1 to Transnuclear, Inc. (TN) Application for Amendment 10 to the Standardized NUHOMS® System (Docket No. 72-1004; TAC NO. L24052)," November 7, 2007.

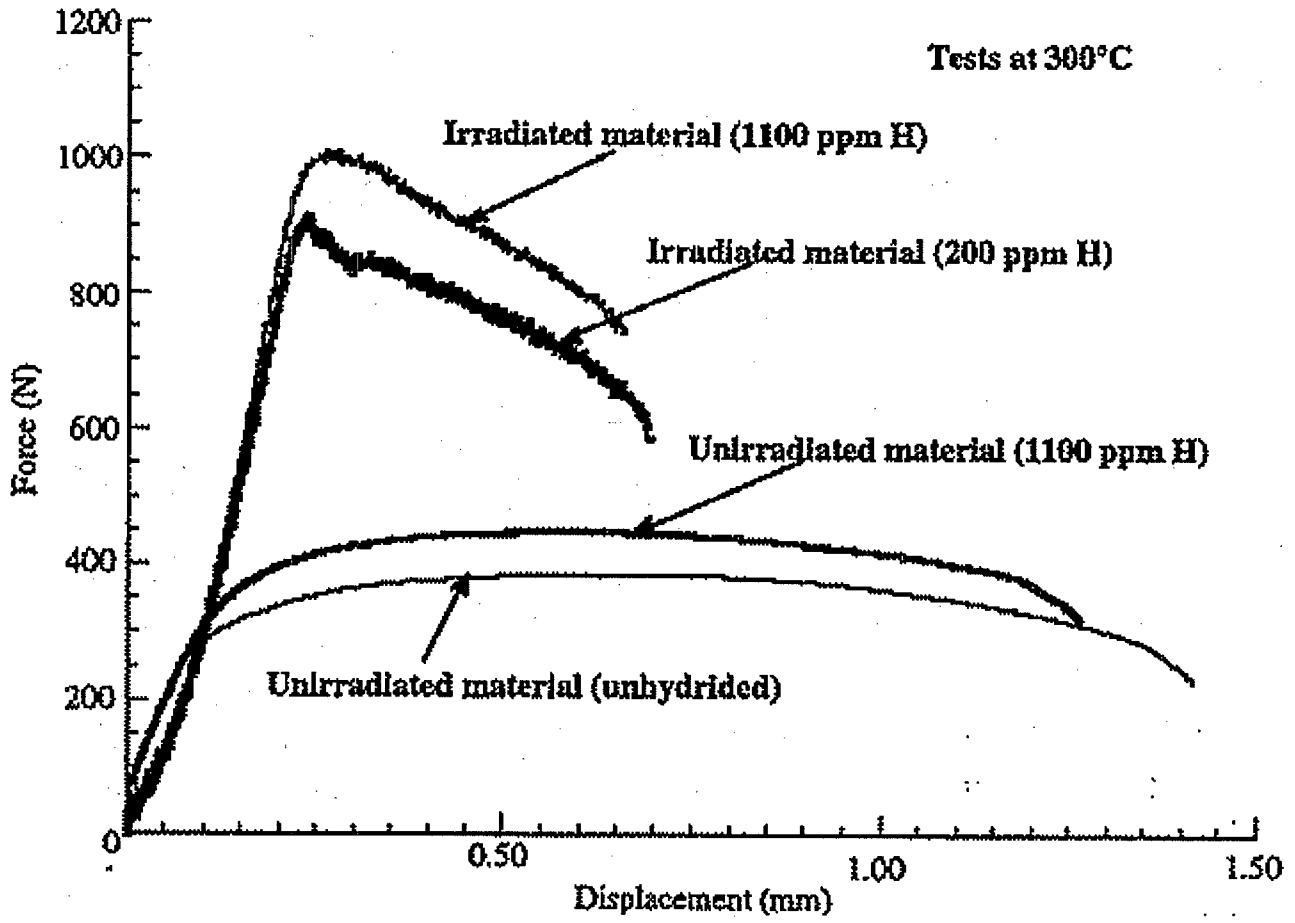


Figure 3-1-1: Comparison between the Irradiated and Unirradiated Materials (Tensile Strength and Displacement as a Function of Hydrogen Concentration)
(From Figure 8-b of Reference 3-1-2)

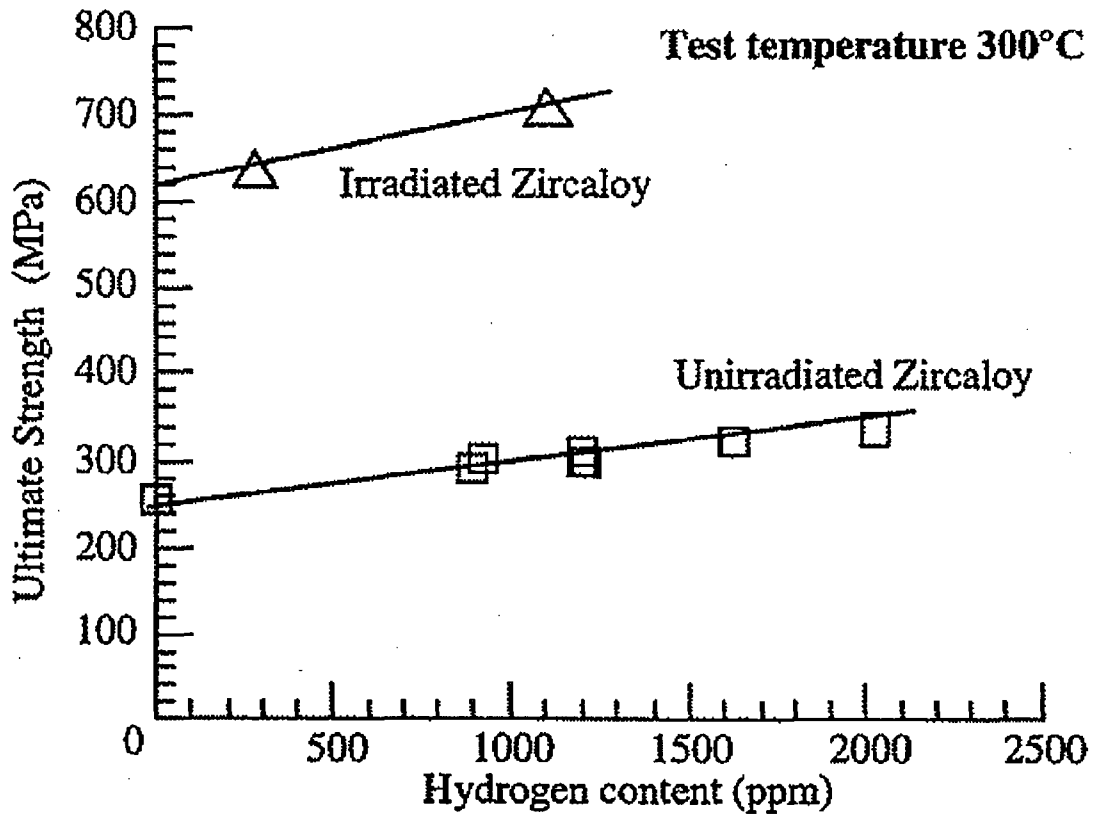


Figure 3-1-2: Ultimate Strength Comparison between the Irradiated and Unirradiated Zircaloy
(From Figure 8-a of Reference 3-1-2)

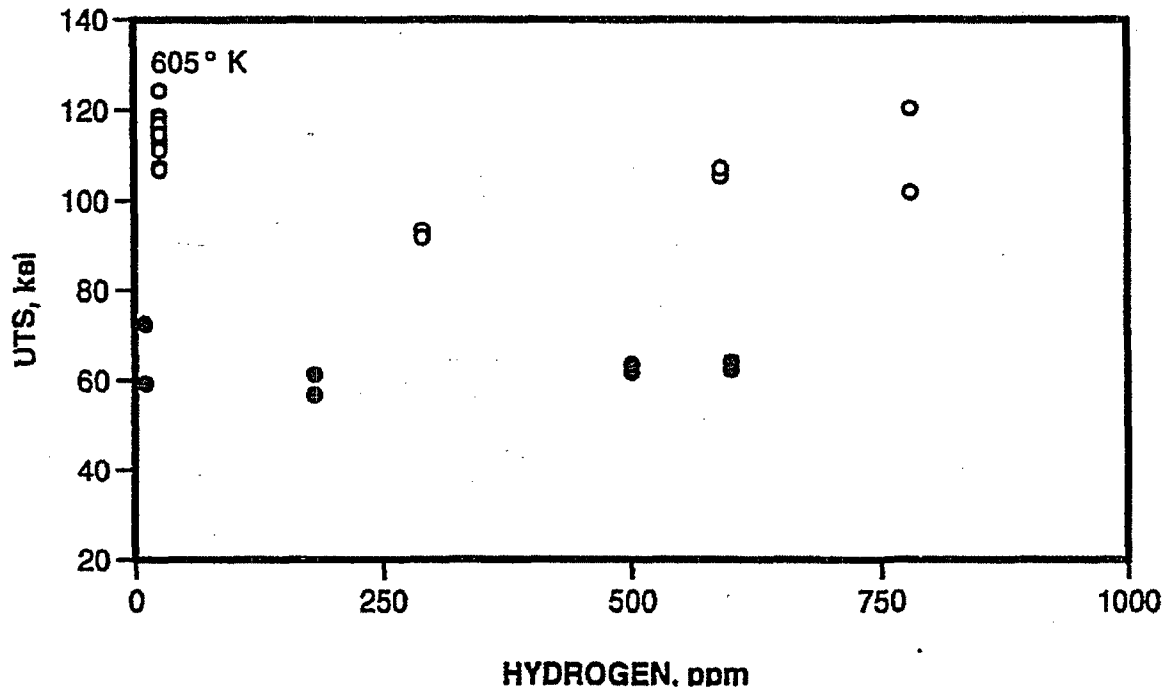


Figure 3-1-3: Ultimate Tensile Strength versus Hydrogen Content for Unirradiated and Irradiated Zircaloy-2 Tested at 605 °K (332 °C)

(From Figure 2 of Reference 3-1-3)

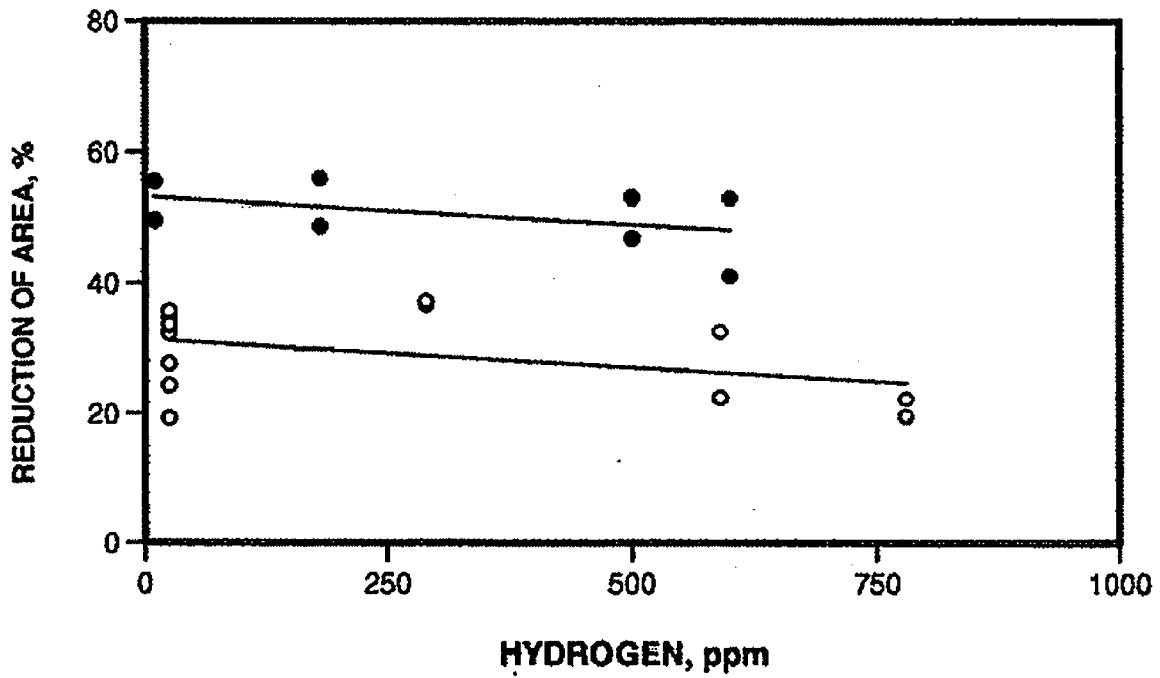


Figure 3-1-4: Reduction of Area for Unirradiated and Irradiated Zircaloy-2 Tested at 605 °K (332 °C)

(From Figure 3 of Reference 3-1-3)

3-2: *In response to RAI 3-12 (Round 1), the NRC staff noted that an "Axial Crack Fracture Mechanics Analysis" was added on pp T-3.6-28 and T.3.6-28A (Rev. 1). As shown on pages T.3.6-28 through T.3.6-31 and T.3.6-84 through T.3.6-85, Fracture Geometry #1 is a through-wall circumferential crack, and Fracture Geometry #2 is a crack emanating from a circular hole. Please clarify whether the axial crack model is a new Fracture Geometry #3.*

Assuming that the axial crack analysis represents a third crack geometry, and not further analysis for Fracture Geometry #1 or #2, staff has a follow-on question. For Fracture Geometry #1 (for a 7 x 7 GE1, GE2, and GE3) the calculated value of $K_I = 1.74 \text{ ksi-in}^{1/2}$ (page T.3.6-29). This value of K_I was computed based on a circumferential crack, with a crack length of 0.22 inches, and a nominal bending stress of 2.33ksi. However, for the new Rev. 1 analysis, the calculated value of $K_I = 0.01 \text{ ksi-in}^{1/2}$ (page T.3.6-28 (new)). This value of K_I was computed based on an axial crack, with a crack length of 10 inches, and a nominal bending stress of 45 ksi.

Please explain how the axial crack analysis performed with approximately 45 times (10" vs. 0.22") longer crack length, and approximately 20 times (45ksi vs. 2.33ksi) more applied bending stress than the circumferential crack analysis, resulted in a demand stress intensity factor of $K_I = 0.01 \text{ ksi-in}^{1/2}$, a value that is 174 times less ($1.74 / 0.01$) than the circumferential crack analysis (fracture geometry #1). Note that in both cases, the allowable stress intensity factor $K_{IC} = 16.36 \text{ ksi-in}^{1/2}$ that was used, is acceptable to the staff.

This information is required by the staff to verify compliance with 10 CFR 72.236.

Response to 3-2

**Proprietary Information Withheld
Pursuant to 10 CFR 2.390**

**Proprietary Information Withheld Pursuant
to 10 CFR 2.390**

**Proprietary Information Withheld Pursuant
to 10 CFR 2.390**

CHAPTER 4 Thermal Evaluation

Section U.4.8.3 32PTH1 DSC Basket Effective Thermal Properties

- 4-1:** Correct the effective specific heat equation in Section U.4.8.3, Page U.4-44 of the SAR. Determine if the correction affects the analyses presented in the SAR, and if so, update those analyses.

Section U.4.8.3 of the SAR (page U.4-44), describes the homogenized DSC internals k-effective model. There appears to be a typographical error in the effective specific heat equation. A term appears to be missing or compressed in the equation for effective specific heat of the DSC. It appears that the equation term "weight of Al x C_{p, fuel}" should be "weight of Al x C_{p, Al} + weight of fuel x C_{p, fuel}" for the Type 2 basket.

In addition, the C_{p, fuel} value appears to be an order of magnitude too large. It should be on the order of 0.06-0.07 Btu/lbm-°F, but is reported as 0.677 Btu/lbm-°F. If the reported value was actually used in the calculation for the blocked vent transient, as described in the SAR, it would result in overestimating the thermal capacity of the DSC. This would tend to reduce the rate of increase in the DSC outer shell temperatures during the transient, which would in turn lead to a lower estimated peak clad temperature, using the decoupled methodology employed in the accident analysis presented in the SAR.

The application should provide reasonable assurance that all analyses are realistic and conservative, and that analysis methods used to evaluate thermal performance of systems are applied properly and appropriately for the designs evaluated.

This information is needed to satisfy the provisions of 10 CFR 72.236(f), and 10 CFR 72.11.

Response to 4-1

There are two typographical errors in the Amendment 10 SAR, Section U.4.8.3, Page U.4-44:

- (1) in the effective specific heat equation, and
- (2) in the value of C_{p, fuel}.

The correct equation for the effective specific heat is:

$$C_p = \frac{\text{weight of SS} \times C_{p, SS} + \text{weight of Al} \times C_{p, Al} + \text{weight of fuel} \times C_{p, fuel}}{\text{basket weight} + \text{fuel assemblies weight}}$$

where the correct value of C_{p, fuel} is **0.0677** Btu/lbm-°F, which is conservatively used based on specific heat for the fuel assembly at 400 °F.

The above typographical errors are corrected in Amendment 10 SAR Revision 3. The original resultant basket effective specific heat capacity reported in the SAR (the table on Page U.4-45 of Section U.4.8.3) is calculated based on the above correct effective specific heat equation and correct value of C_{p, fuel}. Therefore, these typographical errors do not affect the transient thermal analysis results reported in the SAR.

Section U.4.4.3 HSM-H Air Flow Analysis (Stack Effect Calculations)

- 4-2:** Review the NUHOMS cask system SAR and provide corrections to the systems affected by the potential error in the 'dead zone' angle of 4.4° behind the I-beam support rail for the DSC in the HSM. Demonstrate that all NUHOMS system DSC/HSM storage configurations maintain system components below applicable temperature limits.

In a response to the first RAI, (see Enclosure 3 to RN E-25506) the applicant corrected an error in the analysis model related to the convective 'dead zone' that existed in the vicinity of the rail for the 32PTH1 DSC in the HSM-H. The NUHOMS system SAR references Appendix P (from an earlier NUHOMS system amendment for the 24PTH in the HSM-H) for details on the methodology used in the thermal analysis presented in Appendix U. In Appendix P, Figure P.4-2 (page P.4-115) shows a diagram of the convection regions around the 24PTH DSC in the HSM-H. This diagram identifies a 'dead zone' of 4.4° behind the I-beam support rail (between Region 1-T1 and Region 2-T2). Appendix U shows a 'dead zone' angle of 18.9° (see Figure U.4-4, page U.4-89) for the 32PTH1 DSC in the HSM-H, but reports a value of 4° in the Calculation Package NUH32PTH1-0421, "Thermal Analysis of HSM-H Loaded with 32PTH1 DSC," Revision 0, (see Figure 5.5; page 27).

The geometry in Figure 5.5 of TN Calculation Package NUH32PTH1-0421 appears to be erroneous in the analysis of the 32PTH1 DSC in the HSM-H. Since the 'dead zone' region is due to the presence of the I-beam support rail, it appears that an angle of only 4.4° may not be valid in the Appendix P analyses for the 24PTH DSC, or for any other DSC within the HSM-H. If a 'dead zone' angle 4.0-4.4° has been used in other analyses for a DSC within the HSM-H, this could adversely impact reported peak clad temperatures for these configurations. The application should provide reasonable assurance that all analyses are realistic and conservative, and that analysis methods used to evaluate thermal performance of systems are applied properly and appropriately for the designs evaluated. This information is needed to satisfy the provisions of 10 CFR 72.236(f), and 10 CFR 72.11.

Response to 4-2

The dead zone angle is 4.2° both in the Amendment 10 SAR Revision 1 Page P.4-114 (or UFSAR [4-2-1], Appendix P, Figure 4-2, page P.4-118) for the 24PTH DSC and in calculation package NUH32PTH1-0421, Rev. 0, Figure 5-5, Page 27 for the 32PTH1 DSC. Note that calculation package NUH2PTH1-0421, Revision 0 was provided to the staff before the correction of "dead zone" as documented in Enclosure 3 to TN letter E-25506. TN performed two separate calculations to correct the "dead zone," and the results were included in the submittal per TN letter E-25506.

The calculated "dead zone" angle for the 24PTH DSC is 4.2° when the support plate is equipped with 0.5" high slots as shown in UFSAR Appendix P, Figure P.4-2.

Since the HSM-H with a 32PTH1 DSC design has no slots in the support plate, it increases the "dead zone" angle to 18.9° as shown in Amendment 10 SAR Revision 0, Appendix U, Figure U.4-4.

Sensitivity analyses are performed to capture the effect of the increased "dead zone" of 18.9° on the maximum temperatures of the HSM-H, DSC components, and fuel cladding. The evaluations in Amendment 10 SAR Revision 1 account for a "dead zone" of 18.9°.

Similar to the 32PTH1 DSC, the support plate in the HSM-H for the 61BTH DSC has no slots. Therefore, thermal analyses results provided in Appendix T for the 61BTH DSC are based on an 18.9° "dead zone," as shown in Figure T.4-2 of Appendix T. Therefore, the thermal evaluation results for the 61BTH DSC presented in Appendix T are correct and do not need revision.

TN will revise calculation NUH32PTH1-0421, Revision 0 to reference the two new calculations that correct an error in the analysis model of "dead zone" for 32PTH1 DSC from 4.2° to 18.9°.

RAI 4-2 Response References:

- 4-2-1 Updated Final Safety Analysis Report for the Standardized NUHOMS® Horizontal Modular Storage System for Irradiated Nuclear Fuel, NUH-003, Rev. 10, NRC Docket No. 72-1004.

Calculation Package NUH32PTH1-0421 "Thermal Analysis of HSM-H Loaded with 32PTH1 DSC," Revision 0

- 4-3:** *Clarify the statements presented in Section 3 (page 7) and Section 4.2 of Calculation Package NUH32PTH1-0421, which appear to indicate that effective thermal properties from the DSC using the Type 2 basket are used in the analysis for a heat load that is not applicable (40.8 kW) to the Type 2 basket configuration.*

Section 3 of NUH32PTH1-0421 (page 7) lists assumptions and conservatisms "applied in this analysis." One item states that "Effective thermal properties of 32PTH1 DSC alternate 2 basket are conservatively used in this thermal analysis for 31.2 kW and 40.8 kW heat loads." In Section 4.2 (page 10) of NUH32PTH1-0421, the k-effective properties for the Type 2 basket are reported in tabular form and the text states that these calculated thermal conductivity values are "conservatively applied to HSM-H DSC thermal analysis." These statements are not clear, in that they seem to imply that this conservatism is generally applied to all calculations reported for the DSC within the HSM-H.

In Section 5 (page 13) of NUH32PTH1-0421 it states that temperature distributions in the HSM-H are determined "using a steady-state model without contents of the DSC," and that "for the accident blocked vent case," a "homogenized DSC with basket effective properties is used." The statements do not fully counterbalance the effect of the statements in Sections 3 and 4.2. The description of conservatisms or assumptions that apply only to specific calculations in an analysis should clearly identify the limited range of their application.

This information is needed to satisfy the provisions of 10 CFR 72.236(f), and 10 CFR 72.11.

Response to 4-3

As described in Amendment 10 SAR Section U.1, the 32PTH1 DSC basket design is provided with two alternate options: a Type 1 basket with solid aluminum rails and a Type 2 basket with steel transition rails including aluminum inserts. The solid aluminum rail configuration of the basket in 32PTH1 DSC Type 1 better facilitates heat transfer and is required for canisters with high decay heat loads.

Effective thermal conductivities were calculated in the axial and radial directions. In the axial direction, as described in Amendment 10 SAR Section U.4.8.3, the slice model of the 32PTH1 DSC Type 2 used for effective thermal conductivity calculation is independent of any DSC heat load.

In the radial (transverse) direction, the slice model of the 32PTH1 DSC Type 2 used for effective thermal conductivity calculation includes heat generation in fuel regions as described in Amendment 10 SAR Section U.4.8.3. A heat generation rate corresponding to 31.2 kW total heat load is considered for calculation of the radial effective thermal conductivity for this model.

Increase of DSC heat load causes DSC component and fuel cladding temperatures to rise. Effective thermal conductivity of the DSC basket also increases with temperature rise. Therefore, results for effective conductivity using the lower total heat load of 31.2 kW bound those for the higher heat load of 40.8 kW.

Since effective thermal properties of the 32PTH1 DSC Type 2 homogenized basket are lower than those for the Type 1 DSC, it is conservative to use them for the Type 1, which results in higher DSC component heat up rate and fuel cladding temperatures. Additional conservatism is included in the analysis by using 95% of calculated 32PTH1 DSC Type 2 radial effective thermal conductivity values as shown in the Amendment 10 SAR table on page U.4-46.

The note for the table on Amendment 10 SAR page U.4-46 is revised as follows:

95% of the calculated radial effective thermal conductivity is conservatively chosen for HSM-H and transfer cask transient thermal analyses.

It should be noted that only the thermal properties for the 32PTH1 DSC Type 2 are used for the 32PTH1 DSC Type 1 in the transient thermal analyses of the HSM-H and OS200 Transfer Cask. The boundary conditions for the heat loads are separate inputs for the ANSYS models and are applied according to the maximum allowable heat load for each DSC type.

Statement on NUH32PTH1-0421, page 7 will be appended by following: "...when homogenized DSC basket properties used for transient runs".

Statement on NUH32PTH1-0421, page 10 will be modified as follows: "...HSM-H DSC transient thermal analysis."

Statement on NUH32PTH1-0421, page 13 will be clarified as follows: "...for the normal, off-normal and accident ambient conditions are determined using a steady-state model without contents of the DSC."

Section U.4.4.2 Thermal Analysis of HSM-H with 32PTH1 DSC

- 4-4:** Address the inconsistencies related to the correlation approach to analysis of heat transfer in the HSM-H with the 32 PTH1 DSC, or other applicable DSCs and contents requested for modification in this amendment request. Provide revised analyses that utilize the appropriate updated correlations from the most current revisions of the references cited in the Amendment 10 SAR.

The reference for all of the correlations in Amendment 10 is given as Rohsenow and Hartnett, "Handbook of Heat Transfer Fundamentals," 2nd edition, 1985. Some of the coefficients for turbulent forms of a particular correlation are referenced to Kreith, "CRC Handbook of Thermal Engineering," 2000. It appears, however, that some of these correlations have been updated in the latest edition of the Rohsenow and Hartnett reference, which is the "Handbook of Heat Transfer," 3rd edition, McGraw-Hill, 1998. The current correlations should be justified, or the application should be updated to correct the following editorials, updated correlations, and potential errors in used correlations.

This information is needed to satisfy the provisions of 10 CFR 72.236(f), and 10 CFR 72.11.

- (a) For the general form of the correlation for natural convection from a horizontal cylinder (used for DSC shell, except for top region, bottom region, and area of contact with I-beam support rail); a coefficient of $m = 3.3$ is used; the updated reference has $m = 10$. The source of the original coefficient $m=3.3$ could not be determined.
- (b) For the correlation for natural convection from vertical flat surfaces (used for side heat shields, interior concrete walls, and vertical face of DSC end plugs), Nu for fully laminar heat transfer; a coefficient of 2.0 is used; the updated reference has 2.8.
- (c) For the correlation for convection from inclined surfaces (used for flanges and center web of I-beam support rail), Nu for fully laminar heat transfer uses a coefficient of 2.0; the updated reference has 2.8.
- (d) For the correlation for convection from inclined surfaces (used for flanges and center web of I-beam support rail), the definition of Rayleigh number (Ra) is not consistent with updated reference. A multiplier $\cos(\varphi)$ is included, where φ is the angle of inclination of the plate from the vertical. Ra in the updated reference does not include this term, using \cos or \sin of φ only in the definition of the leading coefficient for the Nusselt number for fully turbulent heat transfer.
- (e) The definition of term Nu^T is omitted from documentation of correlation for natural convection from a horizontal cylinder.
- (f) The definition of component "f" in Nusselt number for fully laminar heat transfer is omitted from documentation of the correlation for natural convection from a horizontal cylinder.
- (g) The documentation for the correlation for natural convection from a horizontal surface facing downwards (used for concrete ceiling and lower surface of top heat shield in HSM-H) erroneously defines the equation for Nu^T as the Nusselt number for fully laminar heat transfer, and omits the actual formula for the Nusselt number for fully laminar heat transfer.

Response to 4-4

The correlations and the methodology used in the thermal analysis of the HSM-H are verified and benchmarked based on a thermal test performed on a full scale mockup of the HSM-H. The thermal test report was sent to NRC for CoC 1004, Amendment 8, NUHOMS® 24PTH and for CoC 1030, NUHOMS® HD System [4-4-1]. The applicability ranges and the methodologies to apply these correlations were provided in response to RAI #1 Item 4-9. The test results were used to validate and benchmark the methodology documented in the UFSAR for the Standardized NUHOMS® System (Reference 4-2-1 for RAI 4-2), Appendix P, and the Amendment 10 application.

It is shown in the test report that the correlations and the methodology used for thermal analysis of the HSM-H can conservatively predict the temperature distribution for the HSM-H and its contents, including the DSC shell for heat loads up to 44 kW. The updated correlation in Rohsenow and Hartnett, "Handbook of Heat Transfer," 3rd edition, 1998 were not used in the methodology that was validated against the thermal test results.

However to determine the impact of updated correlations in the Rohsenow Handbook, 3rd edition, this response includes the results of the evaluation that TN performed. In general, updated heat transfer coefficients improve the applicability of the correlation to a wider Ra and Pr range or decrease the margin of error and do not invalidate the previous correlations.

The only coefficient referred to Kreith, "CRC Handbook of Thermal Engineering," 2000 is \overline{C}_i for the calculation of natural convection coefficient on horizontal cylinders. Rohsenow and Hartnett, "Handbook of Heat Transfer," 2nd edition, 1985, Chapter 6, Table 2A suggest a value of 0.103 for \overline{C}_i in circular cylinders with Pr = 0.71. This value is identical to that used for \overline{C}_i in Kreith Handbook. Reference to the Kreith Handbook is changed to Rohsenow Handbook, 2nd edition in the UFSAR for the Standardized NUHOMS® System (Reference 4-2-1 for RAI 4-2), Section P.4.9, pages P.4-62 and P.4-63.

- a) The value of 3.3 for coefficient m is based on Rohsenow and Hartnett, "Handbook of Heat Transfer," 2nd edition, McGraw-Hill, 1985 Chapter 6, equation (65) on page 6-25.

The thermal test report [4-4-1], Table 9 shows that the predicted DSC shell temperatures based on natural convection correlations from Rohsenow Handbook 2nd edition are 4 to 70 °F higher than the measured temperatures for a 44 kW heat load. For comparison purposes, the correlations for natural convection coefficients on horizontal cylinders are taken from Rohsenow Handbook 2nd and 3rd editions and are shown in Table 4-4.1.

The natural convection coefficients for the 32PTH1 DSC shell (D=69.75", air temperature = 154.5 °F) are recalculated based on these correlations for a surface temperature range between 200 and 600 °F and are listed in Table 4-4.2.

As seen in Table 4-4.2, natural convection coefficients for the 32PTH1 DSC based on Rohsenow Handbook 3rd edition are approximately 5% lower than those based on Rohsenow Handbook 2nd edition. This has the potential of increasing the DSC shell temperature by a small amount. At the same time, the temperature increase of the DSC shell enhances the radiation exchange between the DSC shell and the HSM-H inner surfaces. Therefore, the net temperature increase of the DSC shell is expected to be approximately 3 °F. An increase in the DSC shell temperature by a small amount (approximately 3 °F) will be more than offset by the margin demonstrated by the test data and will not affect the thermal evaluations of HSM-H and its contents.

Table 4-4.1 Natural Convection Correlation for Horizontal Cylinder *

| | Rohsenow Handbook 2 nd Edition, Chapter 6, Section B.2.b, Page 6-25 | Rohsenow Handbook 3 rd Edition, Chapter 4, Page 4.21 |
|--------------------|--|--|
| Definitions | $h_c = \frac{Nu k}{D}, D = \text{diameter of cylinder}$ $Ra = Gr Pr$ $Gr = \frac{g \beta (T_w - T_\infty) D^3}{\nu^2}$ | $h_c = \frac{Nu k}{D}, D = \text{diameter of cylinder}$ $Ra = Gr Pr$ $Gr = \frac{g \beta (T_w - T_\infty) D^3}{\nu^2}$ |
| Thin-layer flow | $Nu^T = 0.772 \bar{C}_l Ra^{1/4}$ $\bar{C}_l = 0.515 \text{ for } Pr = 0.71$ | $Nu^T = 0.772 \bar{C}_l Ra^{1/4}$ $\bar{C}_l = 0.515 \text{ for } Pr = 0.71$ |
| Fully laminar flow | $Nu_l = \frac{2f}{\ln(1 + 2f / Nu^T)}$ $f = 1 - \frac{0.13}{(Nu^T)^{0.16}}$ | $Nu_l = \frac{2f}{\ln(1 + 2f / Nu^T)}$ $f = 1 - \frac{0.13}{(Nu^T)^{0.16}}$ |
| Turbulent flow | $Nu_l = \bar{C}_l Ra^{1/3}$ $\bar{C}_l = 0.103 \text{ for } Pr = 0.71 \text{ [Table 2A]}$ | $Nu_l = \bar{C}_l Ra^{1/3}$ $\bar{C}_l = 0.103 \text{ for } Pr = 0.71 \text{ [Table 4.2]}$ |
| Whole flow range | $Nu = [(Nu_l)^m + (Nu_t)^m]^{1/m}$ $\mathbf{m = 3.3} \text{ for } 10^{-10} < Ra < 10^{10}$ | $Nu = [(Nu_l)^m + (Nu_t)^m]^{1/m}$ $\mathbf{m = 10} \text{ for } 10^{-10} < Ra < 10^7$ |
| Error | Close fit to data for $Ra > 10^{-2}$ 8% error for $Ra < 10^{-2}$ | Less than 5% error for $10^{-10} < Ra < 10^7$ |

* Differences between the correlations from Rohsenow Handbook 2nd and 3rd editions are shown in "Bold."

Table 4-4.2 Natural Convection Correlation for Horizontal Cylinder
(32PTH1 DSC Shell)

| T _w (°F) | Ra (---) | Nu _l (---) | Nu _t (---) | Rohsenow Handbook 2 nd Edition | | Rohsenow Handbook 3 rd Edition | | (h _{c,2nd} / h _{c,3rd})-1 (---) |
|------------------------|-------------|--------------------------|--------------------------|--|--|--|--|---|
| | | | | Nu (---) | h _c (Btu/hr-in ² -°F) | Nu (---) | h _c (Btu/hr-in ² -°F) | |
| 200 | 5.85E+09 | 111 | 186 | 195 | 0.0041 | 186 | 0.0039 | 5.2% |
| 225 | 8.31E+09 | 121 | 209 | 219 | 0.0046 | 209 | 0.0044 | 4.7% |
| 250 | 1.03E+10 | 128 | 224 | 234 | 0.0051 | 224 | 0.0048 | 4.4% |
| 275 | 1.20E+10 | 133 | 236 | 246 | 0.0054 | 236 | 0.0052 | 4.3% |
| 300 | 1.34E+10 | 136 | 245 | 255 | 0.0057 | 245 | 0.0054 | 4.2% |
| 325 | 1.45E+10 | 139 | 251 | 262 | 0.0059 | 251 | 0.0057 | 4.1% |
| 350 | 1.54E+10 | 141 | 256 | 267 | 0.0061 | 257 | 0.0059 | 4.0% |
| 375 | 1.61E+10 | 143 | 260 | 270 | 0.0063 | 260 | 0.0061 | 4.0% |
| 400 | 1.65E+10 | 144 | 262 | 273 | 0.0064 | 262 | 0.0062 | 3.9% |
| 425 | 1.68E+10 | 144 | 264 | 274 | 0.0066 | 264 | 0.0063 | 3.9% |
| 450 | 1.70E+10 | 145 | 265 | 275 | 0.0067 | 265 | 0.0064 | 3.9% |
| 475 | 1.72E+10 | 145 | 266 | 276 | 0.0068 | 266 | 0.0065 | 3.9% |
| 500 | 1.72E+10 | 145 | 266 | 276 | 0.0069 | 266 | 0.0066 | 3.9% |
| 525 | 1.72E+10 | 145 | 266 | 276 | 0.0070 | 266 | 0.0067 | 3.9% |
| 550 | 1.71E+10 | 145 | 265 | 276 | 0.0071 | 265 | 0.0068 | 3.9% |
| 575 | 1.70E+10 | 145 | 265 | 275 | 0.0071 | 265 | 0.0069 | 3.9% |
| 600 | 1.69E+10 | 144 | 264 | 274 | 0.0072 | 264 | 0.0069 | 3.9% |

- b) There appears to be a typographical error in part b and part c of this RAI. A coefficient of 2.8 is used in the UFSAR for the Standardized NUHOMS[®] System, Section P.4.9.1 based on Rohsenow Handbook, 2nd edition while the updated value in Rohsenow Handbook, 3rd Edition is 2.0. These values are reversely reported in part b and part c of RAI 4-4.

The above coefficient is used to calculate the Nu number for laminar flow and has secondary effects on the overall heat transfer coefficient. A larger effect is caused by the difference between the correlations for Nu number for turbulent flow in Rohsenow Handbook 2nd and 3rd editions. These correlations are shown in Table 4-4.3.

For comparison purposes, the natural convection coefficients for a vertical flat surface (HSM-H end wall, L = 178", air temperature = 154.5 °F) are recalculated based on correlations from Rohsenow Handbook 2nd and 3rd editions. The recalculated coefficients are listed in Table 4-4.4 for a surface temperature range between 200 and 600 °F.

Table 4-4.4 shows that using correlations from Rohsenow Handbook 3rd edition has negligible effect on the natural convection coefficient values for flat vertical surfaces for surface temperatures up to 250 °F and increases the natural convection coefficient values by up to 4.9% for surface temperatures from 275 to 600 °F. It concludes that using correlations from Rohsenow Handbook 2nd edition is more conservative for flat vertical surfaces.

Table 4-4.3 Natural Convection Correlation for Vertical Flat Surfaces *

| | Rohsenow Handbook 2 nd Edition, Chapter 6, Section B.2.a, Pages 6-16 and 6-17 | Rohsenow Handbook 3 rd Edition, Chapter 4, Page 4.13 |
|--------------------|---|--|
| Definitions | $h_c = \frac{Nu k}{L}, L = \text{height of the plate}$ $Ra = Gr Pr$ $Gr = \frac{g \beta (T_w - T_\infty) L^3}{\nu^2}$ | $h_c = \frac{Nu k}{L}, L = \text{height of the plate}$ $Ra = Gr Pr$ $Gr = \frac{g \beta (T_w - T_\infty) L^3}{\nu^2}$ |
| Thin-layer flow | $Nu^T = \bar{C}_l Ra^{1/4}$ $\bar{C}_l = 0.515 \text{ for } Pr = 0.71$ | $Nu^T = \bar{C}_l Ra^{1/4}$ $\bar{C}_l = 0.515 \text{ for } Pr = 0.71$ |
| Fully laminar flow | $Nu_l = \frac{2.8}{\ln(1 + 2.8 / Nu^T)}$ | $Nu_l = \frac{2.0}{\ln(1 + 2.0 / Nu^T)}$ |
| Turbulent flow | $Nu_t = C_l^V Ra^{1/3}$ $C_l^V = \frac{0.13 Pr^{0.22}}{(1 + 0.61 Pr^{0.81})^{0.42}}$ | $Nu_t = C_l^V Ra^{1/3} / (1 + 1.4 \times 10^9 Pr / Ra)$ <p>For large $\Delta T/T$, replace C_l^V by $C_l^V f$</p> $C_l^V = \frac{0.13 Pr^{0.22}}{(1 + 0.61 Pr^{0.81})^{0.42}}$ $f = 1.0 + 0.078 \left(\frac{T_w}{T_\infty} - 1 \right)$ |
| Whole flow range | $Nu = [(Nu_l)^m + (Nu_t)^m]^{1/m}$ $m = 6 \text{ for } 1 < Ra < 10^{12}$ | $Nu = [(Nu_l)^m + (Nu_t)^m]^{1/m}$ $m = 6 \text{ for } 10^{-1} < Ra < 10^{12}$ |
| Error | Negligible for air | Less than 5% error for $10^{-1} < Ra < 10^{12}$ |

* Differences between the correlations from Rohsenow Handbook 2nd and 3rd editions are shown in "Bold."

Table 4-4.4 Natural Convection Correlation for a Flat Vertical Surface
(HSM-H End Wall)

| T _w (°F) | Ra (---) | Rohsenow Handbook 2 nd Edition | | | | Rohsenow Handbook 3 rd Edition | | | | (h _{c,2nd} / h _{c,3rd})-1 (---) |
|------------------------|-------------|--|--------------------------|-------------|--|--|--------------------------|-------------|--|---|
| | | Nu _i (---) | Nu _t (---) | Nu (---) | h _c (Btu/hr-in ² -°F) | Nu _i (---) | Nu _t (---) | Nu (---) | h _c (Btu/hr-in ² -°F) | |
| 200 | 9.72E+10 | 289 | 472 | 476 | 0.00389 | 289 | 470 | 474 | 0.00388 | 0.4% |
| 225 | 1.38E+11 | 315 | 530 | 534 | 0.00444 | 315 | 531 | 535 | 0.00445 | -0.2% |
| 250 | 1.72E+11 | 333 | 570 | 574 | 0.00485 | 333 | 574 | 578 | 0.00488 | -0.6% |
| 275 | 2.00E+11 | 346 | 600 | 603 | 0.00518 | 345 | 606 | 609 | 0.00523 | -1.0% |
| 300 | 2.23E+11 | 355 | 622 | 625 | 0.00545 | 355 | 630 | 634 | 0.00553 | -1.3% |
| 325 | 2.41E+11 | 362 | 638 | 642 | 0.00569 | 362 | 650 | 653 | 0.00578 | -1.7% |
| 350 | 2.56E+11 | 368 | 651 | 655 | 0.00589 | 367 | 665 | 668 | 0.00601 | -2.0% |
| 375 | 2.68E+11 | 372 | 661 | 664 | 0.00606 | 371 | 677 | 680 | 0.00621 | -2.3% |
| 400 | 2.75E+11 | 374 | 667 | 670 | 0.00620 | 374 | 685 | 688 | 0.00637 | -2.6% |
| 425 | 2.80E+11 | 376 | 671 | 674 | 0.00632 | 376 | 691 | 694 | 0.00651 | -2.9% |
| 450 | 2.83E+11 | 377 | 673 | 677 | 0.00643 | 377 | 696 | 699 | 0.00665 | -3.2% |
| 475 | 2.85E+11 | 378 | 675 | 678 | 0.00653 | 377 | 700 | 702 | 0.00677 | -3.5% |
| 500 | 2.86E+11 | 378 | 675 | 678 | 0.00662 | 378 | 702 | 705 | 0.00688 | -3.8% |
| 525 | 2.85E+11 | 378 | 675 | 678 | 0.00671 | 377 | 704 | 707 | 0.00699 | -4.1% |
| 550 | 2.84E+11 | 377 | 674 | 677 | 0.00678 | 377 | 705 | 708 | 0.00709 | -4.3% |
| 575 | 2.83E+11 | 377 | 672 | 676 | 0.00686 | 376 | 706 | 708 | 0.00719 | -4.6% |
| 600 | 2.80E+11 | 376 | 670 | 674 | 0.00692 | 376 | 706 | 709 | 0.00728 | -4.9% |

- c) See response for part d
- d) As stated previously, the natural convection correlations for thermal analysis of the HSM-H are validated based on a thermal test documented in a report that was submitted to NRC [4-4-1]. The test report shows that the applied methodology predicts the temperature distribution of the components within the HSM-H conservatively.

For comparison purposes, the natural convection coefficients for an inclined surface (flange of the DSC support rail, L = 6.3", angle = 60 degree, air temperature = 106 °F) are recalculated based on correlations from Rohsenow Handbook 2nd and 3rd editions. These correlations are shown in Table 4-4.5.

The recalculated coefficients are listed in Table 4-4.6 for a surface temperature range between 200 and 600 °F. As Table 4-4.6 shows, using correlations from Rohsenow Handbook 3rd results in natural convection coefficients which are more than 6% higher than those from 2nd edition. Using correlations from Rohsenow Handbook 2nd edition is therefore more conservative for this case.

Table 4-4.5 Natural Convection Correlation for Positive Angled,
Inclined Flat Surfaces *

| | |
|--------------------|--|
| | Rohsenow Handbook 2 nd Edition, Chapter 6, Section B.2.e, Page 6-21 |
| Definitions | $h_c = \frac{Nu k}{L}, L = \text{length of the plate}$ $Ra = \frac{g \beta (T_w - T_\infty) L^3}{\nu \alpha} \cos \phi$ |
| Thin-layer flow | $Nu^T = \bar{C}_l Ra^{1/4}$ $\bar{C}_l = 0.515 \text{ for Pr} = 0.71$ |
| Fully laminar flow | $Nu_l = \frac{2.8}{\ln(1 + 2.8 / Nu^T)}$ |
| Turbulent flow | $Nu_t = C_l Ra^{1/3}$ $C_l = C_l^V \cos^{1/3} \phi \text{ for } -90^\circ \leq \phi \leq \tan^{-1} \left(\frac{C_l^V}{C_l^H} \right)^3$ $C_l = C_l^H \sin^{1/3} \phi \text{ for } \tan^{-1} \left(\frac{C_l^V}{C_l^H} \right)^3 \leq \phi \leq 90^\circ$ $C_l^V = \frac{0.13 \text{Pr}^{0.22}}{(1 + 0.61 \text{Pr}^{0.81})^{0.42}}, C_l^H = 0.14 \text{ for Pr} < 100$ |
| Whole flow range | $Nu = [(Nu_l)^m + (Nu_t)^m]^{1/m}$ $m = 6 \text{ for } 1 < Ra < 10^{12}$ |

Table 4-4.5 Natural Convection Correlation for Positive Angled, Inclined Flat Surfaces – Continued *

| | |
|--|---|
| | Rohsenow Handbook 3 rd Edition, Chapter 4, Page 4.19 |
| Definitions | $h_c = \frac{Nu k}{L}$, L = length of the plate |
| | 1) Calculate heat transfer for vertical plate with g replaced by g sinφ 2) Calculate heat transfer for downward facing plate with g replaced by g(0, -cosφ) _{max} 3) Calculate heat transfer for upward facing plate with g replaced by g(0, cosφ) _{max} 4) Take the maximum of the above three heat transfer rates |
| Vertical plate with g replaced by g sinφ | $Ra = \frac{g \sin \phi \beta (T_w - T_\infty) L^3}{\nu \alpha}$, L = length of the plate $Nu^T = \bar{C}_l Ra^{1/4}$, $\bar{C}_l = 0.515$ for Pr = 0.71, $Nu_l = \frac{2.0}{\ln(1 + 2.0 / Nu^T)}$ $Nu_l = C_l^V Ra^{1/3} / (1 + 1.4 \times 10^9 Pr / Ra)$, $C_l^V = \frac{0.13 Pr^{0.22}}{(1 + 0.61 Pr^{0.81})^{0.42}}$ $Nu = [(Nu_l)^m + (Nu_t)^m]^{1/m}$, m = 6 |
| Flat plate facing downward with g replaced by g(0, -cosφ) _{max} | For positive angled plate g(0, -cosφ) _{max} = 0 and the following equations can be ignored $Ra = \frac{g(0, -\cos \phi)_{\max} \beta (T_w - T_\infty) (L^*)^3}{\nu^2}$, $L^* = \frac{A}{p} = \frac{\text{heater area}}{\text{heater perimeter}}$ $Nu^T = \frac{0.527}{(1 + (1.9 / Pr)^{9/10})^{2/9}} Ra^{1/5}$, $Nu_l = \frac{2.5}{\ln(1 + 2.5 / Nu^T)}$, Nu = Nu _l |
| Flat plate facing upward with g replaced by g(0, cosφ) _{max} | For negative angled plate g(0, cosφ) _{max} = 0 and the following equations can be ignored $Ra = \frac{g(0, \cos \phi)_{\max} \beta (T_w - T_\infty) (L^*)^3}{\nu \alpha}$, $L^* = \frac{A}{p} = \frac{\text{heater area}}{\text{heater perimeter}}$ $Nu^T = 0.835 \bar{C}_l Ra^{1/4}$, $\bar{C}_l = 0.515$ for Pr = 0.71, $Nu_l = \frac{1.4}{\ln(1 + 1.4 / Nu^T)}$ $Nu_l = C_l^U Ra^{1/3}$, $C_l^U = 0.140$ for Pr = 0.71 $Nu = [(Nu_l)^m + (Nu_t)^m]^{1/m}$, m = 10 |

* The approaches to calculate the natural convection coefficients for inclined flat surfaces are entirely different in Rohsenow Handbook 2nd and 3rd editions. The differences are shown in "Bold."

Table 4-4.6 Natural Convection Correlation for an Inclined Flat Surface
(Flange of DSC Support Rail)

| T_w (°F) | Ra (---) | Rohsenow Handbook 2 nd Edition | | Rohsenow Handbook 3 rd Edition | $(h_{c,2nd}/h_{c,3rd})-1$ (---) |
|---------------|-------------|--|---------------------------------------|--|------------------------------------|
| | | Nu (---) | h_c (Btu/hr-in ² -°F) | h_c (Btu/hr-in ² -°F) | |
| 200 | 5.31E+06 | 28 | 0.0062 | 0.0067 | -7.1% |
| 225 | 6.13E+06 | 29 | 0.0066 | 0.0071 | -6.9% |
| 250 | 6.79E+06 | 30 | 0.0069 | 0.0074 | -6.7% |
| 275 | 7.30E+06 | 30 | 0.0072 | 0.0077 | -6.6% |
| 300 | 7.70E+06 | 31 | 0.0074 | 0.0079 | -6.5% |
| 325 | 8.01E+06 | 31 | 0.0076 | 0.0081 | -6.4% |
| 350 | 8.24E+06 | 31 | 0.0078 | 0.0083 | -6.4% |
| 375 | 8.40E+06 | 32 | 0.0079 | 0.0085 | -6.3% |
| 400 | 8.51E+06 | 32 | 0.0081 | 0.0086 | -6.3% |
| 425 | 8.54E+06 | 32 | 0.0082 | 0.0088 | -6.3% |
| 450 | 8.50E+06 | 32 | 0.0083 | 0.0089 | -6.3% |
| 475 | 8.43E+06 | 32 | 0.0084 | 0.0090 | -6.3% |
| 500 | 8.33E+06 | 32 | 0.0085 | 0.0091 | -6.3% |
| 525 | 8.23E+06 | 31 | 0.0086 | 0.0092 | -6.4% |
| 550 | 8.11E+06 | 31 | 0.0087 | 0.0092 | -6.4% |
| 575 | 7.98E+06 | 31 | 0.0087 | 0.0093 | -6.4% |
| 600 | 7.84E+06 | 31 | 0.0088 | 0.0094 | -6.4% |

- e) UFSAR, Section P.4.9.1, page P.4-62 is revised to correct this editorial error.
- f) UFSAR, Section P.4.9.1, page P.4-62 is revised to correct this editorial error.
- g) The correlations for natural convection from a horizontal surface facing downwards are based on data in Rohsenow Handbook 2nd edition, Chapter 6, equation (53), page 6-20. These correlations are correctly reflected in the UFSAR for the Standardized NUHOMS[®] System, Section P.4.9.1.

The correlations for natural convection coefficients on horizontal surfaces facing downwards from Rohsenow Handbook 2nd and 3rd editions are shown in Table 4-4.7.

A comparison between the natural convection coefficients for a horizontal surface facing downwards (HSM-H ceiling, $L_c = 31.2''$, air temperature = 203 °F) based on Rohsenow Handbook 2nd and 3rd editions are shown in Table 4-4.8.

This table shows that the natural convection coefficients calculated based on correlations from Rohsenow Handbook 3rd are approximately 4 to 9% higher than those from 2nd edition. Using correlations from Rohsenow Handbook 2nd edition is therefore more conservative for horizontal surfaces facing downwards.

Table 4-4.7 Natural Convection Correlation for Horizontal Surfaces Facing Downwards *

| | Rohsenow Handbook 2 nd Edition, Chapter 6, Section B.1.d, Page 6-20 | Rohsenow Handbook 3 rd Edition Chapter 4, Pages 4.17 and 4.18 |
|--------------------|--|--|
| Definitions | $h_c = \frac{Nu k}{L^*}$ $L^* = \frac{A}{p} = \frac{\text{heater area}}{\text{heater perimeter}}$ $Ra = \frac{g \beta (T_w - T_\infty) (L^*)^3}{\nu \alpha}$ | $h_c = \frac{Nu k}{L^*}$ $L^* = \frac{A}{p} = \frac{\text{heater area}}{\text{heater perimeter}}$ $Ra = \frac{g \beta (T_w - T_\infty) (L^*)^3}{\nu \alpha}$ |
| Thin-layer flow | N/A | $Nu^T = \frac{0.527}{(1 + (1.9/Pr)^{9/10})^{2/9}} Ra^{1/5}$ |
| Fully laminar flow | $Nu_l = \frac{0.527}{(1 + (1.9/Pr)^{9/10})^{2/9}} Ra^{1/5}$ | $Nu_l = \frac{2.5}{\ln(1 + 2.5/Nu^T)}$ |
| Whole flow range | $Nu = Nu_l$ restricted to air and water | $Nu = Nu_l$ for $10^3 < Ra < 10^{10}$ |
| Error | -22 to +30% for $10^6 < Ra < 10^8$ | ±20% for air |

* Differences between correlations from Rohsenow Handbook 2nd and 3rd editions are shown in "Bold."

Table 4-4.8 Natural Convection Correlation for Horizontal Surface Facing Downwards (HSM-H Ceiling)

| T _w (°F) | Ra (---) | Rohsenow Handbook 2 nd Edition | | Rohsenow Handbook 3 rd Edition | | (h _{c,2nd} /h _{c,3rd})-1 (---) |
|------------------------|-------------|--|--|--|--|--|
| | | Nu (---) | h _c (Btu/hr-in ² -°F) | Nu (---) | h _c (Btu/hr-in ² -°F) | |
| 200 | 2.92E+07 | 12 | 0.0006 | 14 | 0.0007 | -8.9% |
| 225 | 1.97E+08 | 18 | 0.0009 | 19 | 0.0010 | -6.3% |
| 250 | 3.89E+08 | 21 | 0.0010 | 22 | 0.0011 | -5.5% |
| 275 | 5.52E+08 | 22 | 0.0011 | 24 | 0.0012 | -5.2% |
| 300 | 6.89E+08 | 23 | 0.0012 | 25 | 0.0013 | -5.0% |
| 325 | 8.02E+08 | 24 | 0.0013 | 25 | 0.0013 | -4.8% |
| 350 | 8.91E+08 | 25 | 0.0013 | 26 | 0.0014 | -4.8% |
| 375 | 9.63E+08 | 25 | 0.0013 | 26 | 0.0014 | -4.7% |
| 400 | 1.02E+09 | 25 | 0.0014 | 27 | 0.0014 | -4.6% |
| 425 | 1.07E+09 | 26 | 0.0014 | 27 | 0.0015 | -4.6% |
| 450 | 1.11E+09 | 26 | 0.0014 | 27 | 0.0015 | -4.6% |
| 475 | 1.13E+09 | 26 | 0.0015 | 27 | 0.0015 | -4.5% |
| 500 | 1.16E+09 | 26 | 0.0015 | 27 | 0.0016 | -4.5% |
| 525 | 1.17E+09 | 26 | 0.0015 | 27 | 0.0016 | -4.5% |
| 550 | 1.18E+09 | 26 | 0.0015 | 27 | 0.0016 | -4.5% |
| 575 | 1.19E+09 | 26 | 0.0015 | 27 | 0.0016 | -4.5% |
| 600 | 1.19E+09 | 26 | 0.0016 | 27 | 0.0016 | -4.5% |

The discussions for item a to g show that using natural convection correlations from Rohsenow Handbook, 3rd edition increases the DSC shell temperature and decreases the other HSM-H components' temperatures by very small amounts. This enhances the radiation exchange between the DSC shell and the HSM-H inner surfaces and limits the overall temperature variation to a few degrees Fahrenheit.

Since the correlations for natural convection from Rohsenow Handbook, 2nd edition are validated and benchmarked against a series of thermal tests and as documented above, the use of updated correlations from Rohsenow Handbook, 3rd edition has an insignificant impact on the results, use of the correlations for natural convection from Rohsenow Handbook, 2nd edition for thermal evaluation of HSM-H is still valid and justified.

RAI 4-4 Response References:

- 4-4-1 Transnuclear, Inc. Letter to USNRC, "Submittal of Revision 1 of Thermal Test Report of the NUHOMS[®] Horizontal Storage Module, Model HSM-H (TN Report E-21625) and Revision 4 of Application No. 8 to the NUHOMS[®] Certificate of Compliance (CoC) No. 1004 (TAC No. L23653), Letter # NUH03-05-06, dated January 14, 2005.

Section U.4.5 Thermal Analysis of OS200 Transfer Casks with 32PTH1 DSCs

- 4-5:** *Provide a discussion of how a circumferentially varying Nusselt number in the liquid neutron shield annulus would effect the temperature distribution of the DSC within the OS-200 TC. Include a discussion of the effects of the stagnation zone at the bottom of the liquid neutron shield annulus. A discussion of the limitations associated with the constant Nusselt number approach, as presented in Section U.4.5.2 and U.4.2 of the SAR, should also be included.*

The staff believes that the Nusselt number values applied in the applicant's analyses may artificially shift and/or incorrectly predict the component temperature distributions within the DSC. The staff has performed independent CFD analyses that have yielded results indicating that the Nusselt number varies around the circumference of the liquid neutron shield of the OS-200 transfer cask, and indicates that a stagnation zone exists in the bottom of the liquid neutron shield annulus. As a result, heat transfer rates vary significantly around the circumference of the OS-200 TC annulus.

The applicant has used a constant Nusselt number about the circumference of the liquid neutron shield, which appears to have yielded conservative temperatures for this specific design configuration and the decay heats requested in this amendment; however, the applicant's approach does not account for the actual physics of the flow in the liquid neutron shield. Rather than constrain the thermal design dimensions and loading operations in the CoC, the staff seeks to document the limitations and associated uncertainties of the applicant's constant Nusselt number approach with correlations to be described as part of the SAR methodology.

The staff has also reviewed the Sandia report (SANDIA report SAND2002-3132, "CFD Calculation of Internal Natural Convection in the Annulus Between Horizontal Concentric Cylinders") provided as a reference in support of the method and approach for the

analysis of the OS200 liquid neutron shield, and does not believe it applies specifically to this analysis, as it is presented in the SAR. For example the SANDIA study focuses on large gap widths (0.5 meter or greater (19.6 inches or greater) and large radius ratios (approx. 3.5), with air as the working fluid. The OS200 TC has a gap of approx. 12 cm (4.93 inches) and a radius ratio of approximately 1.1, with water as the working fluid.

This information is needed to satisfy the provisions of 10 CFR 72.236(f), and 10 CFR 72.11.

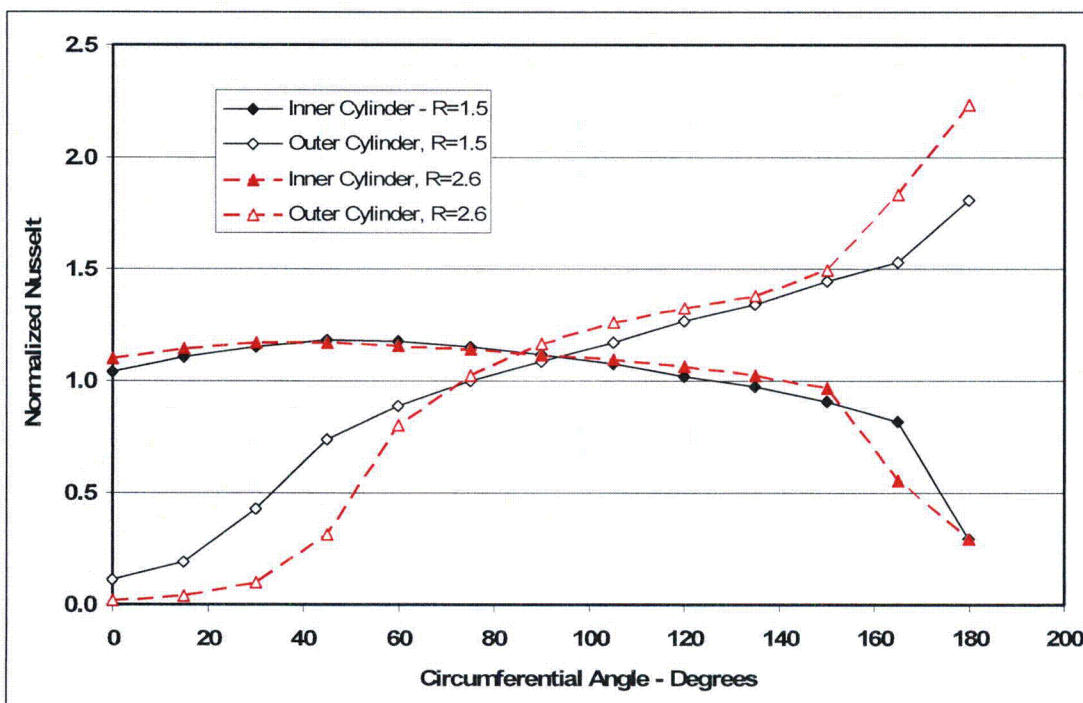
Response to 4-5

The Sandia report was provided for information purposes only and is not used as safety basis for the application.

The staff's observation that the Nusselt number varies around the circumference of the liquid neutron shield of the OS-200 transfer cask and that a stagnation zone exists near the bottom of the annulus is a well known phenomenon that has been noted in numerous experiments and numerical studies used to establish and verify the text book correlations for estimating the heat transfer between the cylinders. As such, the textbook correlations (including those used for this application) do capture the actual physics of the flow in the liquid neutron shield with the effect being reflected in the level of the correlation predicted average Nusselt number. Using a constant, average Nusselt number results in the predicted heat transfer rates being under-estimated over most of the inner cylinder and the upper portion of the outer cylinder and over-estimated over a small section on the upper portion of the inner cylinder and over the lower portion of the outer cylinder.

It is agreed that the correlations do not capture the specific variation in Nusselt number with angle and position within the neutron shield. This level of detail is not reflected in the typical textbook correlation due to a combination of the complexity of including it and the fact that the variation on the heat transfer from the inner cylinder is often sufficiently limited that its inclusion is not warranted for many applications. To verify that this is also the case for this application, an examination was made of the work of Desai and Vafai [4-5-1] who investigate the heat transfer characteristics for annuli with $10^6 < Ra < 10^9$, $0.01 < Pr < 5000$, and diameter ratios of 1.5 to 11. Per Table 4-14 of the NUHOMS[®] HD FSAR (Docket No. 72-1030), the Rayleigh number (Ra) for this application is approximately 10^9 and the Prandtl number (Pr) is approximately 1.5 to 2.5. The diameter ratio (R) is approximately 1.12. While Desai and Vafai did not specifically examine a configuration matching the parameters of the OS200 TC neutron shield, sufficient data is presented to permit an understanding of the sensitivity of the angular variation in heat transfer rates to the pertinent configuration parameters associated with the OS200 TC.

Figure 14 from Desai and Vafai illustrates the Nusselt number distribution over the inner and outer cylinders for a range of diameter ratios (R) at a Ra number of 10^8 and a Pr number of 0.7. To better understand the results for R=1.5 and R=2.6, the data was re-plotted by normalizing the data by the average Nusselt number (as determined by sampling at every 15° and then numerically averaging).



The results show similar variations in the heat transfer rates over the inner cylinder for diameter ratios of 1.5 and 2.6. The same is basically true for the outer cylinder, except that the extent of low flow/stagnation is greater for a diameter ratio of 2.6. As expected, the size of this low flow/stagnation region increases for larger diameter ratios, although the change is not uniform. Figure 8 and Figure 11 from the same source show the sensitivity to Rayleigh and Prandtl number.

Based on these trend lines, it is concluded that the trend lines in Figure 14 can be used to estimate the variation in the Nusselt number with angle for this application. For conservatism, the trend lines for R=2.6 are used to conservatively bound the gradient in heat transfer rates on the outer cylinder. The data points in the figure above are used to convert the average k-effective values presented in Table 4-14 of the NUHOMS[®] HD FSAR to local values as a function of angle and position in the neutron shield. Since the thermal modeling for the OS200 TC neutron shield sub-divides the shield into 3 elements in the radial direction and at every 15° around the circumference, the approach is to use the variation along the inner cylinder (i.e., the structural shell of the TC) vs. the angle for the inside set of elements, the variation along the outer cylinder (i.e., the shell of the neutron shield) for the outside set of elements, and the average of the two for the center set of elements used in modeling the shield. The effect is to vary the k-eff from approximately 112% of the average at the bottom, inside of the neutron shield to approximately 43% of the average at the top, inside of the shield and from approximately 203% of the average at the top, outside of the shield to 4% of the average (i.e., pure conduction/stagnation) at the bottom, outside of the shield.

The transfer condition yielding the lowest fuel cladding thermal margin for the Type 1 basket is HLZC #1 (40.8 kW) for an ambient temperature of 106 °F, while for the Type 2 basket it occurs for HLZC #2 (31.2 kW) and an ambient temperature of 0 °F (see the Amendment 10 SAR, Table U.4-15). A time limit of 15.7 hours or less is applied for

transfer operations with the Type 1 basket and HLZC #1 and steady-state operations can not occur unless the air circulation mode is activated or other corrective actions are implemented. Because of this, the thermal mass of the TC and the payload is the controlling factor on the available transient time and the angular variation in the heat transfer within the neutron shield does not have a significant impact in the determination of the available transfer time limit. Therefore, the steady state evaluation of HLZC #2 for the Type 2 basket for 0 °F ambient is selected as the appropriate transfer condition for determining the impact of the angular variation in the neutron shield heat transfer rates.

Figures 4-5-1 to 4-5-6 provide a comparison between the results obtained using the Amendment 10 SAR methodology (average Nusselt number) and those obtained using the non-constant neutron shield k-effective for the evaluation of steady-state conditions for the Type 2 basket with HLZC #2 at 0 °F ambient. The change to the temperature distribution on the shell of the neutron shield is seen between Figures 4-5-1 and 4-5-2. Alternative views of the outer shell are presented in each figure. The simulation of a stagnation region at the bottom of the neutron shield annulus shifts the location of the peak temperature from the bottom to the lower side of the shield's shell. The temperature at the very bottom of the neutron shield outer shell drops by approximately 70 °F due to the simulated presence of a stagnation region. The peak temperature remains about the same, but its location moves up to about 45° from the bottom.

Figures 4-5-3 and 4-5-4 present the temperature distribution over the inside surface of the inner shell of the OS200 TC for the two modeling methodologies. The decreased heat transfer at the base of the neutron shield annulus under the revised methodology results in a 20 °F increase in the peak temperature of the inner shell. The decrease in the k-effective at the top, inside of the neutron shield annulus assumed for the alternative methodology is largely offset by the higher k-effective around the inner surface and around the upper, outside portion of the shield annulus. As a result, the predicted temperature of the inner shell at the top of the cask is only 3 °F higher than that obtained using the Amendment 10 SAR methodology.

Figures 4-5-5 and 4-5-6 present the temperature distribution over the outside of the DSC obtained via the Amendment 10 SAR and alternative methodologies. As seen, the two methodologies yield similar distributions with the primary difference being an increase of approximately 10 to 14 °F along the bottom of the DSC under the alternative modeling methodology due to the higher temperatures seen in the same vicinity of the TC's inner shell. The peak temperature still occurs at the top of the DSC and at approximately the same level (i.e., 1 °F hotter with the revised methodology).

The DSC shell outer surface temperature distribution using the alternate methodology is included in Table 4-5-1 below.

Table 4-5-1

DSC Shell Outer Surface Temperature Distribution Using the Alternate Methodology
(Page 1 of 2)

| Cylindrical coordinate | | | Temp (F) |
|------------------------|-------|---------|----------|
| R | theta | Z | |
| 34.875 | -90.0 | 67.6562 | 339 |
| 34.875 | -75.0 | 67.6562 | 289 |
| 34.875 | -60.0 | 67.6562 | 357 |
| 34.875 | -45.0 | 67.6562 | 379 |
| 34.875 | -30.0 | 67.6562 | 392 |
| 34.875 | -15.0 | 67.6562 | 401 |
| 34.875 | 0.0 | 67.6562 | 407 |
| 34.875 | 15.0 | 67.6562 | 412 |
| 34.875 | 30.0 | 67.6562 | 416 |
| 34.875 | 45.0 | 67.6562 | 419 |
| 34.875 | 60.0 | 67.6562 | 421 |
| 34.875 | 75.0 | 67.6562 | 422 |
| 34.875 | 90.0 | 67.6562 | 423 |
| 34.875 | -90.0 | 76.3125 | 342 |
| 34.875 | -75.0 | 76.3125 | 292 |
| 34.875 | -60.0 | 76.3125 | 360 |
| 34.875 | -45.0 | 76.3125 | 383 |
| 34.875 | -30.0 | 76.3125 | 396 |
| 34.875 | -15.0 | 76.3125 | 404 |
| 34.875 | 0.0 | 76.3125 | 410 |
| 34.875 | 15.0 | 76.3125 | 416 |
| 34.875 | 30.0 | 76.3125 | 419 |
| 34.875 | 45.0 | 76.3125 | 422 |
| 34.875 | 60.0 | 76.3125 | 424 |
| 34.875 | 75.0 | 76.3125 | 426 |
| 34.875 | 90.0 | 76.3125 | 426 |
| 34.875 | -90.0 | 84.969 | 344 |
| 34.875 | -75.0 | 84.969 | 294 |
| 34.875 | -60.0 | 84.969 | 362 |
| 34.875 | -45.0 | 84.969 | 385 |
| 34.875 | -30.0 | 84.969 | 398 |
| 34.875 | -15.0 | 84.969 | 406 |

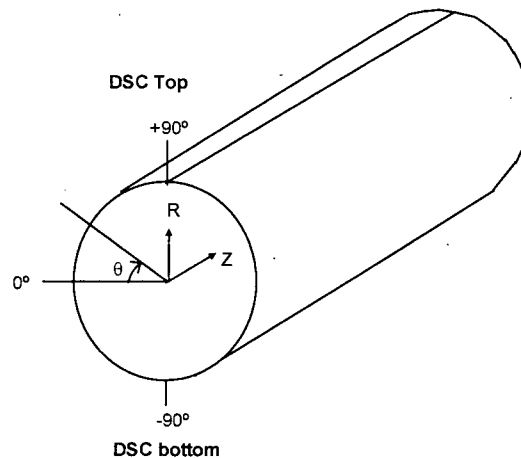
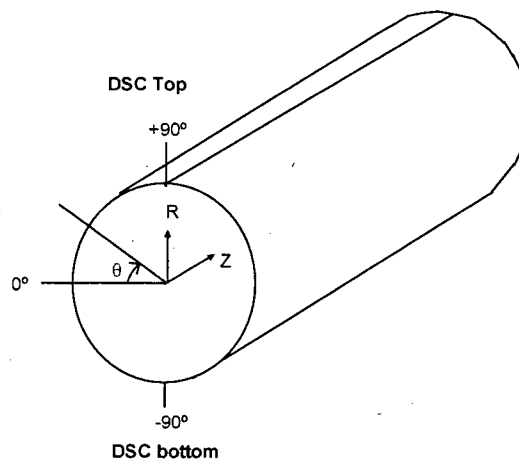


Table 4-5-1

DSC Shell Outer Surface Temperature Distribution Using the Alternate Methodology
(Page 2 of 2)

| Cylindrical coordinate | | | Temp (F) |
|------------------------|-------|---------|----------|
| R | theta | Z | |
| 34.875 | 0.0 | 84.969 | 412 |
| 34.875 | 15.0 | 84.969 | 417 |
| 34.875 | 30.0 | 84.969 | 421 |
| 34.875 | 45.0 | 84.969 | 424 |
| 34.875 | 60.0 | 84.969 | 426 |
| 34.875 | 75.0 | 84.969 | 428 |
| 34.875 | 90.0 | 84.969 | 428 |
| 34.875 | -90.0 | 93.625 | 345 |
| 34.875 | -75.0 | 93.625 | 295 |
| 34.875 | -60.0 | 93.625 | 363 |
| 34.875 | -45.0 | 93.625 | 385 |
| 34.875 | -30.0 | 93.625 | 398 |
| 34.875 | -15.0 | 93.625 | 406 |
| 34.875 | 0.0 | 93.625 | 412 |
| 34.875 | 15.0 | 93.625 | 418 |
| 34.875 | 30.0 | 93.625 | 422 |
| 34.875 | 45.0 | 93.625 | 425 |
| 34.875 | 60.0 | 93.625 | 427 |
| 34.875 | 75.0 | 93.625 | 428 |
| 34.875 | 90.0 | 93.625 | 428 |
| 34.875 | -90.0 | 102.281 | 344 |
| 34.875 | -75.0 | 102.281 | 294 |
| 34.875 | -60.0 | 102.281 | 362 |
| 34.875 | -45.0 | 102.281 | 384 |
| 34.875 | -30.0 | 102.281 | 398 |
| 34.875 | -15.0 | 102.281 | 406 |
| 34.875 | 0.0 | 102.281 | 412 |
| 34.875 | 15.0 | 102.281 | 417 |
| 34.875 | 30.0 | 102.281 | 421 |
| 34.875 | 45.0 | 102.281 | 424 |
| 34.875 | 60.0 | 102.281 | 426 |
| 34.875 | 75.0 | 102.281 | 427 |
| 34.875 | 90.0 | 102.281 | 428 |



The DSC shell temperature profile from the alternate methodology is applied over the detailed DSC and basket model using the methodology described in Amendment 10 SAR, Section U.4.6.5.2. Figure 4-5-7 and 4-5-8 present the temperature distribution over the fuel assemblies calculated based on the DSC shell temperatures profiles from the SAR and the alternate methodologies. As seen in Figures 4-5-7 and 4-5-8, the maximum fuel cladding temperature and the maximum DSC shell temperature predicted by alternate methodology along with those predicted by the SAR methodology are listed below.

| 32PTH1 DSC, Type 2 Cold Transfer Condition in OS200, 0°F, 31.2 kW, HLZC#2 | | | |
|--|-----------------------------------|---|--------------------|
| | SAR Methodology T_{max} (°F) | Alternate Methodology T_{max} (°F) | ΔT (°F) |
| Fuel Cladding | 730 | 732 | +2 |
| DSC Shell Outer Surface | 427.43 | 428.46 | +1 |

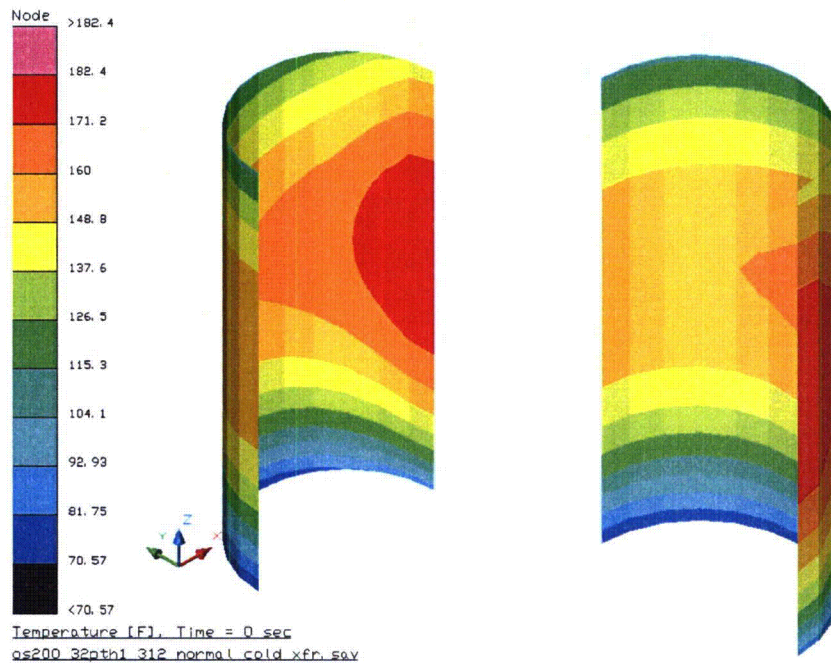
As the above results demonstrate, although the Nusselt number will vary around the circumference of the neutron shield, the Amendment 10 SAR methodology of using a constant value as the basis for estimating the peak fuel cladding temperatures is appropriate. The effects of a varying Nusselt number around the circumference of the liquid neutron shield are seen mainly in the immediate shells attached to the liquid neutron shield. Due to conduction through multiple shells of the TC and the relatively large gap between the DSC and TC inner shell, these effects are reduced to an insignificant level for the DSC shell temperature and for the fuel cladding temperature. The maximum DSC shell temperature and the maximum fuel cladding temperature predicted using the alternative methodology are respectively within 1 and 2 °F of those predicted using the SAR methodology.

The presence of a stagnation region at the base of the annulus is a well established phenomenon the affects of which have been accounted for as part of the development of the textbook correlations. A stagnation region develops when the circulating flow along the outside of the neutron shield descends to the bottom elevation of the inner cylinder. At a short distance below this point the flow will naturally separate from the outer cylinder, turn, and flow towards the inner cylinder since the buoyancy forces do not support continuing the flow further along the outside of the neutron shield. The size of this stagnation zone will increase as the diameter ratio between the inner and outer cylinders increases. Despite this, the overall heat transfer from the inner cylinder adjacent to this stagnation region is not affected, as demonstrated by the level of Nusselt number for the inner cylinder vs. angular position seen for the various cases analyzed in the Desai and Vafai paper.

A new section (Section U.4.5.4.3) is added to the Amendment 10 SAR which discusses the sensitivity analysis and its results.

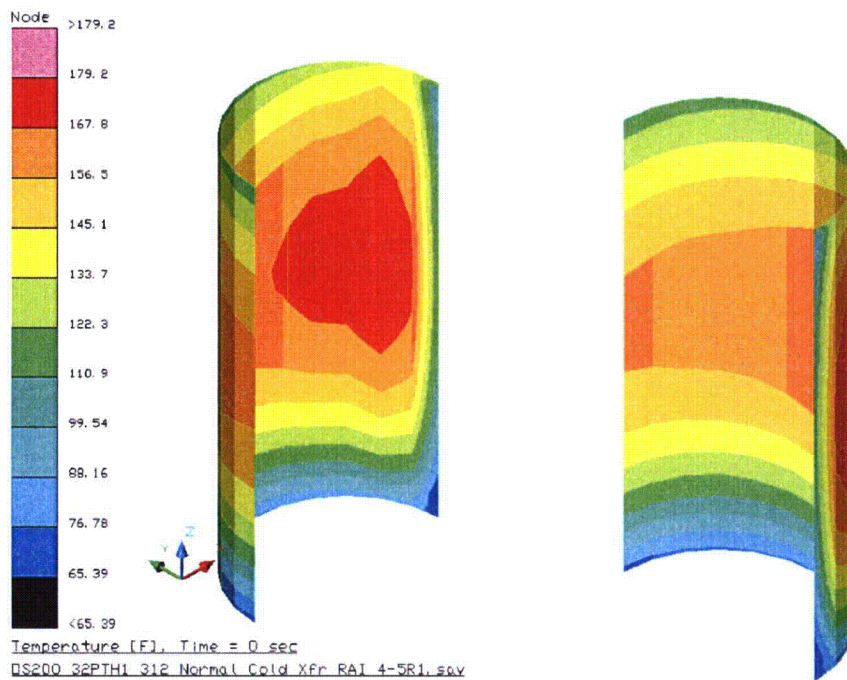
RAI 4-5 Response References:

- 4-5-1 Desai, C. P. and Vafai, K., An Investigation and Comparative Analysis of Two- and Three-dimensional Turbulent Natural Convection in a Horizontal Annulus, International Journal of Heat and Mass Transfer, Vol. 37, No. 16, pp. 2475-2504, 1994.



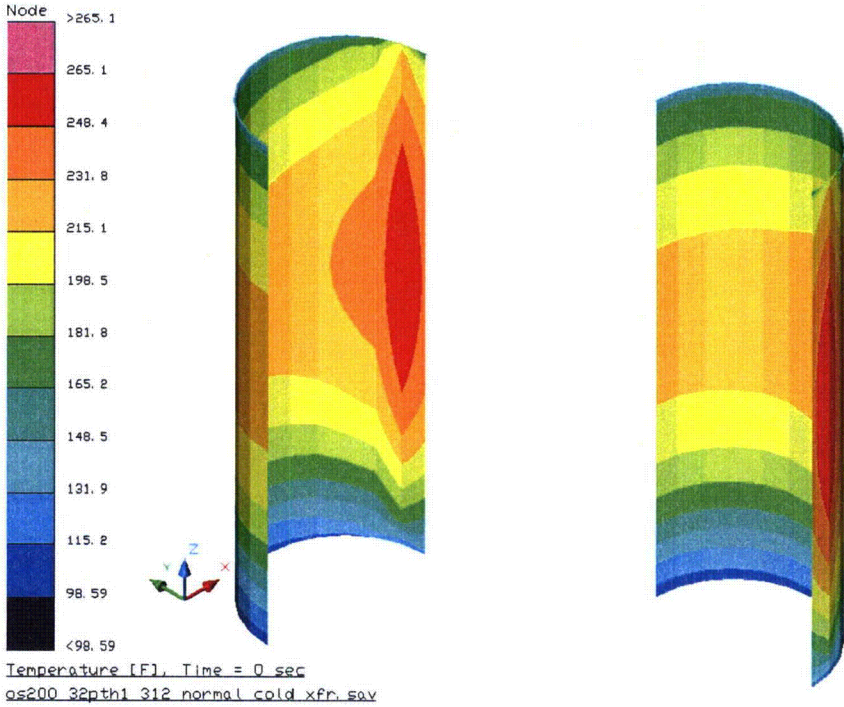
Note: The x-axis points to the bottom of the horizontal TC

Figure 4-5-1 Neutron Shield Surface with SAR Methodology Modeling



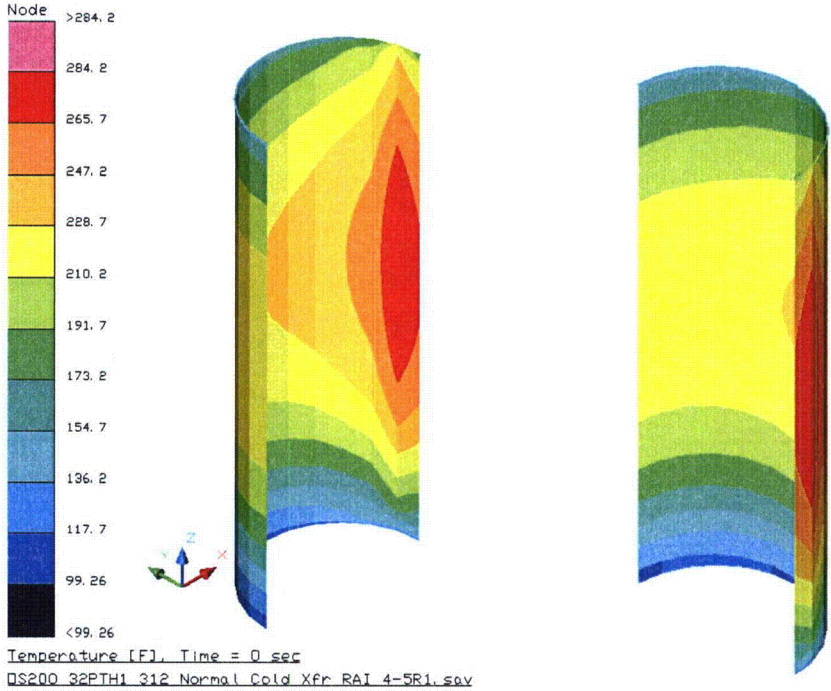
Note: The x-axis points to the bottom of the horizontal TC

Figure 4-5-2 Neutron Shield Surface with RAI 4-5 Response Modeling Approach



Note: The x-axis points to the bottom of the horizontal TC

Figure 4-5-3 Inner Shell Surface with SAR Methodology Modeling



Note: The x-axis points to the bottom of the horizontal TC

Figure 4-5-4 Inner Shell Surface with RAI 4-5 Response Modeling Approach

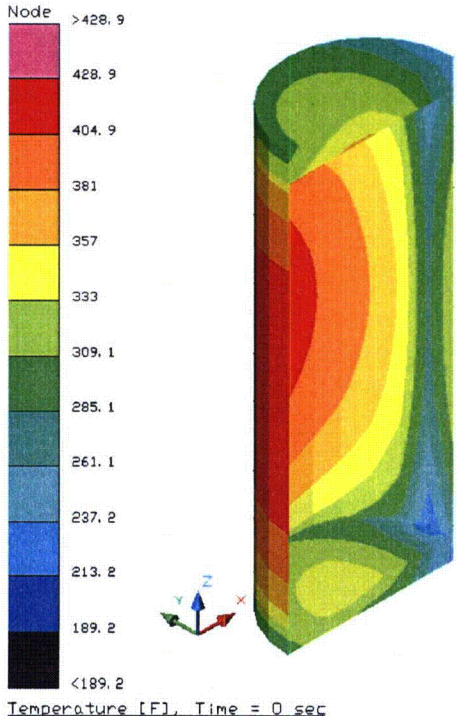


Figure 4-5-5 DSC Shell with SAR Methodology Modeling

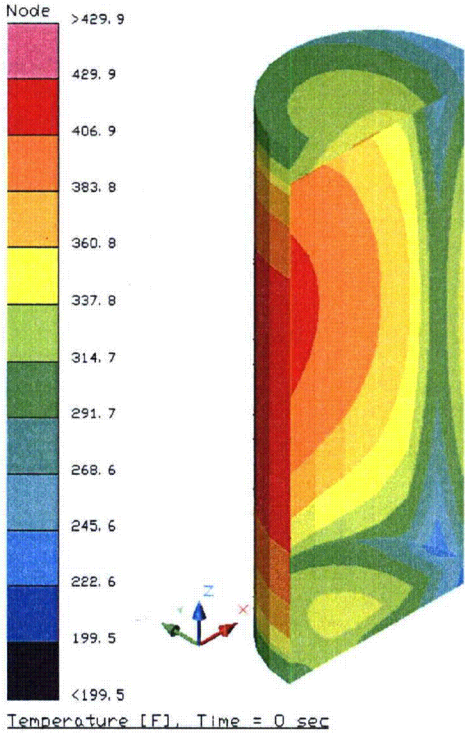
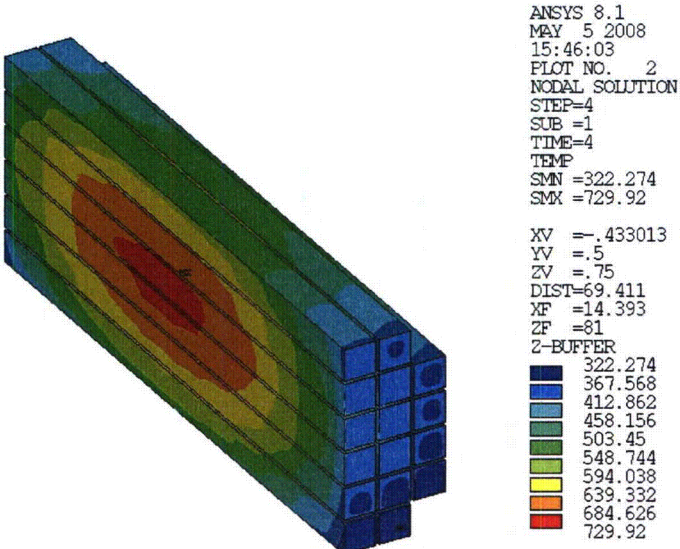
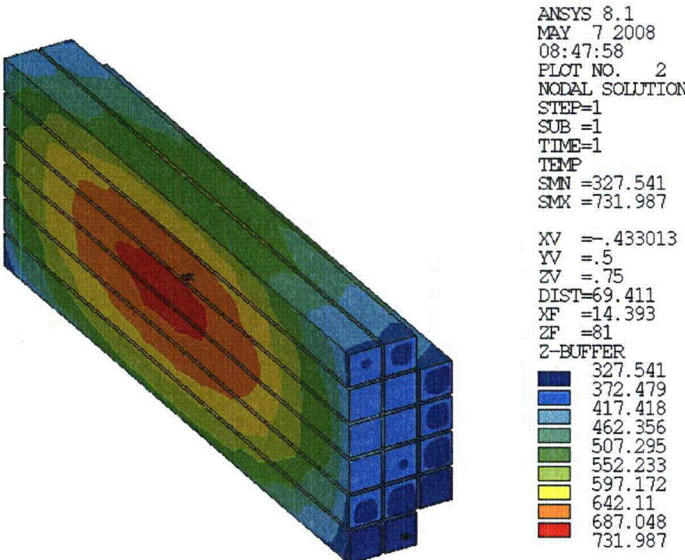


Figure 4-5-6 DSC Shell with RAI 4-5 Response Modeling Approach



32PTH1 Type A, Normal Transfer, 31.2 kW, OF, 0.5" Boral (0.075") paired A1

Figure 4-5-7 Fuel Assemblies with SAR Methodology Modeling



32PTH1 Type C, Normal Transfer, 31.2 kW, OF, Varying Nu

Figure 4-5-8 Fuel Assemblies with RAI 4-5 Response Modeling Approach

- 4-6:** *Demonstrate that extrapolated k-effective values taken from Tables 4-14 and 4-17 of the NUHOMS® HD SAR and applied in the thermal analysis of the OS200 transfer cask for DSC heat loads of 24 kW, 31.2 kW, and 40.8 kW are appropriate. Justify that the extrapolation of a heat transfer correlation developed to provide an average Nusselt number for the annulus between two concentric cylinders at uniform temperatures to conditions where the cylinders have large circumferential temperature gradients, and non-uniform boundary conditions on the exterior surface facing the ambient is appropriate.*

The values of the neutron shield effective thermal conductivity reported in Appendix U (page U.4-10) are taken directly from Chapter 4 of the Safety Analysis Report for the NUHOMS® HD Horizontal Modular Storage System for Irradiated Fuel, NRC Docket No. 72-1030, Revision 4 (specifically, Table 4-14 and Table 4-17.) This is justified on the grounds that the neutron shield for the OS187 transfer cask is identical to that of the OS200. The methodology described in Chapter 4 of the SAR for the NUHOMS® HD shows that the Nusselt number for free convection within each neutron shield segment is determined using a heat transfer correlation for free convection between concentric cylinders. This correlation was developed and validated using heat transfer data obtained in test sections small enough to ensure a uniform temperature distribution on the inner and outer cylinder surfaces.

In addition, the k-effective values listed in Tables 4-14 and 4-17 were calculated using a total decay heat load of 34.8 kW, but the OS200 transfer cask will be carrying DSCs with maximum heat load capacities of 24 kW, 31.2 kW, and 40.8 kW. Instead of directly applying the heat transfer correlation for this methodology to calculate the Nusselt number and k-effective values as part of the energy solution for the OS200 neutron shield, the tabulated values of k-effective for the OS187 were used for the OS200. This approach decouples the k-effective values from the decay heat load of 34.8 kW which was used to derive these specific values.

This information is needed to satisfy the provisions of 10 CFR 72.236(f), and 10 CFR 72.11.

Response to 4-6

The temperature difference required to transfer a given amount of heat from the inner cylinder to the outer cylinder is a measure of the thermal resistance associated with the boundary layers on the inner and outer cylinders and the mechanical energy required to circulate the flow within the neutron shield. These parameters remain approximately the same for a given fluid type and temperature level whether the uniform or non-uniform temperatures exist along the boundaries of the cylinders. The methodology described in the NUHOMS® HD FSAR (NRC Docket No. 72-1030) does not calculate the temperature of the inner and outer cylinders directly from the heat transfer correlations, only an average effective thermal conductivity of the fluid as a function of fluid temperature and approximate Rayleigh number. The 'large circumferential temperature gradients' are actually relatively modest in terms of their impact on the thermo-physical properties of the fluid and it is these properties that determine the behavior of the fluid in the neutron shield.

The non-uniform temperature distribution on the surfaces of the neutron shield are addressed in the Amendment 10 SAR model by the segmentation of the neutron shield into 12 sections over the circumference and 3 sections in the radial direction. This

modeling connects the local temperature of the inner cylinder to the local temperature of the outer cylinder. As such, a higher temperature on the top of the neutron shield shell due to the presence of solar loading, etc. will cause the opposing section of the inner surface of the neutron shield to rise in temperature, as it will in reality.

While the Amendment 10 SAR modeling approach is not perfect, it is appropriate for the purpose of computing the peak fuel cladding temperatures within the DSC during transfer conditions. This conclusion was confirmed in the SER for NUHOMS® HD System (NRC Docket No. 72-1030). Further confirmation of this conclusion is taken from the staff's findings that the use of a constant Nusselt number about the circumference of the liquid neutron shield appears to have yielded conservative temperatures for this specific design configuration and the decay heats as stated in RAI 4-5.

In regards to the use of the k-effective values in the NUHOMS® HD FSAR, Tables 4-14 and 4-17 for decay heat loads of 24 kW, 31.2 kW, and 40.8 kW, the computed k-effective values are a function of the shield's geometry and Rayleigh number. As pointed out in the Amendment 10 SAR, the design of the OS200/OS200FC TC is similar to the design of the OS187 TC. Thus there will be no difference in the k-effective values due to geometry. The Rayleigh number is a function of the neutron shield's thickness, the fluid properties, and the temperature difference needed to transfer the decay heat across the neutron shield. Again, there is no change in the shield's thickness and the fact that the k-effective values are calculated as a function of mean fluid temperature means that the computer model will interpolate the k-effective values to fit the temperature profile determined under each decay heat loading. This leaves only the assumed temperature difference across the neutron shield as the only difference separating the k-effective values for each decay heat level.

The values in the NUHOMS® HD FSAR, Table 4-14 are calculated for a 10 to 13 °F difference, depending on the position along the cask, based on a 34.8 kW decay heat load. Since the required temperature difference is proportional to the decay heat load, a 40.8 kW decay heat load would require an approximately $40.8/34.8 \times 13^\circ\text{F} = 15.2^\circ\text{F}$ difference over the center portion of the cask. The larger temperature difference would yield higher Rayleigh numbers and, in turn, higher k-effective value than those presented in the NUHOMS® HD FSAR, Table 4-14. These higher values are conservatively ignored for the purposes of the Amendment 10 SAR calculations.

For 31.2 kW, the required temperature difference is approximately $31.2\text{ kW}/34.8\text{ kW} \times 13^\circ\text{F} = 11.7^\circ\text{F}$ difference. Since the Nusselt number is a function of the Rayleigh number to the 0.25 power and the Rayleigh number is proportional to the temperature difference, the effect on the computed k-effective values would be $(11.7^\circ\text{F}/13^\circ\text{F})^{0.25} = 0.97$. Thus, the k-effective values in the NUHOMS® HD FSAR, Table 4-14 are within 3% of the values that would have been computed specifically for 31.2 kW. This level of change, combined with the approximate 12 °F difference across the neutron shield, means the computed temperatures would have increased by only approximately 0.4 °F. This level of temperature difference was judged as insignificant.

For 24 kW, the required temperature difference is approximately $24\text{ kW}/34.8\text{ kW} \times 13^\circ\text{F} = 9^\circ\text{F}$ difference. Again, the Nusselt number is a function of the Rayleigh number to the 0.25 power meaning that the effect on the computed k-effective values would be $(9^\circ\text{F}/13^\circ\text{F})^{0.25} = 0.91$. Thus, the k-effective values in the NUHOMS® HD FSAR, Table 4-14 are within 9% of the values that would have been computed specifically for

24 kW. When combined with the approximately 9 °F difference across the neutron shield, this means the computed temperatures would have increased by only approximately 0.8 °F. This level of temperature difference was also judged insignificant, especially given the thermal margins shown for the HLZC #3 (24 kW) conditions.

Similar situations exist for the data in the NUHOMS® HD FSAR, Table 4-17 (i.e., an air-filled neutron shield), except that heat transfer by radiation dominates. The Amendment 10 SAR thermal model used only the convection portion of the k-effective from the NUHOMS® HD FSAR, Table 4-17. The radiation heat transfer was calculated independently within the Amendment 10 SAR model of the OS200 TC.

Therefore, the use of a single set of k-effective values for all heat loads evaluated by the Amendment 10 SAR is appropriate.

Discussion is added to Amendment 10 SAR Section U.4.5.2 regarding decay heat loading effects on effective thermal properties.

Section T.8 Procedures for Loading Cask, T.8.1.2 DSC Fuel Loading

- 4-7:** *Remove permissive language from the Technical Specifications (TS) that could potentially allow operators to deviate from the actions stated in the TSs related to cask handling, drying, and sealing.*

Appendix T, Section T.8, "Procedures for Loading Cask, T.8.1.2 DSC Fuel Loading," (page T.8-5) has a revised Step 16 which adds that "provision should be made to assure that air will not enter the DSC cavity. This may be achieved by replenishing the helium in the DSC cavity during cask movement from fuel pool to the decon area in case of malfunction of equipment used for cask movement." This information is needed to satisfy the provisions of 10 CFR 72.236(f), and 10 CFR 72.11.

Response to 4-7

TN finds permissive language in Amendment 10 SAR Chapter T.8 and also Chapter U.8, but not the Technical Specifications. In Chapters T.8 and U.8 the language has been changed to "provision shall be made to assure that air will not enter the DSC cavity. One way to achieve this is by replenishing the helium in the DSC cavity during cask movement from the fuel pool to the decon area in case of malfunction of equipment used for cask movement."

- 4-8:** *Clarify what quantities of water may be drained from NUHOMS system DSCs prior to removal from the spent fuel pool.*

Appendix T, Section T.8, "Procedures for Loading Cask, T.8.1.2 DSC Fuel Loading," (page T.8-5) adds a new Step 17A, to refill the partially drained cask once it is in the decon area, "If option of draining approximately 1100 gallons of water in Step 15 was selected... then slowly refill the DSC cavity" with about same amount of water that was drained.

This guidance appears to offer only one option as to the quantity drained from the DSC, specifically, 1100 gallons, in the case of the 61BTH. This also applies to the 32PTH1, in Section U.8.1.2 of Appendix U.

This information is needed to satisfy the provisions of 10 CFR 72.236(f).

Response to 4-8

Amendment 10 SAR, Step T.8.1.2.17a and Step U.8.1.2.18a have been revised such that the amount of water drained from the DSC prior to removal from the Spent Fuel Pool and the amount of water refilled into the DSC in the cask decon area are consistent. These instructions are also consistent with the loading procedures described for the other DSCs in the Standardized NUHOMS® system.

Section U.4.5.4 OS200 TC Thermal Model Results

4-9: *Insert revised page U.4-23*

It appears that Page U.4-23 should show revisions, if only because of shifted text, as a result of additions to page U.4-22. Otherwise, some text will be deleted from the document. This information is needed to satisfy the provisions of 10 CFR 72.11.

Response to 4-9

TN agrees. Page U.4-23 had shifted text and should have been included with Amendment 10 SAR Revision 1 pages. The information on Page U.4-23 is again shifted as a result of changes made for RAI No. 2 Items 4-5 and 4-6. All pages with changes or shifted information are included as Amendment 10 SAR Revision 3 pages with this submittal.

Section U.4.6.5.3 Maximum Temperatures

4-10: *Provide clarification in the SAR text to state precisely what the footnote to Table U.4-16 means.*

In Appendix U, Chapter U.4, new tables U.4-15 (Fuel cladding peak temperatures for normal conditions of transfer and storage; Type 1 and Type 2 basket) and U.4-16 (DSC component temperatures for Type 1 configuration only) have been added. A footnote stating "Temperatures adjusted based on effect of correction to "Dead Zone"/No correction DSC shell-support structure interface."

The staff requires additional clarification as to what is meant by the footnote. This information is needed to satisfy the provisions of 10 CFR 72.236(f), and 10 CFR 72.11.

Response to 4-10

Per the discussion for RAI #1 Item 4-9 it was recognized that the size of the dead zone angle for the DSC shell was incorrectly implemented as 7.9°. The correct dead zone angle of 18.9° for a 32PTH1 DSC in the HSM-H model is shown in Amendment 10 SAR Revision 0 Figure U.4-4.

Based on reanalyzing the HSM-H with the correct dead zone of 18.9°, results listed in Table U.4-2, Table U.4-3, Table U.4-15 through Table U.4-17, Table U.4-20 through Table U.4-22, and Table U.4-24 through Table U.4-26 were updated in Amendment 10 SAR Revision 1.

The footnotes added to Table U.4-15 through Table U.4-17, Table U.4-20 through Table U.4-22, and Table U.4-24 through Table U.4-26, were to indicate that this correction was implemented. Those footnotes contain a typographical error. The second instance of the word "correction" was meant to be "convection." The footnotes for these tables are rewritten and associated Amendment 10 SAR Revision 3 pages are included in this submittal.

Sections U.4.4.6 Description of Cases Evaluated for the HSM-H and U.4.4.7.1 Normal and Off-Normal Operating Condition Results

- 4-11:** *Revise the appropriate analyses to account for the potential rise in mean air temperature and total air mass flow rates based on the new DSC shell and HSM-H surface temperatures provided in the response to the first RAI (RAI 4-10, Round #1).*

New DSC shell surface temperatures and HSM-H surface temperatures (corresponding to new peak values reported in Rev. 1, for Table U.4-2) should also result in new values for mean air temperature, the T_n air temperatures for the eight 'levels' within the DSC, and the air exit temperature. The SAR changes for Revision 1 should also include a new Table U.4-1 (Air Flow Calculation Results Summary), and new total air mass flow rate values for the limiting cases with Type 1 and Type 2 baskets. This information is needed to satisfy the provisions of 10 CFR 72.236(f), and 10 CFR 72.11.

Response to 4-11

The changes for the DSC shell and HSM-H surface temperatures reflected in Amendment 10 SAR Revision 1 Table U.4-2 are caused by the correction of the "dead zone" area as described above in the response to RAI # 2 Item 4-2. The results and evaluation of the bounding cases (sea level conditions) are reported in Amendment 10 SAR Revision 1 Section U.4.4.7.1. Note that all the required analyses were revised to evaluate this correction and changes were made to the SAR. These changes are not caused by the effect of elevation on air density which was the subject of RAI #1 Item 4-10.

It is shown in the response to RAI #1 Item 4-10, Table 4-10-3 that the storage at elevations up to 5000 ft does not have any adverse effect on the thermal performance of the HSM-H and the maximum temperatures for all components are bounded by the values calculated for storage at sea level conditions. Therefore, airflow calculation results documented in Table U.4-1 for the storage conditions at sea level described in Sections U.4.4.1 and U.4.4.6 bound those for higher elevation and no changes were required to the Amendment 10 SAR.

Section U.4.4.5 – Description of HSM-H Model for the Blocked Vent Transient

- 4-12:** *Clarify the phrase: "7.9° No Convection Zone," which appears in Figures U.4-11 and U.4-13 for the Blocked Vent accident condition transient.*

Captions for Figures U.4-11 thru U.4-13 include the added phrase "7.9° No Convection Zone." Given that the blocked vents accident neglects convection (i.e., conduction only to cavity air) within HSM-H, according to SAR text (see Section U.4.4.5 – Description of

HSM-H Model for the Blocked Vent Transient, page U.4-16), this caption does not appear to apply to the Blocked Vent Transient.

This information is needed to satisfy the provisions of 10 CFR 72.236(f), and 10 CFR 72.11.

Response to 4-12

The NRC staff observation is correct. The HSM-H Model for the blocked vent accident condition assumes no convection within the HSM-H cavity.

Due to HSM-H model local mesh size in the DSC shell-support structure interface, a dead zone angle of 7.9° was used for the calculated dead zone angle of 4.2° in Chapter U.4 of Amendment 10, Revision 0.

The evaluations in Amendment 10 SAR, Rev. 1 account for a "dead zone" of 18.9° for the normal and off-normal analyses of an HSM-H with a 32PTH1 DSC. Since the initial conditions for the blocked vent transient analysis are based on off-normal conditions, the maximum temperatures for the blocked vent accident conditions were also affected by increasing the dead zone angle to 18.9°. This change resulted in corrections in Rev. 1 of Table U.4-3, Table U.4-24 through Table U.4-26, and Figure U.4-10. Since the temperature distributions for HSM-H components except for the DSC shell are similar before and after the correction of the dead zone angle, the temperature distributions and the time histories in Figure U.4-11 through Figure U.4-14 do not include new information and are not updated. The intention of the phrase "7.9° No Convection Zone" is to indicate that the content of the corresponding figures is not updated. This phrase is revised in Revision 3 of Amendment 10 to clarify the intention.

CHAPTER 7 Confinement Evaluation

7-1: *Modify the Operating Procedure T.8.1.3 (and the corresponding section for the other designs) to reflect that the vacuum pump needs to be shut off, or its isolated suction open to the atmosphere, when complying with Technical Specification 1.2.2 requirements for maintaining a stable vacuum pressure for 30 minutes to ensure that the water has been removed from the DSC*

Steps 21 and 27 of T.8.1.4 "DSC Drying and Backfilling" just isolate the vacuum pump when performing the pressure rise test as required by the TS. However, a leaking isolation valve (single failure) would negate the results. To prevent this possibility and to perform a valid test, the vacuum pump needs to be shut off or the isolation valve closed and the suction of the vacuum pump exposed to atmospheric pressure.

10CFR 72.162 requires that, in part, that a test program is established to ensure that the system will perform satisfactorily in service.

Response to 7-1

Section T.8.1.3 has been modified as requested. The corresponding section for the other design associated with Amendment 10, U.8.1.3 for the 32PTH1 system, has also been modified in the same fashion.

CHAPTER 8 Operating Systems

Note: RAI 8-1 is related to the materials review of the application.

- 8-1:** *Provide a TS section and wording to incorporate SAR section 8.1.3 into the TS by reference.*

10 CFR 72.122(h) requires: "The spent fuel cladding to be protected during storage against degradation that leads to gross rupture. . . ." The staff has identified, through the guidance in ISG-22 (Potential Rod Splitting Due to Exposure to an Oxidizing Atmosphere During Short-Term Cask Loading Operations in LWR or Other Uranium Oxide Based Fuel), that the loading/unloading process risks gross rupture of the cladding if precautions are not made to prevent or limit air exposure. SAR section 8.1.3 provides appropriate measures in accordance with the staff guidance of ISG-22. However, these measures need to be incorporated into the TS to ensure compliance with 10 CFR 72.122(h).

This information is required for compliance with 10 CFR 72.122(h).

Response to 8-1

In response to RAI #1 Item 4-1, TN created new Technical Specification 1.2.19, "61BTH and 32PTH1 DSC Bulkwater Removal Medium." Technical Specification 1.2.19 states that "Helium shall be used for drainage of bulk water (blowdown or draindown) from the DSC." This prevents any oxidizing atmosphere from coming in contact with the spent fuel cladding and provides appropriate measures to meet ISG-22. It would be redundant, and is not necessary, to incorporate dozens of steps from the UFSAR operating procedures in order to accomplish this same purpose. Therefore no changes have been made regarding RAI 8-1.

Although the Amendment 10 Revision 1 Technical Specifications included new TS 1.2.19, the TS table of contents did not reflect the new TS. Updated table of contents pages are therefore included with this submittal.

CHAPTER 9 Materials Evaluation (and Technical Specifications)

- 9-1:** *Clarify TN's position regarding helium leak rate testing for the vent and siphon port cover welds of the 24P and 52B DSC's.*

TS 1.2.4 (Amendment 10, SAR page A-117) specifies a helium leakage rate test of the inner top cover seal weld. However, this TS wording is silent with respect to helium leakage rate testing of the vent and siphon port cover welds.

In the previous RAI, (RAI 9-1, Round #1) this question was posed somewhat differently. However, in that RAI question, the staff misunderstood the design intent, thinking the acceptable leak rate should be 10E-7 instead of 10E-4 as stated in the SAR. The TN response correctly stated that TS 1.2.4 applies only to the 24P and 52B, which have a design leak rate limit of 10E-4. However, the response did not address helium leakage rate testing of the vent and siphon port covers.

TS 1.2.4a (Amendment 10, SAR page A-118) has been amended by way of another response to the first Amendment 10 RAI to include helium leakage rate testing of these cover plates for all the other designs covered by amendment 10. Thus, there is an apparent oversight.

This information is required for compliance with 10 CFR 72.236(j).

Response to 9-1

TS 1.2.4 has been edited to include the vent and siphon port cover welds as part of the helium leak rate testing of the inner top cover seal weld.

Enclosure 7 to TN E-26486

**Amendment 10 Revision 3 Proposed changes to the NUHOMS® CoC 1004 Amendment 9
Technical Specifications, and the UFSAR, Revision 10 (Non-proprietary version)**

TABLE OF CONTENTS

| <u>Section</u> | <u>Page</u> |
|---|-------------|
| 1.0 INTRODUCTION..... | A-1 |
| 1.1 General Requirements and Conditions | A-1 |
| 1.1.1 Regulatory Requirements for a General License..... | A-1 |
| 1.1.2 Operating Procedures | A-3 |
| 1.1.3 Quality Assurance | A-3 |
| 1.1.4 Heavy Loads Requirements..... | A-3 |
| 1.1.5 Training Module..... | A-3 |
| 1.1.6 Pre-Operational Testing and Training Exercise | A-4 |
| 1.1.7 Special Requirements for First System in Place..... | A-4 |
| 1.1.8 Surveillance Requirements Applicability..... | A-5 |
| 1.1.9 Supplemental Shielding..... | A-5 |
| 1.1.10 HSM-H Storage Configuration..... | A-5 |
| 1.1.11 Hydrogen Gas Monitoring for 61BTH and 32PTH1 DSCs..... | A-5 |
| 1.1.12 Codes and Standards | A-5 |
| 1.2 Technical Specifications, Functional and Operating Limits..... | A-6 |
| 1.2.1 Fuel Specifications | A-6 |
| 1.2.2 DSC Vacuum Pressure During Drying..... | A-114 |
| 1.2.3 24P and 52B DSC Helium Backfill Pressure | A-115 |
| 1.2.3a 61BT, 32PT, 24PHB, 24PTH and 61BTH DSC Helium Backfill Pressure..... | A-116 |
| 1.2.4 24P and 52B DSC Helium Leak Rate of Inner Seal Weld..... | A-117 |
| 1.2.4a 61BT, 32PT, 24PHB, 24PTH, 61BTH and 32PTH1 DSC Helium Leak Rate of Inner Seal Weld | A-118 |
| 1.2.5 DSC Dye Penetrant Test of Closure Welds..... | A-119 |
| 1.2.6 Deleted..... | A-120 |
| 1.2.7 HSM Dose Rates with a Loaded 24P, 52B or 61BT DSC | A-121 |
| 1.2.7a HSM Dose Rates with a Loaded 32PT DSC Only | A-122 |
| 1.2.7b HSM Dose Rates with a Loaded 24PHB DSC Only | A-123 |
| 1.2.7c HSM-H Dose Rates with a Loaded 24PTH-S or 24PTH-L DSC Only | A-124 |
| 1.2.7d HSM or HSM-H Dose Rates with a Loaded 24PTH-S-LC DSC Only | A-125 |
| 1.2.7e HSM-H Dose Rates with a Loaded Type 2 61BTH DSC Only | A-126 |
| 1.2.7f HSM or HSM-H Dose Rates with a Loaded Type 1 61BTH DSC Only | A127 |
| 1.2.7g HSM-H Dose Rates with a 32PTH1 DSC Only | A128 |
| 1.2.8 HSM Maximum Air Exit Temperature with a Loaded 24P, 52B, 61BT, 32PT, 24PHB or 24PTH-S-LC or a Type 1 61BTH DSC Only | A-129 |
| 1.2.8a HSM-H Maximum Air Exit Temperature with a Loaded 24PTH DSC..... | A-130 |
| 1.2.8b HSM-H Maximum Air Exit Temperature with a Loaded 61BTH DSC | A-131 |

| | | |
|---------|---|---------------|
| 1.2.8c | HSM-H Maximum Air Exit Temperature with a Loaded 32PTH1 DSC..... | A-133 |
| 1.2.9 | Transfer Cask Alignment with HSM or HSM-H | A-134 |
| 1.2.10 | TC/DSC Handling Height Outside the Spent Fuel Pool Building | A-135 |
| 1.2.11 | Transfer Cask Dose Rates with a Loaded 24P, 52B, 61BT, or 32PT DSC | A-136 |
| 1.2.11a | Transfer Cask Dose Rates with a Loaded 24PHB DSC | A-137 |
| 1.2.11b | Transfer Cask Dose Rates with a Loaded 24PTH-S or 24PTH-L DSC | A-138 |
| 1.2.11c | Transfer Cask Dose Rates with a Loaded 24PTH-S-LC DSC | A-139 |
| 1.2.11d | Transfer Cask Dose Rates with a Loaded 61BTH DSC..... | A-140 |
| 1.2.11e | Transfer Cask Dose Rates with a Loaded 32PTH1 DSC | A-141 |
| 1.2.12 | Maximum DSC Removable Surface Contamination | A-142 |
| 1.2.13 | TC/DSC Lifting Heights as a Function of Low Temperature and Location | A-143 |
| 1.2.14 | TC/DSC Transfer Operations at High Ambient Temperatures (24P, 52B, 61BT, 32PT, 24PHB, 24PTH, or 61BTH only)..... | A-144 |
| 1.2.14a | TC/DSC Transfer at High Ambient Temperatures (32PTH1 DSC Only)..... | A-145 |
| 1.2.15 | Boron Concentration in the DSC Cavity Water for the 24-P Design Only..... | A-146 |
| 1.2.15a | Boron Concentration in the DSC Cavity Water for the 32PT Design Only..... | A-148 |
| 1.2.15b | Boron Concentration in the DSC Cavity Water for the 24PHB Design Only | A-149 |
| 1.2.15c | Boron Concentration in the DSC Cavity Water for the 24PTH Design Only | A-150 |
| 1.2.15d | Boron Concentration in the DSC Cavity Water for the 32PTH1 Design Only | A-151 |
| 1.2.16 | Provision of TC Seismic Restraint Inside the Spent Fuel Pool Building as a Function of Horizontal Acceleration and Loaded Cask Weight | A-152 |
| 1.2.17 | 61BT DSC Vacuum Drying Duration Limit | A-153 |
| 1.2.17a | 32PT DSC Vacuum Drying Duration Limit..... | A-154 |
| 1.2.17b | 24PHB DSC Vacuum Drying Duration Limit | A-155 |
| 1.2.17c | 24PTH DSC Vacuum Drying Duration Limit..... | A-156 |
| 1.2.18 | Time Limit for Completion of 24PTH DSC Transfer Operation | A-157 |
| 1.2.18a | Time Limit for Completion of Type 2 61BTH DSC Transfer Operation | A-158 |
| 1.2.18b | Time Limit for Completion of 32PTH1 DSC Transfer Operation | A-159 |
| 1.2.19 | 61BTH and 32PTH1 DSC Bulkwater Removal Medium | A-159a |
| 1.3 | Surveillance and Monitoring..... | A-160 |
| 1.3.1 | Visual Inspection of HSM or HSM-H Air Inlets and Outlets (Front Wall and Roof Birdscreen)..... | A-160 |
| 1.3.2 | HSM or HSM-H Thermal Performance | A-161 |

Table 1-11
PWR Fuel Specification for the Fuel to be Stored in the NUHOMS®-24PTH DSC

| | |
|---|--|
| PHYSICAL PARAMETERS: | |
| Fuel Class | Intact or damaged unconsolidated B&W 15x15, WE 17x17, CE 15x15, WE 15x15, CE 14x14 and WE 14x14 class PWR assemblies (with or without control components) that are enveloped by the fuel assembly design characteristics listed in Table 1-1m. Equivalent reload fuel manufactured by other vendors but enveloped by the design characteristics listed in Table 1-1m is also acceptable. |
| Fuel Damage | Damaged PWR fuel assemblies are assemblies containing missing or partial fuel rods or fuel rods with known or suspected cladding defects greater than hairline cracks or pinhole leaks. The extent of cladding damage in the fuel rods is to be limited such that a fuel pellet is not able to pass through the damaged cladding opening during handling and retrievability is assured following normal and off-normal conditions. |
| Partial Length Shield Assemblies (PLSAs) | WE 15x15 class PLSAs which have only ever been irradiated in peripheral core locations with following characteristics are authorized: <ul style="list-style-type: none"> • Maximum burnup, 40 GWd/MTU • Minimum cooling time, 6.5 years • Maximum decay heat, 900 watts |
| Reconstituted Fuel Assemblies: <ul style="list-style-type: none"> • Maximum No. of Reconstituted Assemblies per DSC with Irradiated Stainless Steel Rods • Maximum No. of Irradiated Stainless Steel Rods per Reconstituted Fuel Assembly • Maximum No. of Reconstituted Assemblies per DSC with unlimited number of low enriched UO₂ rods and/or Unirradiated Stainless Steel Rods and/or Zr Rods or Zr Pellets | 4 10 24 |
| Control Components (CCs) | <ul style="list-style-type: none"> • Up to 24 CCs are authorized for storage in 24PTH-L and 24PTH-S-LC DSCs only. • Authorized CCs include Burnable Poison Rod Assemblies (BPRAs), Thimble Plug Assemblies (TPAs), Control Rod Assemblies (CRAs), Rod Cluster Control Assemblies (RCCAs), Axial Power Shaping Assembly Rods (APSRAs), Orifice Rod Assemblies (ORAs), Vibration Suppression Inserts (VSIs), Neutron Source Assemblies (NSAs), and Neutron Sources. • Design basis thermal and radiological characteristics for the CCs are listed in Table 1-1n. |
| Nominal Assembly Width | 8.536 inches |
| No. of Intact Assemblies | ≤24 |
| No. and Location of Damaged Assemblies | <p>Maximum of 12 damaged fuel assemblies. Balance may be intact fuel assemblies, empty slots, or dummy assemblies depending on the specific heat load zoning configuration.</p> <p>Damaged fuel assemblies are to be placed in Location A and/or B as shown in Figure 1-16. The DSC basket cells which store damaged fuel assemblies are provided with top and bottom end caps to assure retrievability.</p> |
| Maximum Assembly plus CC Weight | 1682 lbs |

Table 1-1bb
PWR Fuel Assembly Design Characteristics for the NUHOMS®-32PTH1 DSC

| Assembly Class | | B&W 15x15 | WE 17x17 | CE 15x15 | WE 15x15 | CE 14x14 | WE 14x14 | CE 16x16 |
|---|----------|--------------------------|-----------------------|-----------------------|-----------------------|-----------------------|-----------------------|-----------------------|
| <i>Max Unirradiated Length (in)⁽¹⁾</i> | 32PTH1-S | 162.6 | 162.6 | 162.6 | 162.6 | 162.6 | 162.6 | 162.6 |
| | 32PTH1-M | 170.0 | 170.0 | 170.0 | 170.0 | 170.0 | 170.0 | 170.0 |
| | 32PTH1-L | 178.3 | 178.3 | 178.3 | 178.3 | 178.3 | 178.3 | 178.3 |
| <i>Fissile Material</i> | | <i>UO₂</i> | <i>UO₂</i> | <i>UO₂</i> | <i>UO₂</i> | <i>UO₂</i> | <i>UO₂</i> | <i>UO₂</i> |
| <i>Maximum MTU/Assembly⁽²⁾</i> | | <i>0.49</i> | <i>0.49</i> | <i>0.49</i> | <i>0.49</i> | <i>0.49</i> | <i>0.49</i> | <i>0.49</i> |
| <i>Maximum Number of Fuel Rods</i> | | <i>208</i> | <i>264</i> | <i>216</i> | <i>204</i> | <i>176</i> | <i>179</i> | <i>236</i> |
| <i>Maximum Number of Guide/ Instrument Tubes</i> | | <i>17</i> | <i>25</i> | <i>9</i> | <i>21</i> | <i>5</i> | <i>17</i> | <i>5</i> |

Notes:

- (1) *Maximum Assembly + Control Component Length (unirradiated)*
- (2) *The maximum MTU/assembly is based on the shielding analysis. The listed value is higher than the actual.*

1.2.4 24P and 52B DSC Helium Leak Rate of Inner Seal Weld

Limit/Specification:

$\leq 1.0 \times 10^{-4}$ atm · cubic centimeters per second (atm · cm³/s) at the highest DSC limiting pressure.

Applicability: This specification is applicable to the inner top cover seal weld, *including the vent and siphon port covers*, of the 24P and 52B DSCs only.

Objective:

1. To limit the total radioactive gases normally released by each canister to negligible levels. Should fission gases escape the fuel cladding, they will remain confined by the DSC confinement boundary.
2. To retain helium cover gases within the DSC and prevent oxygen from entering the DSC. The helium improves the heat dissipation characteristics of the DSC and prevents any oxidation of fuel cladding.

Action: If the leak rate test of the inner seal weld exceeds 1.0×10^{-4} (atm · cm³/s):

1. Check and repair the DSC drain and fill port fittings for leaks.
2. Check and repair the inner seal weld.
3. Check and repair the inner top cover for any surface indications resulting in leakage.

Surveillance: After the welding operation has been completed, perform a leak test with a helium leak detection device.

Bases: If the DSC leaked at the maximum acceptable rate of 1.0×10^{-4} atm · cm³/s for a period of 20 years, about 63,100 cc of helium would escape from the DSC. This is about 1% of the 6.3×10^6 cm³ of helium initially introduced in the DSC. This amount of leakage would have a negligible effect on the inert environment of the DSC cavity. (Reference: American National Standards Institute, ANSI N14.5-1987, For Radioactive Materials—Leakage Tests on Packages for Shipment," Appendix B3).

The value of h_{fin} used in the model is 0.031 Btu/hr-in²-°F which bounds all ambient conditions and decay heat loads. Alternatively, flat stainless side heat shields are also evaluated.

The distance between the base plate of the HSM-H side heat shield and the HSM-H side wall is 2". The intersections of the HSM-H base plate and the HSM-H side walls create a narrow channels behind the side heat shield. The convection coefficient for these narrow channels are calculated using the same methodology described above.

The value of $h_{channel}$ used in the model is 0.003 Btu/hr-in²-°F which bounds all ambient conditions and decay heat loads.

Convection Coefficients for a Horizontal Cylinders (DSC):

The following equations from Reference [4.17] are used to calculate the free convection coefficients.

$$Nu = [(Nu_l)^m + (Nu_t)^m]^{1/m} \quad \text{with } m = 3.3 \quad \text{for } 10^{-10} < Ra < 10^{10}$$

$$h_c = \frac{Nu k}{D}$$

with:

- D = diameter of the horizontal cylinder,
- k = air conductivity.

$$Ra = Gr Pr, \quad Gr = \frac{g \beta (T_w - T_\infty) D^3}{\nu^2}$$

$$Nu_l = \frac{2f}{\ln(1 + 2f / Nu^T)} \quad (\text{Nusselt number for fully laminar heat transfer})$$

$$Nu^T = 0.772 \bar{C}_l Ra^{1/4}, \quad \bar{C}_l = 0.515 \quad \text{for gases [4.17]}$$

$$f = 1 - \frac{0.13}{(Nu^T)^{0.16}}$$

$$Nu_t = \bar{C}_l Ra^{1/3} \quad (\text{Nusselt number for fully turbulent heat transfer})$$

$$\bar{C}_l = 0.103 \quad \text{for horizontal cylinders [4.17].}$$

Convection Coefficients for the HSM-H Vertical Flat Surfaces (End Wall, Side Wall, Vertical Surface of the DSC Plugs, and Side Heat Shield without Fins):

$$Nu = [(Nu_l)^m + (Nu_t)^m]^{1/m} \quad \text{with } m = 6 \quad \text{for } 1 < Ra < 10^{12}$$

$$h_c = \frac{Nu k}{L}$$

with:

- L = height of the vertical surface

k = air conductivity

$$Nu_l = \frac{2.8}{\ln(1 + 2.8 / Nu^T)} \quad (\text{Nusselt number for fully laminar heat transfer})$$

$$Nu^T = \bar{C}_l Ra^{1/4} \quad , \quad \bar{C}_l = 0.515 \quad \text{for gases [4.17],}$$

$$Nu_t = C_l^V Ra^{1/3} \quad (\text{Nusselt number for fully turbulent heat transfer})$$

$$C_l^V = \frac{0.13 Pr^{0.22}}{(1 + 0.61 Pr^{0.81})^{0.42}}$$

Convection Coefficients for the HSM-H Horizontal Surfaces Facing Upwards (Basemat) and the 22.5° Segment of DSC Top Surface:

$$Nu = [(Nu_l)^m + (Nu_t)^m]^{1/m} \quad \text{with } m = 10 \quad \text{for } Ra > 1$$

$$h_c = \frac{Nu k}{L}$$

with:

$$L = A/P$$

A = Surface area of heated surface

P = perimeter of the heated surface

k = air conductivity

$$Ra = Gr Pr \quad , \quad Gr = \frac{g \beta (T_w - T_e) L^3}{\nu^2}$$

$$Nu_l = \frac{1.4}{\ln(1 + 1.4 / Nu^T)} \quad (\text{Nusselt number for fully laminar heat transfer})$$

$$Nu^T = 0.835 \bar{C}_l Ra^{1/4} \quad , \quad \text{and } \bar{C}_l = 0.515 \quad \text{for gases [4.17]}$$

$$Nu_t = C_l^H Ra^{1/3} \quad (\text{Nusselt number for fully turbulent heat transfer})$$

$$C_l^H \approx 0.14 \quad \text{for } Pr < 100 \quad [4.17]$$

Convection Coefficients for the HSM-H Horizontal Surfaces Facing Downwards (Ceiling):

$$Nu = Nu_l$$

$$h_c = \frac{Nu k}{L}$$

with:

$$L = A/P$$

A = surface area of heated surface

P = perimeter of the heated surface

k = air conductivity

Proprietary Information withheld under 10CFR2.390

Proprietary – Trade Secret

Proprietary Information withheld under 10 CFR 2.390

- b. Position the lifting yoke and the top shield plug and lower the shield plug into the DSC. Note that separate rigging may be used to install the shield plug prior to engaging the trunnions with the lifting yoke.

CAUTION: Verify that all the lifting height restrictions as a function of temperature specified in Technical Specification 1.2.13 can be met in the following steps which involve lifting of the transfer cask.

9. Visually verify that the top shield plug is properly seated within the DSC.
10. Position the lifting yoke with the cask trunnions and verify that it is properly engaged.
11. Raise the transfer cask to the pool surface. Prior to raising the top of the cask above the water surface, stop vertical movement.
12. Inspect the top shield plug to verify that it is properly seated within the DSC. If not, lower the cask and reposition the top shield plug and or remove the shield plug and reposition the hold down ring. Repeat Steps 8 through 12 as necessary.
13. Continue to raise the cask from the pool and spray the exposed portion of the cask with water until the top region of the cask is accessible.
14. Drain any excess water from the top of the DSC shield plug back to the fuel pool. Check the radiation levels at the center of top shield plug and around the perimeter of the cask. Disconnect the top shield plug rigging.
15. Drain a minimum of 50 gallons of water. Optionally approximately 1100 gallons of water (as indicated on the flow meter) may be drained from the DSC back into the fuel pool or other suitable location to meet the weight limit on the crane. Use 1-3 psig of helium to backfill the DSC with an inert gas per ISG-22 [8.2] guidance as water is being removed from the DSC.
16. Lift the cask from the fuel pool. As the cask is raised from the pool, continue to spray the cask with water and decon as directed. Provisions *shall* be made to assure that air will not enter the DSC cavity. *One way to achieve this is* by replenishing the helium in the DSC cavity during cask movement from *the* fuel pool to the decon area in case of malfunction of equipment used for cask movement.
17. Move the cask with loaded DSC to the cask decon area.
- 17A. *Replace the water removed from the DSC cavity in Step 15 with water from the fuel pool or an equivalent source.*
18. Install cask seismic restraints if required by Technical Specification 1.2.16 (required only on plant specific basis).
19. Verify that the transfer cask dose rates are compliant with limits specified in Technical Specification 1.2.11d.

extent of the pressure increase. Vacuum drying is complete when the pressure stabilizes for a minimum of 30 minutes at 3 mm Hg or less as specified in Technical Specification 1.2.2.

Note: The user shall ensure that the vacuum pump is isolated from the DSC cavity when demonstrating compliance with TS 1.2.2 requirements. Simply closing the valve between the DSC and the vacuum pump is not sufficient, as a faulty valve allows the vacuum pump to continue to draw a vacuum on the DSC. Turning off the pump, or opening the suction side of the pump to atmosphere are examples of ways to assure that the pump is not continuing to draw a vacuum on the DSC.

CAUTION: Radiation dose rates are expected to be high at the vent and siphon port locations. Use proper ALARA practices (e.g., use of temporary shielding, appropriate positioning of personnel, etc.) to minimize personnel exposure.

22. Open the valve to the vent port and allow the helium to flow into the DSC cavity.
23. Pressurize the DSC with helium (up to 10 psig for Type 1 DSC or 15 psig for Type 2 DSC).
24. Helium leak test the inner top cover plate weld for a leak rate of 1×10^{-4} atm cm³/sec. This test is optional.
25. If a leak is found, repair the weld, repressurize the DSC and repeat the helium leak test.
26. Once no leaks are detected, depressurize the DSC cavity by releasing the helium through the VDS to the plant's spent fuel pool or radioactive waste system.
27. Re-evacuate the DSC cavity using the VDS. The cavity pressure should be reduced in steps of approximately 10 mm Hg, 5 mm Hg, and 3 mm Hg. After pumping down to each level, the pump is valved off and the cavity pressure is monitored (these levels are optional). When the cavity pressure stabilizes, the pump is valved in to continue the vacuum drying process. Vacuum drying is complete when the pressure stabilizes for a minimum of 30 minutes at 3 mm Hg or less in accordance with Technical Specification 1.2.2 limits.

Note: The user shall ensure that the vacuum pump is isolated from the DSC cavity when demonstrating compliance with TS 1.2.2 requirements. Simply closing the valve between the DSC and the vacuum pump is not sufficient, as a faulty valve allows the vacuum pump to continue to draw a vacuum on the DSC. Turning off the pump, or opening the suction side of the pump to atmosphere are examples of ways to assure that the pump is not continuing to draw a vacuum on the DSC.

28. Open the valve on the vent port and allow helium to flow into the DSC cavity to pressurize the DSC between 14.5 to 16.0 psig for 61BTH Type 1 and 18.5 to 20.0 psig for 61BTH Type 2 psig and hold for 10 minutes. Depressurize the DSC cavity by releasing the helium through the VDS to the plant spent fuel pool or radioactive waste system to about 2.5 psig in accordance with Technical Specification 1.2.3a limits.

CAUTION: Radiation dose rates are expected to be high at the vent and siphon port locations. Use proper ALARA practices (e.g., use of temporary shielding, appropriate positioning of personnel, etc.) to minimize personnel exposure.

29. Close the valves on the helium source.
30. Remove the strongback, if installed in step 14 above, decontaminate as necessary, and store.

T.8.1.4 DSC Sealing Operations

CAUTION: During performance of steps listed in Section T.8.1.4, monitor the cask/DSC annulus water level and replenish as necessary to maintain cooling.

1. Disconnect the VDS from the DSC. Seal weld the prefabricated plugs over the vent and siphon ports. Inject helium into blind space just prior to completing welding and perform a dye penetrant weld examination in accordance with the Technical Specification 1.2.5 requirements.
2. Temporary shielding may be installed as necessary to minimize personnel exposure. Install the automatic welding machine onto the outer top cover plate and place the outer top cover plate with the automatic welding system onto the DSC. Optionally, outer top cover plate may be installed separately from the welding machine. Verify proper fit up of the outer top cover plate with the DSC shell.
3. Tack weld the outer top cover plate to the DSC shell. Place the outer top cover plate weld root pass.
4. Helium leak test the inner top cover plate and vent/siphon port plate welds using the leak test port in the outer top cover plate in accordance with Technical Specification 1.2.4a limits. Verify that the personnel performing the leak test are qualified in accordance with SNT-TC-1A [8.5]. Alternatively, this can be done with a test head in step 1 of Section T.8.1.4.
5. If a leak is found, remove the outer cover plate root pass (if not using test head), the vent and siphon port plugs and repair the inner cover plate welds. Then install the strongback (if used) and repeat procedure steps from T.8.1.1 step 21.
6. Perform dye penetrant examination of the root pass weld. Weld out the outer top cover plate to the DSC shell and perform dye penetrant examination on the weld surface in accordance with the Technical Specification 1.2.5 requirements.
7. Install and seal weld the prefabricated plug, if applicable, over the outer cover plate test port and perform dye penetrant weld examinations in accordance with Technical Specification 1.2.5 requirements.
8. Remove the automatic welding machine from the DSC.
9. Open the cask drain port valve and drain the water from the cask/DSC annulus.

10. Rig the cask top cover plate and lower the cover plate onto the transfer cask.
11. Bolt the cask cover plate into place, tightening the bolts to the required torque in a star pattern.

CAUTION: Monitor the applicable time limits of Technical Specification 1.2.18a until the completion of DSC transfer step 6 of Section T.8.1.6, if loading Type 2 61BTH DSC.

12. Verify that the TC dose rates are compliant with limits specified in Technical Specification 1.2.11d.

T.8.1.5 Transfer Cask Downending and Transport to ISFSI

NOTE:

Alternate Procedure for Downending of Transfer Cask: Some plants have limited floor hatch openings above the cask/trailer/skid, which limit crane travel (within the hatch opening) that would be needed in order to downend the TC with the trailer/skid in a stationary position. For these situations, alternate procedures are to be developed on a plant-specific basis, with detailed steps for downending.

1. Re-attach the transfer cask lifting yoke to the crane hook, as necessary. Ready the transport trailer and cask support skid for service.
2. Move the scaffolding away from the cask as necessary. Engage the lifting yoke and lift the cask over the cask support skid on the transport trailer.
3. The transport trailer should be positioned so that the cask support skid is accessible to the crane with the trailer supported on the vertical jacks.
4. Position the cask lower trunnions onto the transfer trailer support skid pillow blocks.
5. Move the crane forward while simultaneously lowering the cask until the cask upper trunnions are just above the support skid upper trunnion pillow blocks.
6. Inspect the positioning of the cask to insure that the cask and trunnion pillow blocks are properly aligned.
7. Lower the cask onto the skid until the weight of the cask is distributed to the trunnion pillow blocks.
8. Inspect the trunnions to insure that they are properly seated onto the skid and install the trunnion tower closure plates if required.
9. Remove the bottom ram access cover plate from the cask if integral ram/trailer is not used. Install the two-piece temporary neutron/gamma shield plug to cover the bottom ram access. Install the ram trunnion support frame on the bottom of the transfer cask. (The temporary shield plug and ram trunnion support frame are not required with the integral ram/trailer.)

T.8.1.6 DSC Transfer to the HSM

1. Prior to transporting the cask to the ISFSI or prior to positioning the transfer cask at the HSM designated for storage, remove the HSM door using a porta-crane, inspect the cavity of the HSM, removing any debris and ready the HSM to receive a DSC. The doors on adjacent HSMs should remain in place.

CAUTION: Very high dose rates in the empty HSM are expected if they are adjacent to a loaded HSM due to high heat loads in 61BTH DSC. Proper ALARA practices should be followed during these operations.

2. Inspect the HSM air inlet and outlets to ensure that they are clear of debris. Inspect the screens on the air inlet and outlets for damage.

CAUTION: Verify that the requirements of Technical Specification 1.2.14, "TC/DSC Transfer Operations at High Ambient Temperatures," are met prior to the next step.

3. Using a suitable vehicle, transport the cask from the plant's fuel/reactor building to the ISFSI along the designated transfer route.
4. Once at the ISFSI, position the transport trailer to within several inches of the HSM.
5. Check the position of the trailer to ensure the centerline of the HSM and cask approximately coincide. If the trailer is not properly oriented, reposition the trailer, as necessary.
6. Using a crane, unbolt and remove the cask top cover plate.

CAUTION: Verify that the applicable time limits of Technical Specification 1.2.18a are met if loading Type 2 61BTH DSC.

7. Back the cask to within a few inches of the HSM, set the trailer brakes and disengage the tractor. Drive the tractor clear of the trailer. Extend the transfer trailer vertical jacks.
8. Remove the skid tie-down bolts and use the skid positioning system to bring the cask into approximate vertical and horizontal alignment with the HSM. Using optical survey equipment and the alignment marks on the cask and the HSM, adjust the position of the cask until it is properly aligned with the HSM.
9. Using the skid positioning system, fully insert the cask into the HSM access opening docking collar.
10. Secure the cask trunnions to the front wall embedments of the HSM using the cask restraints.
11. After the cask is docked with the HSM, verify the alignment of the transfer cask using the optical survey equipment.

12. Position the hydraulic ram behind the cask in approximate horizontal alignment with the cask and level the ram. Remove either the bottom ram access cover plate or the outer plug of the two-piece temporary shield plug if installed. Power up the ram hydraulic power supply and extend the ram through the bottom cask opening into the DSC grapple ring.
13. Activate the hydraulic cylinder on the ram grapple and engage the grapple arms with the DSC grapple ring.
14. Recheck all alignment marks in accordance with the Technical Specification 1.2.9 limits and ready all systems for DSC transfer.
15. Activate the hydraulic ram to initiate insertion of the DSC into the HSM. Stop the ram when the DSC reaches the support rail stops at the back of the module.
16. Disengage the ram grapple mechanism so that the grapple is retracted away from the DSC grapple ring.
17. Retract and disengage the hydraulic ram system from the cask and move it clear of the cask. Remove the cask restraints from the HSM.
18. Using the skid positioning system, disengage the cask from the HSM access opening. Insert the DSC axial retainer.
19. Install the HSM door using a portable crane and secure it in place. Door may be welded for security. Verify that the HSM dose rates are compliant with the limits specified in Technical Specification 1.2.7e or 1.2.7f as appropriate.
20. Replace the transfer cask top cover plate. Secure the skid to the trailer, retract the vertical jacks and disconnect the skid positioning system.
21. Tow the trailer and cask to the designated equipment storage area. Return the remaining transfer equipment to the storage area.
22. Close and lock the ISFSI access gate and activate the ISFSI security measures.
23. Ensure the HSM-H maximum air exit temperature requirements of Technical Specification 1.2.8b are met.

T.8.1.7 Monitoring Operations

1. Perform routine security surveillance in accordance with the licensee's ISFSI security plan.
2. Perform one of the two alternate daily surveillance activities listed below:
 - a. A daily visual surveillance of the HSM air inlets and outlets to insure that no debris is obstructing the HSM vents in accordance with Technical Specification 1.3.1 requirements.
 - b. A temperature measurement of the thermal performance, for each HSM, on a daily basis in accordance with Technical Specification 1.3.2 requirements.

**Table U.2-3
PWR Fuel Assembly Design Characteristics for the NUHOMS®-32PTH1 DSC**

| Assembly Class | | B&W 15x15 | WE 17x17 | CE 15x15 | WE 15x15 | CE 14x14 | WE 14x14 | CE 16x16 |
|---|----------|-----------------|-----------------|-----------------|-----------------|-----------------|-----------------|-----------------|
| Max Unirradiated Length (in) ⁽¹⁾ | 32PTH1-S | 162.6 | 162.6 | 162.6 | 162.6 | 162.6 | 162.6 | 162.6 |
| | 32PTH1-M | 170.0 | 170.0 | 170.0 | 170.0 | 170.0 | 170.0 | 170.0 |
| | 32PTH1-L | 178.3 | 178.3 | 178.3 | 178.3 | 178.3 | 178.3 | 178.3 |
| Fissile Material | | UO ₂ | UO ₂ | UO ₂ | UO ₂ | UO ₂ | UO ₂ | UO ₂ |
| Maximum MTU/Assembly ⁽²⁾ | | 0.49 | 0.49 | 0.49 | 0.49 | 0.49 | 0.49 | 0.49 |
| Maximum Number of Fuel Rods | | 208 | 264 | 216 | 204 | 176 | 179 | 236 |
| Maximum Number of Guide/ Instrument Tubes | | 17 | 25 | 9 | 21 | 5 | 17 | 5 |

Notes:

- (1) Maximum Assembly + Control Component Length (unirradiated)
- (2) The maximum MTU/assembly is based on the shielding analysis. The listed value is higher than the actual.

The thermal model of the OS200 TC represents a 180° segment of the cask. The use of a 180° model permits the accurate simulation of the temperature distribution within the cask when the cask is in the horizontal or vertical orientation and the axis of the DSC is eccentric to that of the cask. Symmetry conditions are assumed to exist along the symmetry plane of the cask.

Figure U.4-15 presents a perspective view of the thermal model of the cask and DSC shell assembly (i.e., the cask body, closure lid, DSC, and spacer wedges). Figure U.4-16 presents a perspective view of the thermal model for the cask body. The model uses approximately 9,080 nodes, 6,225 solids, and 5,075 planar elements to define the cask body geometry and to provide thermal resolution. The modeling divides the cask circumference into 15° segments with axial lengths of 8 inches or less. Temperature dependent thermal properties are used for the cask components.

While the thermal model captures an increase in the structural shell thickness at the upper portion of the cask, the thermal model is based on an increase of 1.5-inches to 2-inches, instead of the current design configuration calling for an increase from 1.5-inches to 2.38-inches. The primary impact of this design change is that the effective thermal properties within the adjacent neutron shield sections are reduced by approximately 20% from values presented in Section U.4.2 for the portion of the TC affected by this design change (i.e., the column heading 'Middle/Top Sections'). The decrease in the local effective thermal properties is partially offset by the fact that the associated neutron shield width is also reduced by approximately 9% and the fact that the peak system temperatures do not occur at this location. The impact of the design change on the thermal performance of the TC was evaluated via a sensitivity run for the bounding heat load of 40.8 kW and is shown to have a negligible impact on the predicted peak temperatures. As such, use of the thermal model based on the TC design with a change in structural shell thickness from 1.5-inches to 2-inches is valid for the purposes of computing the thermal performance for the current design of the OS200 TC with a structural shell thickness change of 1.5-inches to 2.38-inches.

Since the geometry of water filled neutron shield for OS200/OS200FC TC is identical to that of OS187 described in [4.28], the heat transfer coefficients across the neutron shield are taken from [4.28], Table 4-14 and Table 4-17. These values are presented in Section U.4.2.

As explained in [4.28], the heat transfer coefficients are computed using a standard textbook correlation for the heat transfer between two concentric cylinders [4.13]. While these calculations are based on a heat load of 34.8 kW, the values are also appropriate for the evaluation of the thermal performance of the OS200/OS200FC TC at heat loads of 24, 31.2, and 40.8 kW. The basis for this conclusion is the fact that the effect of decay heat loading on the heat transfer within the neutron shield occurs via its impact on the fluid properties due to a change in operating temperature levels and via the temperature difference required to transfer the decay heat across the neutron shield. Since the k-effective values in Section U.4.2 are presented as a function of the mean fluid temperature, the computer thermal model will effectively account for the impact on fluid properties by interpolating the k-effective values to fit the temperature profile determined under each decay heat loading. This leaves the assumed temperature difference across the neutron shield as the only difference separating the k-effective values for each decay heat level.

Per the correlation presented in [4.28], the Nusselt number is a function of the Rayleigh number to the 0.25 power and the Rayleigh number is proportional to the temperature difference. Table

4-14 shows that a 10 to 13 °F difference is required to dissipate 34.8 kW across the neutron shield, depending on the position along the cask. The larger temperature difference required to transfer 40.8 kW will yield higher Rayleigh numbers and, in turn, higher k-effective values than those presented in Section U.4.2. As such, ignoring these higher k-effective values is conservative when determining the thermal performance of the OS200/OS200FC TC at a heat load of 40.8 kW.

Conversely, the lower temperature differences associated with the OS200/OS200FC TC at heat loads of 24, and 31.2 kW will yield lower k-effective values than those presented in Section U.4.2. However, since the Nusselt number is a function of the Rayleigh number to the 0.25 power and the Rayleigh number is proportional to the temperature difference, the effect of the change in the decay heat loading on the computed k-effective values will be proportional to the ratio of the decay heats raised to the 0.25 power. For the 31.2 kW heat loading, this equates to a $(31.2 \text{ kW}/34.8 \text{ kW})^{0.25} = 0.97$ factor. Thus, the k-effective values in Section U.4.2 are within 3% of the values that would have been computed specifically for the 31.2 kW decay heat condition. This level of change, combined with the approximate 12 °F difference across the neutron shield, results in a level of temperature difference that is judged as insignificant. Similarly, the factor for 24 kW is 0.91, which when combined with the approximate 9 °F difference across the neutron shield, results in less than a 1 °F temperature rise in the temperature difference across the neutron shield. As such, the use of the k-effective values in Section U.4.2 to evaluate the thermal performance of the OS200/OS200FC TC for decay heat loadings of 24 to 40.8 kW is appropriate for determining the safety basis of the design.

Under accident conditions where the neutron shield is assumed to be filled with air, radiation exchange is added to the appropriate effective thermal conductivity values. Axial heat transfer within the neutron shield is based on conduction (i.e., a Nusselt number = 1). Heat transfer from the outer skin of the neutron shield is computed based on natural convection correlation and thermal radiation exchange.

Figure U.4-17 through Figure U.4-19 illustrate the thermal modeling used for the cask closure lid and associated NS-3 shielding. The modeling utilizes approximately 1,680 thermal nodes, 1,070 solids, and 1,200 planar surfaces. The incorporation of the geometry for the slots in the closure lid within the thermal model can be seen in the Figure U.4-18 'solids' view of the modeled closure lid.

The methodology to apply boundary conditions for the OS200 / OS200FC TC is identical to the methodology described in Appendix P, Sections P.4.2.3 and P.4.5.2.4.

Convection and radiation heat transfer to ambient are considered for the exterior surfaces of TC. Radiation heat transfer is also considered between the DSC shell and the TC inner cavity surfaces. The emissivity values are listed in Section U.4.2.

Insulation is considered over exterior surfaces of the TC for hot ambient conditions according to orientation and solar absorptivity of surfaces. Solar absorptivity of stainless steel is considered conservatively equal to its emissivity value of 0.6. The values of the applied solar heat fluxes are listed below:

| OS200 TC Surface | Insolation (gcal/cm ²) | Applied heating averaged over 12 hours (Btu/hr-ft ²) with absorptivity |
|------------------------|------------------------------------|--|
| Cask Cylindrical Shell | 400 | 72.15 |
| Cask Vertical Ends | 200 | 36.08 |

The sensitivity of the model to the thermal resolution was tested based on a preliminary thermal model that used model uses approximately 6,900 nodes, 4,560 solids, and 3,600 planar elements to define the cask body and DSC geometry. The peak cask temperature obtained for the loss of neutron shield accident was 3% lower than the results obtained with the current modeling based on the use of approximately 9,080 nodes, 6,225 solids, and 5,075 planar elements to define the cask body and DSC geometry. Based on the fact that a 30 to 40% increase in the modeling elements results in only a 3% change in the peak temperature it is concluded that the current modeling provides an accurate representation of the OS200 TC's thermal performance.

U.4.5.3 Description of Cases Evaluated for the OS200 TC

The thermal analyses of the OS200 TC are performed for the design basis ambient air temperatures defined in Section U.4.5.1. The evaluated cases include the vertical loading condition inside of the fuel handling facility, normal and off-normal horizontal transfer conditions without and with air circulation, and four accident scenarios. The first accident scenario evaluates the potential interruption of the air circulation system and establishes the time available to re-establish the air circulation, complete the transfer operation, or initiate some other recovery mode. The second accident scenario evaluated the potential loss of both the air circulation system and the water in the neutron shield. The evaluation establishes the transient heat up trend and the ultimate temperatures achieved under steady-state conditions. The third accident scenario involves a 15-minute hypothetical fire. The maximum duration of the fire event will be controlled under actual operations by administratively limiting the available fuel sources within the vicinity of the TC. The evaluation establishes the maximum temperatures reached as a result of the fire event, as well as the post-fire, steady-state conditions. The fourth final accident scenario involves an undamaged TC under an elevated ambient condition of 133°F. The evaluation addresses the maximum steady-state temperatures that would be achieved should this accidental ambient condition occur.

Table U.4-4, Table U.4-5, and Table U.4-6 summarize the cases evaluated for OS200 TC with the 32PTH1 DSC with the HLZC #1, HLZC #2, and HLZC #3 heat load configurations, respectively. Since the OS200 TC is able to accommodate the HLZC #3 heat load configuration without air circulation, fewer design cases are needed to establish the thermal performance of the TC with this payload.

U.4.5.4 OS200 TC Thermal Model Results

The following sections present the predicted thermal results for the OS200 TC with the 32PTH1 DSC. The resultant DSC shell temperatures from these analyses are used as boundary conditions in the 32PTH1 DSC basket analysis presented in Section U.4.6.

U.4.5.4.1 Normal and Off-Normal Transfer Conditions Results

Table U.4-11 presents the maximum steady state component temperatures achieved for transfer operation for 32PTH1 DSC with Type 1 basket and decay heat load of 31.2 kW or less (i.e., HLZC #2 or HLZC #3) under normal and off-normal conditions. The resultant maximum component temperatures for steady state transfer operation for 32PTH1 DSC with Type 2 basket and decay heat load of 24 kW or less (i.e., HLZC #3) are presented in Table U.4-34. All component temperatures are well below their associated allowable limits.

To maintain fuel cladding temperatures below allowable limits, operational time limits are determined for transfer operation when decay heat load of 32PTH1 DSC with Type 1 basket

exceeds 31.2 kW (i.e., HLZC #1) or decay heat load of 32PTH1 DSC with Type 2 basket exceeds 24 kW (i.e., HLZC #2 and HLZC #3). Administrative measures ensure that the transfer operation is completed within the allotted time or some form of recovery operation such as air circulation is initiated.

Figure U.4-20 and Figure U.4-33 illustrate the predicted transient performance of the TC containing 32PTH1 DSC with Type 1 and Type 2 baskets during vertical loading operations, respectively.

The transient begins with the TC and DSC at the steady-state conditions existing for the TC and DSC in the vertical orientation, the annulus between the TC and the DSC filled with water at a temperature of 223°F (i.e., the boiling point of water assuming a mean annulus height of approximately 8 feet). The ambient air temperature in the fuel handling facility is assumed to be at its design maximum of 140°F and the DSC is conservatively assumed to be centered within the TC annulus. At time = 0, the water is assumed to be drained, the closure lid is placed on the cask and the lid bolting is initiated, the TC and DSC are assumed to be left in their upright position, and the system begins to heat up. The transient concludes with a steady-state analysis.

The maximum time the TC can be left in this orientation is determined by the time it takes for the maximum DSC shell temperature to reach a temperature of 450°F when it contains Type 1 basket with a decay heat loading of 40.8 kW. For the same purpose, the maximum DSC shell temperature is selected at 400°F when the DSC contains Type 2 basket with a decay heat loading of 31.2 kW. The targeted maximum DSC shell temperatures are based on a detailed model of the DSC basket, rails and fuel assemblies described in Section U.4.6. Based on the results of the detailed DSC model, the maximum allowable DSC shell temperature is determined and the associated time point in the TC transient analysis is used to establish the allowable time period for completing the transfer process. These transfer times are valid for all ambient conditions and TC orientations.

Similar transient analyses for the normal hot, normal cold, and off-normal hot conditions of transfer are summarized in Table U.4-9 and Table U.4-13.

Table U.4-9 presents the maximum TC component temperatures achieved under the evaluated transient operating conditions at the point when the DSC shell temperature containing a Type 1 basket reaches 450°F. All component temperatures are within their associated maximum allowable temperature limits. Figure U.4-27 and Figure U.4-28 illustrates alternate perspective views of the predicted temperature distribution existing within the DSC shell and the OS200 TC at 15.75 hours after the start of the vertical loading operation. Figure U.4-29 and Figure U.4-30 illustrate similar views of the predicted temperature distributions for the normal hot horizontal transfer operation.

Table U.4-13 presents the maximum TC component temperatures achieved under the evaluated transient operating conditions for DSC with Type 2 basket. Figure U.4-39 and Figure U.4-40 illustrates alternate perspective views of the predicted temperature distribution existing within the DSC shell and the OS200 TC at 16.25 hours after the start of the vertical loading operation.

Figure U.4-41 and Figure U.4-42 illustrate similar views of the predicted temperature distributions for the normal hot horizontal transfer operation.

Table U.4-8 presents the maximum component temperatures achieved under the normal hot, normal cold, and off-normal hot horizontal transfer conditions with 450 cfm of air circulation for DSC 32PTH1 with Type 1 basket and decay heat load of 40.8 kW. The results demonstrate that

the air circulation yield steady state DSC shell temperatures that are below the target value of 450°F for all considered conditions.

Figure U.4-30 and Figure U.4-31 illustrate the expected temperature distributions within the DSC shell and the TC for the normal hot horizontal transfer condition with 450 cfm of air circulation.

Table U.4-11 presents the maximum TC component temperatures achieved under steady state operating conditions for the DSC with Type 1 basket and a maximum heat load of 31.2 kW.

Table U.4-12 presents the maximum component temperatures achieved under the normal hot, normal cold, and off-normal hot conditions of horizontal transfer with 450 cfm of air circulation for 32PTH1 DSC with Type 2 basket and decay heat load of 31.2 kW. The results demonstrate that the air circulation option will yield steady-state DSC shell temperatures that are below the target value of 420°F for all conditions.

Figure U.4-43 and Figure U.4-44 illustrate the expected temperature distribution within the DSC shell and the TC for the normal hot horizontal transfer condition with 450 cfm of air circulation.

Alternatively, steady-state operations for decay heat dissipations of 24 kW or less (i.e., HLZC #3) are permitted under all conditions for either the Type 1 or Type baskets. Table U.4-34 presents the maximum TC component temperatures achieved under steady-state operating conditions.

U.4.5.4.2 Transfer Accident Conditions Results

Four accident scenarios are evaluated for the OS200 TC with the 32PTH1 DSCs. The first accident scenario evaluates the potential interruption of the air circulation system and establishes the time available to re-establish the air circulation, complete the transfer operation, or initiate some other recovery mode. The predicted heat up rate for the OS200 TC with the 32PTH1 DSC and 40.8 kW of decay heat is illustrated in Figure U.4-24. The analysis assumes that the TC and DSC are initially at steady-state under the normal hot condition with air circulation. At time = 0, the air circulation is assumed to be lost and the system begins to heat up. As seen from the figure, approximately 5.5 hours are available before exceeding the target DSC shell temperature limit of 450°F established in consideration of the peak cladding temperature. This time period is available to complete the transfer to the storage module, re-establish the fan airflow, or initiate some other recovery operation. The transient evaluation is continued for a total of 20 hours to illustrate the rate of heat up and is concluded with a steady-state evaluation. Figure U.4-36 illustrates a similar response for the 32PTH1 DSC with 31.2 kW of decay heat. In this case, approximately 17 hours are available before exceeding the target DSC shell temperature limit of 420°F established in consideration of the peak cladding temperature.

The second accident scenario evaluated the potential loss of both the air circulation and the water in the neutron shield. The evaluation establishes the transient heat up trend and the ultimate temperatures achieved under steady-state conditions. Figure U.4-25 and Figure U.4-37 illustrate the predicted thermal response for the OS200 TC with the 32PTH1 DSC and decay heat loads of 40.8 and 31.2 kW, respectively. In each case, the transient is assumed to start at the point where the maximum operational time allowed without air circulation is reached (see Section U.4.5.4.1) since that temperature condition yields the hottest allowable operating temperatures within the DSC and TC and provides a conservative starting point. At time = 0, the water in the neutron shield jacket is lost (drained) and the air circulation option is assumed not to be available. The

transient evaluation is continued for 30 hours to illustrate the rate of heat up expected. The analysis concludes with a steady-state evaluation. In each case, in excess of 30 hours is available to re-establish the water in the neutron shield jacket before steady-state conditions are achieved. The maximum temperatures achieved at steady-state conditions are presented in Table U.4-10 and Table U.4-14 for decay heat loads of 40.8 and 31.2 kW, respectively.

The third accident scenario involves an undamaged OS200 TC under an elevated ambient condition of 133°F. The evaluation addresses the maximum steady-state temperatures that would be achieved. No air circulation is considered for this accident scenario. The maximum steady-state temperatures are presented in Table U.4-10 and Table U.4-14 for decay heat loads of 40.8 and 31.2 kW, respectively.

The fourth accident scenario evaluated for the OS200 TC involves a 15-minute hypothetical fire. The maximum duration of the fire event will be controlled under actual operations by administratively limiting the available fuel sources within the vicinity of the TC. The fire properties are based the 10 CFR §71.73 fire criteria with a flame temperature of 1,475°F and a flame emittance of 0.9. The fire is assumed to fully engulf the TC for the duration of the 15-minute fire event with the heat transfer between the fire and the TC being via radiation and forced convection. Following the fire, the ambient condition is set to 117°F with the maximum insolation. The heat transfer between the TC and the ambient is via radiation and natural convection. The emittance of the TC exterior surfaces is raised to 0.8 at the start of the fire event and is assumed to remain constant for the remainder of the transient.

The initial temperature condition for the fire accident transient is the same as used for the start of the loss of the neutron shield accident scenario. The neutron shield is assumed to be filled with water during the fire event, but the water is assumed to be lost at the end of the fire. This assumption maximizes the heat input to the TC from the fire since it is expected that the pressure relief valves on the shield will activate early in the fire transient, allowing the water to boil off and, in the process, absorbing a significant amount of the energy imparted to the TC from the fire. The calculation of the effective conductivity for water or air-filled neutron shield is described in [4.28] and reported in Section U.4.2 (14).

The analysis demonstrates that, with the exception of the exterior surfaces of the cask, the thermal mass of the DSC and cask components is sufficient to absorb the heat flux from the fire without a significant increase in temperature. Figure U.4-26 and Figure U.4-38 present the predicted transient temperature response for the OS200 TC and the 32PTH1 DSC shell with 40.8 and 31.2 kW of decay heat loading, respectively, under the evaluated hypothetical fire event. As seen from each figure, with the exception of the exterior surfaces of the cask, the maximum cask component temperatures achieved under the fire accident scenario will occur at the post-fire steady-state condition.

It is assumed that liquid neutron shield (water) is present throughout the 15-minute fire transient even though it is expected to be lost and replaced with air very early in the fire transient. This assumption maximizes the heat input from the fire to the canister because of the high conductivity of water compared to air. To maximize the canister temperature during the post-fire transient, it is assumed that water in the neutron shield cavity is lost at the beginning of the post-fire transient and replaced by air as the heat flow is now from the canister to the ambient.

The conditions and material properties during the post-fire period are the same as those for the accident case of loss of neutron shield and sun shade. The only exception is the emissivity of the

cask outer surface. It is assumed that the outer surface is covered with soot for the post-fire conditions with an emissivity of 0.8.

The gaps included in the thermal model of the 32PTH1 DSC basket are summarized in Figure U.4-49 through Figure U.4-51. These gaps are not removed for calculating the cladding temperatures during accident conditions. The DSC shell temperature changes by a small amount during the accident fire transient. This change is small during the fire transient due to the large thermal mass of the transfer cask. This shows that heat input from the fire to the DSC is not significant. Since the DSC shell temperature is almost unchanged, the cladding temperatures during the 15-minute fire transient also are almost unchanged. Therefore, the assumption of not removing the gaps during the fire transient has a negligible impact on cladding temperatures.

Table U.4-10 and Table U.4-14 present the peak component temperatures achieved with decay heat loads of 40.8 and 31.2 kW, respectively, at the end of the fire (i.e., 15 minutes into the transient) and for the post-fire steady-state condition. A comparison of the post-fire steady-state temperatures in each table with those for the 'loss of neutron shield' accident scenario in the same table shows that the 'loss of neutron shield' temperatures bound by a slight margin those seen for the post-fire steady-state condition. This occurs because the sooting and oxidation of the exterior surfaces that is assumed for the fire event raises the surface emissivity, thus increasing the heat transfer between the cask and the ambient. No specific evaluation for the 32PTH1 DSC with HLZC #3 (i.e., 24 kW of decay heat loading) is provided. Instead, the results for 24 kW will be bounded by those seen for 40.8 and 31.2 kW.

U.4.5.4.3 Sensitivity Analysis For Constant Nusselt Number in Neutron Shield

The heat transfer coefficients derived in [4.28] are computed using a standard textbook correlation for the heat transfer between two concentric cylinders [4.13]. The correlation yields an average Nusselt number which, when multiplied by the thermal conductivity of water, yields the effective thermal conductivity of the fluid filling the neutron shield. While this correlation does not explicitly provide an estimate of the variation in Nusselt number as a function of the position in the neutron shield annulus, the actual physics of the flow patterns in the neutron shield which drives the variation in Nusselt number is implicitly captured via the level of the correlation's predicted average Nusselt number. This occurs since the correlation is based on the results of a wide range of physical experiments wherein the complexity of the flow patterns and heat transfer in the annulus is present and their effect on the overall heat transfer is correlated to the parameters chosen for the correlation. This includes the fact that a stagnation region exists near the bottom of the horizontal annulus. Using a constant, average Nusselt number results in the predicted heat transfer rates being under-estimated over most of the inner cylinder (i.e., the structural shell of the TC) and the upper portion of the outer cylinder (i.e., the shell of the neutron shield) and over-estimated over a small section on the upper portion of the inner cylinder and over the lower portion of the outer cylinder.

To verify that the variation in Nusselt number is insignificant for the purposes of predicting the peak fuel cladding temperature, the work of Desai and Vafai [4.40] was used as the basis for a sensitivity analysis. Desai and Vafai investigated the heat transfer characteristics for annuli with $10^6 < \text{Rayleigh number} < 10^9$, $0.01 < \text{Prandtl number} < 5000$, and diameter ratios of 1.5 to 11 and plotted the resulting local Nusselt numbers as function of position on the inner and outer cylinders. Based on this data, the sensitivity analysis replaced the constant Nusselt number derived k-effective values with values that varied from approximately 112% of the average at the

bottom of the structural shell to approximately 43% of the average at the top, and from approximately 203% of the average at the top of the neutron shield's shell to 4% of the average (i.e., pure conduction/stagnation) at the bottom the shield's shell.

To select the transfer condition for the basis of the sensitivity analysis, the various transfer conditions evaluated in Section U.4.5.4.1 were examined to determine the conditions yielding the lowest fuel cladding thermal margin. For the Type 1 basket with HLZC #1 (40.8 kW) this occurs for an ambient temperature of 106 °F, while for the Type 2 basket with HLZC #2 (31.2 kW) it occurs for an ambient temperature of 0 °F (see Table U.4-15). A time limit of 15.7 hours or less is enforced for transfer operations with the Type 1 basket and HLZC #1 and steady-state operations can not occur unless the air circulation mode is activated or other corrective actions are implemented. Because of this, the thermal mass of the TC and the payload is the controlling factor on the available transient time and the angular variation in the heat transfer within the neutron shield will not have a significant impact in the determination of the available transfer time limit. Therefore, the steady-state evaluation of HLZC #2 for the Type 2 basket for 0 °F ambient is selected as the appropriate transfer condition for determining the impact of the angular variation in the neutron shield heat transfer rates.

Re-evaluation of the Type 2 basket for steady-state conditions, a HLZC #2, 0 °F ambient condition, and non-constant Nusselt number within the neutron shield annulus resulted in 3 °F higher temperature for the TC's inner shell at the top of the cask than that obtained using the constant Nusselt number methodology.

The effects of a varying Nusselt number around the circumference of the neutron shield are seen mainly in the immediate shells forming the boundaries of the neutron shield. These effects are reduced to an insignificant level for the DSC shell temperature and for the fuel cladding temperature due to the heat spreading that occurs from conduction through the multiple shells of the TC and the DSC and the relatively large gap between the DSC and TC inner shell, which causes radiation effects to dominate. The maximum basket and fuel cladding temperatures are predicted in the same manner as used for the safety basis calculations (i.e., the temperature distribution on the DSC shell predicted from the TC thermal model is used as a boundary condition for the detailed DSC thermal model). The results demonstrate that maximum DSC shell temperature and the maximum fuel cladding temperature using the varying Nusselt number methodology are within 1 and 2 °F, respectively, of those predicted using the constant Nusselt number methodology.

Therefore, the sensitivity analysis demonstrates that safety evaluations based on a constant, average Nusselt number methodology is appropriate for estimating the peak fuel cladding temperatures despite that fact that the local Nusselt number varies with position within the neutron shield.

U.4.5.5 Evaluation of OS200 TC Performance

The analyses presented above demonstrate that NUHOMS® OS200 TC is qualified for on-site fuel transfer operations with the 32PTH1 DSC and for decay heat loads up to 40.8 kW. All of the OS200 TC component temperatures remain within their allowable limits for the normal, off-normal, and accident conditions.

As determined by the finite element thermal analysis (see Figure 4.4-60), the 1" thick NSP Top Support Ring, which is an attachment to the Top Flange (Top Forging), is the only item where the short term temperature limit may be exceeded. This is a non-structural, non load-bearing component wherein this short duration temperature excursion has no effect on cask performance.

As determined by the finite element thermal analysis (see Figure 4.4-61), the 3/4" thick Bottom Neutron Shield Plate, which is an attachment to the Bottom Support Ring (Bottom Forging), is the only item where the temperature may exceed 1,067° F. This is a non-structural, non load-bearing component wherein this short duration temperature excursion has no affect on cask performance. However, there is a small region around the circumference of the ring, located at the bottom-outer most corner of the machined forging, where temperatures may slightly exceed the short term limit (up to a maximum temperature of 1,067° F). The effected region represents a small fraction of the load bearing section, and is remote from the primary load path between the Structural Shell and the Bottom End Plate. Furthermore, the amount of time the material spends in the elevated temperature range is insufficient to permit creep or sensitization phenomena to occur. Thus, this short duration fire transient temperature excursion has no affect on cask performance.

The 32PTH1 DSC is available in three lengths and with two fuel basket configurations. The analyses are bounding for all DSC lengths, but are dependent on the combination of fuel basket configuration and the decay heat loading. Tables U.4-8 through U.4-14 and U.4-34 list the DSC shell maximum allowable limit of 800 °F for long term. Similarly, Table U.4-14 also lists 1000 °F as the maximum allowable limit for short term. Note that these limits are not the thermal analyses limits. They are limits for the structural analysis in Section U.3 to ensure structural integrity for stainless steel components.

Steady-state operations under all conditions are permissible for heat loads of 24 kW or less for either Type 1 or Type 2 basket. Likewise, steady-state operations under all conditions are permissible for heat loads of 24 kW to 31.2 kW for the DSC with Type 1 basket, but not for the Type 2 basket. Operations for decay heat loads exceeding 24 kW for the DSC with Type 2 basket and 31.2 kW for the DSC with Type 1 basket must be limited in time duration permitted or some form of recovery operation, such as air circulation, must be initiated. The allowable duration for the transfer operations (defined as the time elapsed after the initiation of draining of Cask/DSC annulus water until the completion of insertion of the DSC into the HSM-H) will vary depending on the DSC configuration and the heat load, and whether or not the air circulation option for the TC is utilized. The following table summarizes the permissible operational conditions:

| Fuel Basket Type | DSC Heat Load Zoning Configurations | Transfer Time Limit ^{(1) (2) (4)} |
|--------------------------|-------------------------------------|--|
| Type 1 with intact fuel | HLZC 2 (≤31.2 kW) | No time limit |
| Type 1 with damaged fuel | HLZC 2 (≤31.2 kW) | 38 hrs. ⁽³⁾ |
| Type 1 | HLZC 1 (≤40.8 kW) | 13 hrs. ⁽³⁾ |
| Type 2 with intact fuel | HLZC 2 (24 kW to 31.2 kW) | 14 hrs. ⁽³⁾ |
| Type 2 with damaged fuel | HLZC 2 (>24 kW to ≤31.2 kW) | 10 hrs. ⁽³⁾ |
| Type 1 or Type 2 | HLZC 2 (≤24 kW) | No time limit |

Notes:

- (1) Transfer time is defined as the time elapsed after the initiation of draining of Cask/DSC annulus water until the completion of insertion of the DSC into the HSM-H.
- (2) Initiate recovery operations such as air circulation if the operation time exceeds the limit.
- (3) Initiate recovery operations such as air circulation if the operation time exceeds the limit. Two hours is considered sufficient time to initiate the air circulation option.
- (4) The transfer operation time limit is reset only if the transfer cask annulus is refilled with water.

The properties of Zircaloy-4 and UO₂ are provided in Section U.4.2.

The calculated bounding values of effective specific heat and density for FAs to store in the 32PTH1 DSC are summarized in Section U.4.2.

U.4.8.3 32PTH1 DSC Basket Effective Thermal Properties

The 32PTH1 DSC basket effective density, thermal conductivity and specific heat are calculated for use in the transient analyses of the 32PTH1 DSC in the OS200 transfer cask and in the HSM-H. This section includes calculation of the bounding basket properties among 32PTH1-S, 32PTH1-M and 32PTH1-L DSCs with maximum heat load per DSC up to 40.8 kW.

The calculation of these thermal effective properties is based on the DSC component weights. The 32PTH1 DSC effective density and specific heat are calculated as volumetric and weight average values, respectively. Weight of the basket components are calculated in Chapter U.3. The effective density and effective specific heat are calculated as follows:

$$\rho_{\text{eff}} = \frac{\text{basket weight} + \text{fuel assemblies weight}}{\text{cavity volume}}$$

$$C_{p,\text{eff}} = \frac{\text{weight of SS} \times C_{p,\text{ss}} + \text{weight of Al} \times C_{p,\text{Al}} + \text{weight of fuel} \times C_{p,\text{fuel}}}{\text{basket weight} + \text{fuel assemblies weight}}$$

where

$$\text{Total cavity volume} = \pi/4 \times D_i^2 \times L$$

$$D_i = \text{DSC inner diameter} = 68.75''$$

L = cavity length

$C_{p,\text{ss}}$ is specific heat of stainless steel (SS) (=0.114 Btu/lbm-°F@100°F [4.2]).

$C_{p,\text{Al}}$ is specific heat of aluminum (=0.216 Btu/lbm-°F@100°F [4.2]).

$C_{p,\text{fuel}}$ is specific heat of fuel (=0.0677 Btu/lbm-°F at 400°F [Section U.4.8.2]).

Selecting low specific heat capacities for stainless steel and aluminum at 100°F and the fuel assembly at 400°F is conservative since it reduces the amount of stored heat in the basket and results in a higher fuel cladding temperatures. The bounding PWR fuel assembly weight of 1715 lb in U.4.2 is conservatively applied in the above calculation.

The effective thermal properties of 32PTH1 DSC with Type 2 basket (steel rail) bounds those for 32PTH1 DSC with Type 1 basket (aluminum rail). These properties are used in thermal analysis.

The resultant effective density and specific heat capacity of the three 32PTH1 DSC configurations are listed below.

$$k_{\text{eff_rad}} = \frac{Q}{4\pi \cdot L \cdot (T_c - T_s)}$$

where Q = total heat load – reaction solution for the outermost nodes (Btu/hr)
 L = cylinder (DSC cavity) length (15" length of the slice model)
 T_c = maximum temperature at the cylinder center (°F)
 T_s = temperature at the cylinder outer surface (°F)

Since the surface area of the fuel assemblies at the basket cross section is much larger than the other components, assuming a uniform heat generation is a reasonable approximation to calculate the radial effective conductivity. The temperatures from 100°F to 1000°F are applied uniformly to the DSC shell. An average, (T_s+T_c)/2, is used for the basket temperature, for which *k_{eff_rad}* is reported. Applied boundary conditions are shown in Figure U.4-59.

The resulting values of DSC basket effective axial and radial conductivity are listed in table below.

32PTH1 DSC Basket Axial and Radial Effective Thermal Conductivity

| T (°F) | Calculated <i>k_{eff_rad}</i> (Btu/hr-in-°F) | Bounding Value (95%)* (Btu/hr-in-°F) |
|--------|--|--------------------------------------|
| 290 | 0.1576 | 0.1497 |
| 380 | 0.1664 | 0.1581 |
| 469 | 0.1771 | 0.1682 |
| 560 | 0.1879 | 0.1785 |
| 651 | 0.1989 | 0.1890 |
| 744 | 0.2082 | 0.1978 |
| 840 | 0.2147 | 0.2040 |
| 937 | 0.2193 | 0.2084 |
| 1034 | 0.2229 | 0.2118 |
| 1133 | 0.2254 | 0.2141 |

| T (°F) | Calculated <i>k_{eff_axl}</i> (Btu/hr-in-°F) | Bounding Value (95%)* (Btu/hr-in-°F) |
|--------|--|--------------------------------------|
| 350 | 0.8701 | 0.8266 |
| 450 | 0.8877 | 0.8433 |
| 550 | 0.9029 | 0.8578 |
| 650 | 0.9172 | 0.8714 |
| 750 | 0.9294 | 0.8829 |
| 850 | 0.9417 | 0.8946 |
| 950 | 0.9506 | 0.9031 |
| 1050 | 0.9572 | 0.9094 |
| 1150 | 0.9585 | 0.9106 |

* 95% of the calculated radial effective thermal conductivity is conservatively chosen for HSM-H and transfer cask *transient* thermal analyses.

- 4.34. Section 4 of Amendment No. 1 to the Certificate of Compliance No. 1029 for the Standardized Advanced NUHOMS[®] Storage System, NRC Docket No. 72-1029, May 31, 2005.
- 4.35. ASHRAE Handbook Fundamentals 4th Edition, American Society of Heating, Refrigerating, and Air-Conditioning Engineers, New York, NY, 1983.
- 4.36. Guyer, "Handbook of Applied Thermal Design", McGraw-Hill, Inc., 1989.
- 4.37. Bucholz, J. A., Scoping Design Analysis for Optimized Shipping Casks Containing 1, 2, 3, 5, 7, or 10 Year Old PWR Spent Fuel, Oak Ridge National Laboratory, January, 1983, ORNL/CSD/TM-149.
- 4.38. Gubareff, G. G., Janssen, J. E. and Torborg, R. H. "Thermal Radiation Properties Survey", 2nd Edition, Honeywell Research Center, 1960.
- 4.39. McAdams, William H., "Heat Transmission", McGraw-Hill Book Company, New York, NY, 1954.
- 4.40 *Desai, C. P. and Vafai, K., An Investigation and Comparative Analysis of Two- and Three-dimensional Turbulent Natural Convection in a Horizontal Annulus, International Journal of Heat and Mass Transfer, Vol. 37, No. 16, pp. 2475-2504, 1994.*

**Table U.4-15
Fuel Cladding Normal Operating Condition Maximum Temperatures**

For Intact Fuel Assemblies

| Operating Condition | DSC with Type 1 Basket | | DSC with Type 2 Basket | | Limit ⁽⁴⁾ (°F) |
|--|------------------------|-----------------|------------------------|-----------------|------------------------------|
| | HLZC #1 | HLZC #2 | HLZC #2 | HLZC #3 | |
| | 40.8 kW (°F) | 31.2 kW (°F) | 31.2 kW (°F) | 24.0 kW (°F) | |
| Storage, 0°F ambient ^{(1) (5)} | 658 | <640 | 640 | <640 | 752 |
| Storage, 106°F ambient ^{(1) (5)} | 733 | <717 | 717 | <717 | |
| Transfer (Loading), 0°F ambient | 717 | 665 | 730 | 624 | |
| Transfer (Loading), 106°F ambient | 722 | 713 | 728 | 680 | |
| Transfer (Loading), 120°F ambient ⁽²⁾ | <730 | <737 | <727 | <702 | |
| Time Limit for Transfer Operation ⁽³⁾ | 15.75 hr | No time Limit | 16.25 hr | No time limit | |

For Intact and Damaged Fuel Assemblies

| Operating Condition | DSC with Type 1 Basket | | DSC with Type 2 Basket | | Limit ⁽⁴⁾ (°F) |
|--|------------------------|-----------------|------------------------|-----------------|------------------------------|
| | HLZC #1 | HLZC #2 | HLZC #2 | HLZC #3 | |
| | 40.8 kW (°F) | 31.2 kW (°F) | 31.2 kW (°F) | 24.0 kW (°F) | |
| Storage, 106°F ambient ⁽⁵⁾ | 742 | 673 | 733 | 676 | 752 |
| Transfer (Loading), 120°F ambient ⁽²⁾ | <741 | <731 | <731 | <714 | |
| Time Limit for Transfer Operation ⁽³⁾ | 15.75 hr | 40.0 hr | 12.0 hr | No time limit | |

Notes:

- (1) HLZC #2 (31.2 kW) for DSC with Type 1 basket and HLZC #3 (24.0 kW) for DSC with Type 2 basket are bounded by HLZC #2 (31.2 kW) for DSC with Type 2 basket.
- (2) Vertical loading normal transfer 120°F ambient case is bounded by vertical loading off-normal transfer 140°F ambient case. The fuel cladding temperatures for the vertical loading off-normal transfer are provided in Table U.4-20.
- (3) The time limit for transfer operation denotes the time allowed for transfer before air circulation is required. The time limit is governed by the vertical loading off-normal 140°F ambient case.
- (4) The fuel cladding limit is provided in ISG-11, Revision 3 [4.15].
- (5) Temperatures *calculated* based on effect of correction to "Dead Zone".

Table U.4-16
32PTH1 DSC with Type 1 Basket Assembly Component Normal Operating Condition
Maximum Temperatures

For Intact Fuel Assemblies

| Operating Condition | Fuel Compartment | | Neutron Absorber | | R45 & R90 Rails | |
|--|------------------|-----------------|------------------|-----------------|-----------------|-----------------|
| | HLZC #1 | HLZC #2 | HLZC #1 | HLZC #2 | HLZC #1 | HLZC #2 |
| | 40.8 kW (°F) | 31.2 kW (°F) | 40.8 kW (°F) | 31.2 kW (°F) | 40.8 kW (°F) | 31.2 kW (°F) |
| Storage, 0°F ambient ^(1, 4) | 619 | <602 | 619 | <601 | 424 | <424 |
| Storage, 106°F ambient ^(1, 4) | 701 | <685 | 701 | <684 | 511 | <511 |
| Transfer (Loading), 0°F ambient | 676 | 625 | 676 | 625 | 503 | 466 |
| Transfer (Loading), 106°F ambient | 683 | 677 | 683 | 676 | 506 | 520 |
| Transfer (Loading), 120°F ambient ⁽²⁾ | <699 | <704 | <699 | <704 | <508 | <531 |

For Intact & Damaged Fuel Assemblies

| Operating Condition | Fuel Compartment | | Neutron Absorber | | R45 & R90 Rails | |
|--|---------------------|-----------------|---------------------|-----------------|---------------------|-----------------|
| | HLZC #1 | HLZC #2 | HLZC #1 | HLZC #2 | HLZC #1 | HLZC #2 |
| | 40.8 kW (°F) | 31.2 kW (°F) | 40.8 kW (°F) | 31.2 kW (°F) | 40.8 kW (°F) | 31.2 kW (°F) |
| Storage, 106°F ambient ⁽⁴⁾ | 688 | 615 | 688 | 615 | 509 | 440 |
| Transfer (Loading), 120°F ambient ⁽²⁾ | <699 ⁽³⁾ | <678 | <699 ⁽³⁾ | <678 | <508 ⁽³⁾ | <507 |

Notes:

- (1) HLZC #2 (31.2 kW) is bounded by the HLZC #1 (40.8 kW) for DSC with Type 1 basket and HLZC #2 (31.2 kW) for DSC with Type 2 basket (listed in Table U.4-17).
- (2) Vertical loading normal transfer 120°F ambient case is bounded by vertical loading off-normal transfer 140°F ambient case. The basket assembly component temperatures for the vertical loading off-normal transfer are provided in Table U-4-21.
- (3) The maximum temperatures for the structural components are bounded by the 32 intact fuel assemblies in DSC with 40.8 kW heat load.
- (4) Temperatures *calculated* based on effect of correction to "Dead Zone".

Table U.4-17
32PTH1 DSC with Type 2 Basket Assembly Component Normal Operating Condition
Maximum Temperatures

For Intact Fuel Assemblies

| Operating Condition | Fuel Compartment | | Neutron Absorber | | R45 & R90 Rails | |
|--|------------------|-----------------|------------------|-----------------|-----------------|-----------------|
| | HLZC #2 | HLZC #3 | HLZC #2 | HLZC #3 | HLZC #2 | HLZC #3 |
| | 31.2 kW (°F) | 24.0 kW (°F) | 31.2 kW (°F) | 24.0 kW (°F) | 31.2 kW (°F) | 24.0 kW (°F) |
| Storage, 0°F ambient ^(1, 3) | 602 | <602 | 601 | <601 | 442 | <442 |
| Storage, 106°F ambient ^(1, 3) | 685 | <685 | 684 | <684 | 529 | <529 |
| Transfer (Loading), 0°F ambient | 695 | 589 | 695 | 588 | 552 | 469 |
| Transfer (Loading), 106°F ambient | 694 | 648 | 693 | 648 | 547 | 529 |
| Transfer (Loading), 120°F ambient ⁽²⁾ | <694 | <673 | <694 | <672 | <536 | <543 |

For Intact & Damaged Fuel Assemblies

| Operating Condition | Fuel Compartment | | Neutron Absorber | | R45 & R90 Rails | |
|--|------------------|-----------------|------------------|-----------------|-----------------|-----------------|
| | HLZC #2 | HLZC #3 | HLZC #2 | HLZC #3 | HLZC #2 | HLZC #3 |
| | 31.2 kW (°F) | 24.0 kW (°F) | 31.2 kW (°F) | 24.0 kW (°F) | 31.2 kW (°F) | 24.0 kW (°F) |
| Storage, 106°F ambient ⁽³⁾ | 681 | 629 | 681 | 628 | 528 | 502 |
| Transfer (Loading), 120°F ambient ⁽²⁾ | <678 | <669 | <678 | <669 | <523 | <542 |

Notes:

- (1) HLZC #3 (24.0 kW) is bounded by HLZC #2 (31.2 kW).
- (2) Vertical loading normal transfer 120°F ambient case is bounded by vertical loading off-normal transfer 140°F ambient case. The basket assembly component temperatures for the vertical loading off-normal transfer are provided in Table U.4-22.
- (3) Temperatures *calculated* based on effect of correction to "Dead Zone".

**Table U.4-20
Fuel Cladding Off-Normal Condition Maximum Temperatures**

For Intact Fuel Assemblies

| Operating Condition | DSC with Type 1 Basket | | DSC with Type 2 Basket | | Limit ⁽⁴⁾ (°F) |
|--|------------------------|--------------------|------------------------|--------------------|------------------------------|
| | HLZC #1 | HLZC #2 | HLZC #2 | HLZC #3 | |
| | 40.8 kW (°F) | 31.2 kW (°F) | 31.2 kW (°F) | 24.0 kW (°F) | |
| Storage, -40°F ambient ^(1, 6) | 629 | <610 | 610 | <610 | 1,058 |
| Storage, 117°F ambient ^(1, 6) | 741 | <724 | 724 | <724 | |
| Transfer (Loading), 117°F ambient | 722 | 709 | 730 | 675 | 752 |
| Transfer (Loading), 117°F ambient, with air circulation, Steady State | 690 | --- ⁽³⁾ | 669 | --- ⁽³⁾ | |
| Transfer (Loading), 140°F ambient | 730 | 737 | 727 | 702 | |
| Time Limit for Transfer Operation ⁽²⁾ | 15.75hr | No time Limit | 16.25 hr | No time limit | |

For Intact and Damaged Fuel Assemblies

| Operating Condition | DSC with Type 1 Basket | | DSC with Type 2 Basket | | Limit ⁽⁴⁾ (°F) |
|--|------------------------|-----------------|------------------------|-----------------|------------------------------|
| | HLZC #1 | HLZC #2 | HLZC #2 | HLZC #3 | |
| | 40.8 kW (°F) | 31.2 kW (°F) | 31.2 kW (°F) | 24.0 kW (°F) | |
| Storage, 117°F ambient ⁽⁶⁾ | ~750 ⁽⁵⁾ | 681 | 740 | 684 | 1,058 |
| Transfer (Loading), 140°F ambient ⁽²⁾ | ~741 ⁽⁵⁾ | 731 | 731 | 714 | 752 |
| Time Limit for Transfer Operation ⁽²⁾ | 15.75hr | 40.0 hr | 12.0 hr | No time limit | |

Notes:

- (1) HLZC #2 (31.2 kW) for DSC with Type 1 basket and HLZC #3 (24.0 kW) for DSC with Type 2 basket are bounded by HLZC #2 (31.2 kW) for DSC with Type 2 basket.
- (2) The time limit for transfer operation denotes the time allowed for transfer before air circulation is required. The time limit is governed by the vertical loading off-normal 140°F ambient case.
- (3) No air circulation is required for DSC with Type 1 basket, HLZC #2 (31.2 kW) and DSC with Type 2 basket, HLZC #3 (24.0 kW).
- (4) The fuel cladding limit is provided in ISG-11, Revision 3 [4.15].
- (5) These temperatures are estimated based on the difference between the maximum fuel cladding temperatures for the intact and damaged fuel assemblies under 106°F ambient storage conditions reported in Table U.4-15.
- (6) Temperatures *calculated* based on effect of correction to "Dead Zone".

Table U.4-21
32PTH1 DSC with Type 1 Basket Assembly Component Off-Normal Operating Condition
Maximum Temperatures

For Intact Fuel Assemblies

| Operating Condition | Fuel Compartment | | Neutron Absorber | | R45 & R90 Rails | |
|---|------------------|--------------------|------------------|--------------------|-----------------|--------------------|
| | HLZC #1 | HLZC #2 | HLZC #1 | HLZC #2 | HLZC #1 | HLZC #2 |
| | 40.8 kW (°F) | 31.2 kW (°F) | 40.8 kW (°F) | 31.2 kW (°F) | 40.8 kW (°F) | 31.2 kW (°F) |
| Storage, -40°F ambient ⁽¹⁾⁽⁴⁾ | 587 | <570 | 587 | <569 | 390 | <390 |
| Storage, 117°F ambient ⁽¹⁾⁽⁴⁾ | 710 | <693 | 710 | <692 | 520 | <520 |
| Transfer (Horizontal), 117°F ambient | 684 | 674 | 684 | 674 | 505 | 514 |
| Transfer (Horizontal), 117°F ambient, with air circulation, Steady State | 649 | --- ⁽²⁾ | 648 | --- ⁽²⁾ | 485 | --- ⁽²⁾ |
| Transfer (Loading), 140°F ambient | 699 | 704 | 699 | 704 | 508 | 532 |

For Intact & Damaged Fuel Assemblies

| Operating Condition | Fuel Compartment | | Neutron Absorber | | R45 & R90 Rails | |
|---------------------------------------|---------------------|-----------------|---------------------|-----------------|-----------------|-----------------|
| | HLZC #1 | HLZC #2 | HLZC #1 | HLZC #2 | HLZC #1 | HLZC #2 |
| | 40.8 kW (°F) | 31.2 kW (°F) | 40.8 kW (°F) | 31.2 kW (°F) | 40.8 kW (°F) | 31.2 kW (°F) |
| Storage, 117°F ambient ⁽⁴⁾ | <710 ⁽³⁾ | 624 | <710 ⁽³⁾ | 624 | 497 | 449 |
| Transfer (Loading), 140°F ambient | <699 ⁽³⁾ | 678 | 672 | 678 | 492 | 507 |

Notes:

- (1) HLZC #2 (31.2 kW) is bounded by the HLZC #1 (40.8 kW) for DSC with Type 1 basket and HLZC #2 (31.2 kW) for DSC with Type 2 basket (listed in Table U.4-22).
- (2) No air circulation is required for DSC with Type 1 basket, HLZC #2 (31.2 kW).
- (3) The maximum temperatures for the structural components are bounded by the results for 32 intact fuel assemblies in DSC with 40.8 kW heat load.
- (4) Temperatures *calculated* based on effect of correction to "Dead Zone".

Table U.4-22
32PTH1 DSC with Type 2 Basket Assembly Component Off-Normal Operating Condition
Maximum Temperatures

For Intact Fuel Assemblies

| Operating Condition | Fuel Compartment | | Neutron Absorber | | R45 & R90 Rails | |
|---|------------------|--------------------|------------------|--------------------|-----------------|--------------------|
| | HLZC #2 | HLZC #3 | HLZC #2 | HLZC #3 | HLZC #2 | HLZC #3 |
| | 31.2 kW (°F) | 24.0 kW (°F) | 31.2 kW (°F) | 24.0 kW (°F) | 31.2 kW (°F) | 24.0 kW (°F) |
| Storage, -40°F ambient ^(1, 3) | 570 | <570 | 569 | <569 | 409 | <409 |
| Storage, 117°F ambient ^(1, 3) | 693 | <693 | 692 | <692 | 537 | <537 |
| Transfer (Horizontal), 117°F ambient | 695 | 644 | 695 | 643 | 488 | 523 |
| Transfer (Horizontal), 117°F ambient, with air circulation, Steady State | 631 | --- ⁽²⁾ | 630 | --- ⁽²⁾ | 488 | --- ⁽²⁾ |
| Transfer (Loading), 140°F ambient | 694 | 673 | 694 | 672 | 536 | 543 |

For Intact & Damaged Fuel Assemblies

| Operating Condition | Fuel Compartment | | Neutron Absorber | | R45 & R90 Rails | |
|---------------------------------------|------------------|-----------------|------------------|-----------------|-----------------|-----------------|
| | HLZC #2 | HLZC #3 | HLZC #2 | HLZC #3 | HLZC #2 | HLZC #3 |
| | 31.2 kW (°F) | 24.0 kW (°F) | 31.2 kW (°F) | 24.0 kW (°F) | 31.2 kW (°F) | 24.0 kW (°F) |
| Storage, 117°F ambient ⁽³⁾ | 690 | 637 | 689 | 637 | 536 | 511 |
| Transfer (Loading), 140°F ambient | 678 | 669 | 678 | 669 | 523 | 542 |

Notes:

- (1) HLZC #2 (24.0 kW) is bounded by HLZC #2 (31.2 kW).
- (2) No air circulation is required for DSC with Type 2 Basket, HLZC #3 (24.0 kW).
- (3) Temperatures *calculated* based on effect of correction to "Dead Zone".

**Table U.4-24
Fuel Cladding Accident Condition Maximum Temperatures**

For Intact Fuel Assemblies

| Operating Condition | DSC with Type 1 Basket | | DSC with Type 2 Basket | | Limit ⁽⁴⁾ (°F) |
|--|------------------------|-----------------|------------------------|---------------------|------------------------------|
| | HLZC #1 | HLZC #2 | HLZC #2 | HLZC #3 | |
| | 40.8 kW (°F) | 31.2 kW (°F) | 31.2 kW (°F) | 24.0 kW (°F) | |
| Storage, 133°F ambient ^(1, 6) | 752 | <736 | 736 | <736 | 1,058 |
| Storage, Blocked Vents @40 hr, 117°F ambient ^(1, 6) | 887 | <849 | 849 | <849 | |
| Transfer loss of sunshade, ⁽²⁾ neutron shield, & air circulation, 117°F ambient, Steady State | 886 | 796 | 858 | <858 ⁽³⁾ | |

For Intact and Damaged Fuel Assemblies

| Operating Condition | DSC with Type 1 Basket | | DSC with Type 2 Basket | | Limit ⁽⁴⁾ (°F) |
|--|------------------------|-----------------|------------------------|-----------------|------------------------------|
| | HLZC #1 | HLZC #2 | HLZC #2 | HLZC #3 | |
| | 40.8 kW (°F) | 31.2 kW (°F) | 31.2 kW (°F) | 24.0 kW (°F) | |
| Storage, Blocked Vents @40 hr, 117°F ambient ⁽⁶⁾ | ~896 ⁽⁵⁾ | 805 | 863 | 809 | 1,058 |
| Transfer loss of sunshade, ⁽²⁾ neutron shield, & air circulation, 117°F ambient, Steady State | ~897 ⁽⁵⁾ | 809 | 870 | 816 | |

Notes:

- (1) HLZC #2 (31.2 kW) for DSC with Type 1 basket and HLZC #3 (24.0 kW) for DSC with Type 2 basket are bounded by HLZC #2 (31.2 kW) for DSC with Type 2 basket.
- (2) The transfer accident case bounds the accident transfer at 133°F ambient, and the fire-accident.
- (3) HLZC #3 (24.0 kW) is bounded by the HLZC #2 (31.2 kW) for DSC with Type 2 basket.
- (4) The fuel cladding limit is provided in ISG-11, Revision 3 [4.15].
- (5) These temperatures are estimated based on the difference between the maximum fuel cladding temperatures for the intact and damaged fuel assemblies under 106°F ambient storage conditions reported in Table U.4-15.
- (6) Temperatures *calculated* based on effect of correction to "Dead Zone".

Table U.4-25
32PTH1 Type 1 Basket DSC Basket Assembly Component Accident Condition Maximum
Temperatures

For Intact Fuel Assemblies

| Operating Condition | Fuel Compartment | | Neutron Absorber | | R45 & R90 Rails | |
|--|------------------|-----------------|------------------|-----------------|-----------------|-----------------|
| | HLZC #1 | HLZC #2 | HLZC #1 | HLZC #2 | HLZC #1 | HLZC #2 |
| | 40.8 kW (°F) | 31.2 kW (°F) | 40.8 kW (°F) | 31.2 kW (°F) | 40.8 kW (°F) | 31.2 kW (°F) |
| Storage, 133°F ambient ^(1, 4) | 722 | <705 | 722 | <705 | 533 | <533 |
| Storage, Blocked Vents @ 40hr, 117°F ambient ^(1, 4) | 865 | <825 | 865 | <825 | 685 | 674 |
| Transfer loss of sunshade, ⁽²⁾ neutron shield, & air circulation, 117°F ambient, Steady State | 858 | 766 | 858 | 766 | 692 | 609 |

For Intact & Damaged Fuel Assemblies

| Operating Condition | Fuel Compartment | | Neutron Absorber | | R45 & R90 Rails | |
|--|---------------------|-----------------|---------------------|-----------------|---------------------|-----------------|
| | HLZC #1 | HLZC #2 | HLZC #1 | HLZC #2 | HLZC #1 | HLZC #2 |
| | 40.8 kW (°F) | 31.2 kW (°F) | 40.8 kW (°F) | 31.2 kW (°F) | 40.8 kW (°F) | 31.2 kW (°F) |
| Storage, Blocked Vents @ 40hr, 117°F ambient ⁽⁴⁾ | <865 | 761 | <865 ⁽³⁾ | 761 | <685 ⁽³⁾ | 593 |
| Transfer loss of sunshade, ⁽²⁾ neutron shield, & air circulation, 117°F ambient, Steady State | <853 ⁽³⁾ | 762 | <843 ⁽³⁾ | 762 | <692 ⁽³⁾ | 609 |

Notes:

- (1) HLZC #2 (31.2 kW) is bounded by the HLZC #1 (40.8 kW) for DSC with Type 1 basket and HLZC #2 (31.2 kW) for DSC with Type 2 basket (listed in Table U.4-26).
- (2) The transfer accident case bounds the accident transfer at 133°F ambient, and the fire-accident.
- (3) The maximum temperatures for the structural components are bounded by the results for 32 intact fuel assemblies in DSC with 40.8 kW heat load.
- (4) Temperatures *calculated* based on effect of correction to "Dead Zone".

**Table U.4-26
32PTH1 DSC with Type 2 Basket Assembly Component Accident Condition Maximum
Temperatures**

For Intact Fuel Assemblies

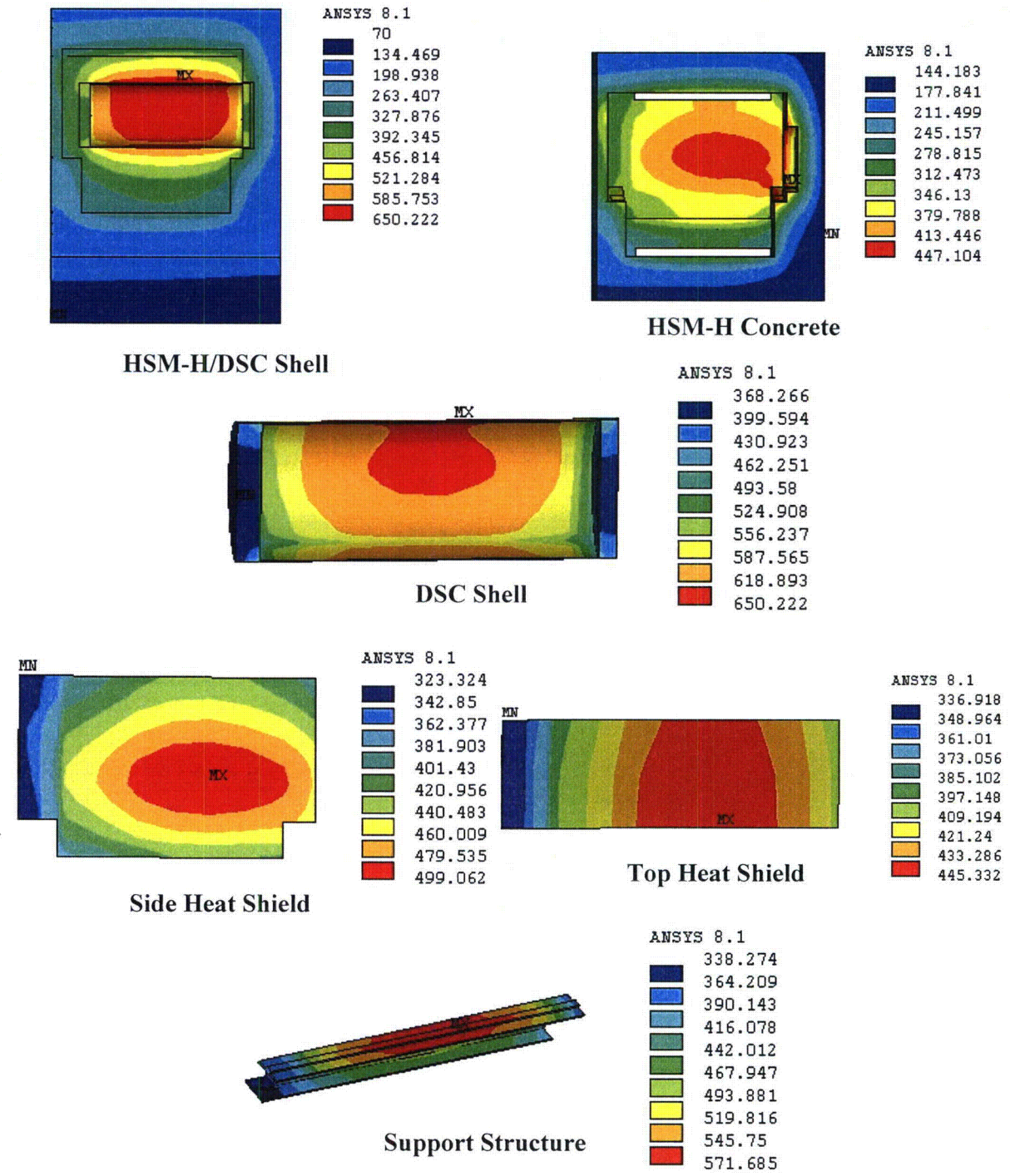
| Operating Condition | Fuel Compartment | | Neutron Absorber | | R45 & R90 Rails | |
|---|------------------|-----------------|------------------|-----------------|-----------------|-----------------|
| | HLZC #1 | HLZC #2 | HLZC #1 | HLZC #2 | HLZC #1 | HLZC #2 |
| | 40.8 kW (°F) | 31.2 kW (°F) | 40.8 kW (°F) | 31.2 kW (°F) | 40.8 kW (°F) | 31.2 kW (°F) |
| Storage, 133°F ambient ⁽¹⁾ | 705 | <705 | 705 | <705 | 550 | <550 |
| Storage, Blocked Vents @ 40hr, 117°F ambient ^(1, 3) | 825 | <825 | 824 | <824 | 674 | <674 |
| Transfer loss of sunshade, ^(1, 2) neutron shield, & air circulation, 117°F ambient, Steady State | 831 | <831 | 830 | <830 | 689 | <689 |

For Intact & Damaged Fuel Assemblies

| Operating Condition | Fuel Compartment | | Neutron Absorber | | R45 & R90 Rails | |
|--|------------------|-----------------|------------------|-----------------|-----------------|-----------------|
| | HLZC #1 | HLZC #2 | HLZC #1 | HLZC #2 | HLZC #1 | HLZC #2 |
| | 40.8 kW (°F) | 31.2 kW (°F) | 40.8 kW (°F) | 31.2 kW (°F) | 40.8 kW (°F) | 31.2 kW (°F) |
| Storage, Blocked Vents @ 40hr, 117°F ambient ⁽³⁾ | 822 | 773 | 822 | 773 | 673 | 650 |
| Transfer loss of sunshade, ⁽²⁾ Neutron shield, & air circulation, 117°F ambient, Steady State | 827 | 778 | 827 | 778 | 688 | 665 |

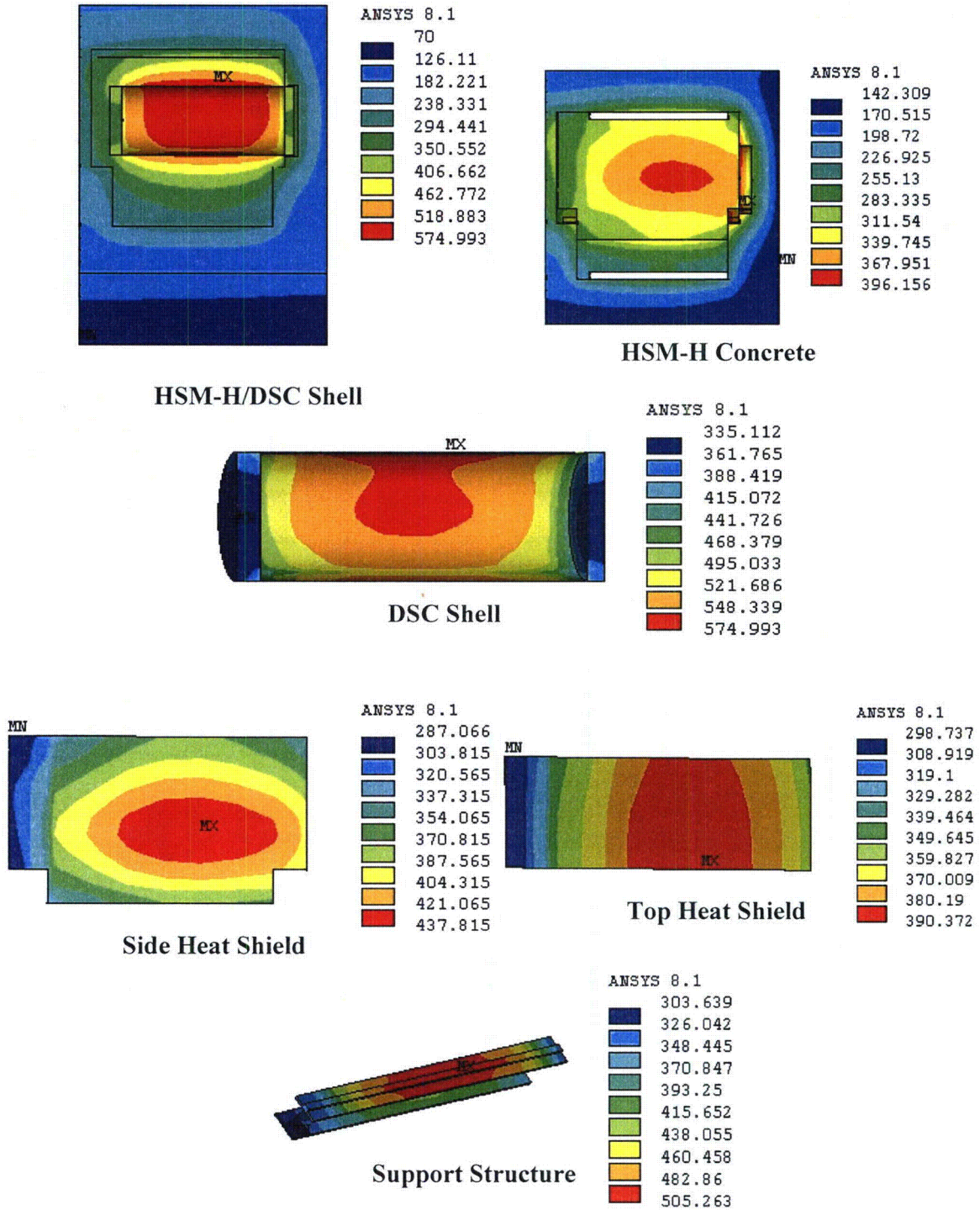
Notes:

- (1) HLZC #3 (24.0 kW) is bounded by HLZC #2 (31.2 kW).
- (2) The transfer accident case bounds the accident transfer at 133°F ambient, and the fire-accident.
- (3) Temperatures *calculated* based on effect of correction to "Dead Zone".



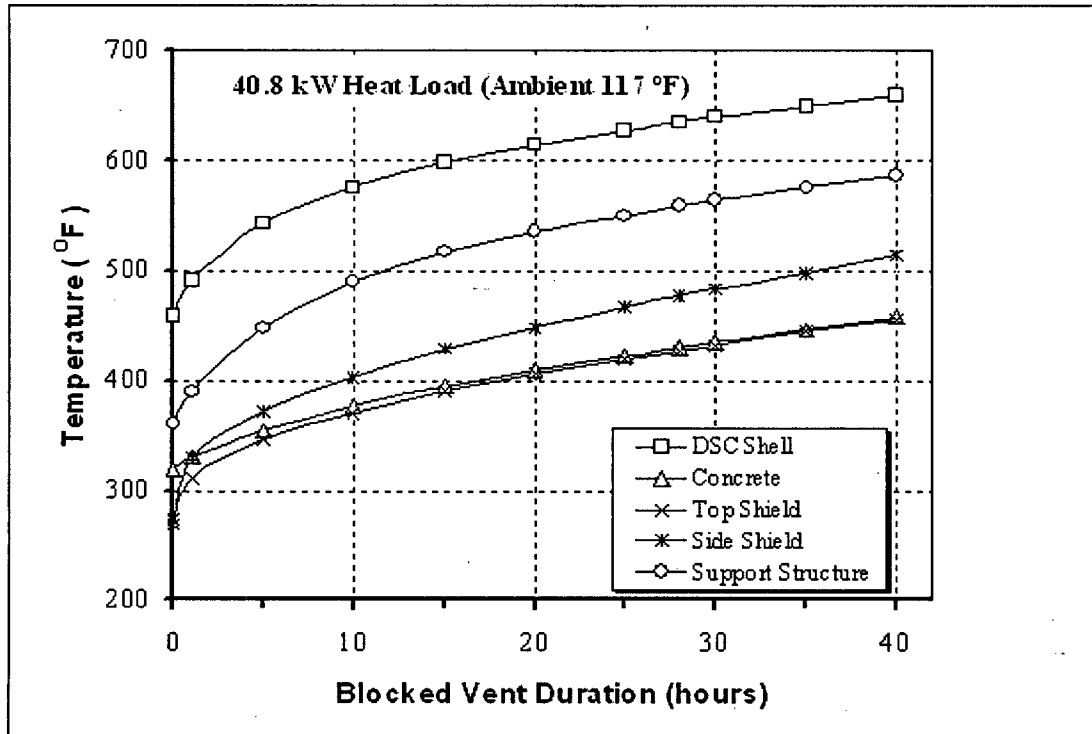
Note: These temperature profiles are based on a dead zone angle of 7.9° instead of 18.9°. The effects of the enlarged dead zone area are considered in Table U.4-3.

Figure U.4-11
HSM-H Component Temperature Distributions for
Blocked Vents Accident Storage Condition @ 35 hr, DSC with 40.8 kW, 117°F Ambient



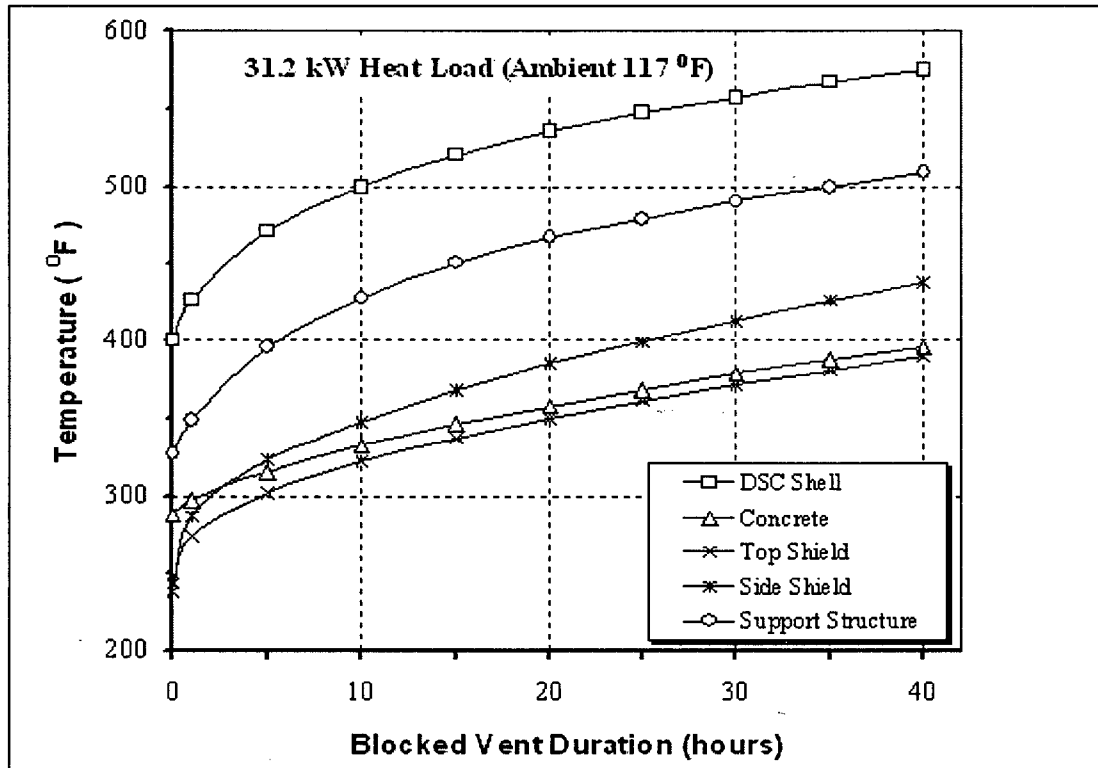
Note: These temperature profiles are based on a dead zone angle of 7.9° instead of 18.9°. The effects of the enlarged dead zone area are considered in Table U.4-3.

Figure U.4-12
HSM-H Component Temperature Distributions for
Blocked Vents Accident Storage Condition @ 40 hr, DSC with 31.2 kW, 117°F Ambient



Note: These temperature profiles are based on a dead zone angle of 7.9° instead of 18.9°. The effects of the enlarged dead zone area are considered in Table U.4-3.

Figure U.4-13
HSM-H Component Temperature Time Histories for
DSC with 40.8 kW, Blocked Vents Accident Condition, 117°F Ambient



Note: These temperature profiles are based on a dead zone angle of 7.9° instead of 18.9°. The effects of the enlarged dead zone area are considered in Table U.4-3.

Figure U.4-14
HSM-H Component Temperature Time Histories for
DSC with 31.2 kW, Blocked Vents Accident Condition, 117°F Ambient

9. Visually verify that the top shield plug is properly seated onto the DSC.
10. Position the lifting yoke with the TC trunnions and verify that it is properly engaged.
11. Raise the TC to the pool surface. Prior to raising the top of the cask above the water surface, stop vertical movement.
12. Inspect the top shield plug to verify that it is properly seated onto the DSC. If not, lower the cask and reposition the top shield plug. Repeat Steps 8 through 12 as necessary.
13. Continue to raise the TC from the pool and spray the exposed portion of the cask with water until the top region of the cask is accessible.
14. Drain any excess water from the top of the DSC shield plug back to the fuel pool.
15. Check the radiation levels at the center of the top shield plug and around the perimeter of the cask. Disconnect the top shield plug rigging.
16. Drain a minimum of 50 gallons of water from the DSC cavity. Optionally, approximately 900 gallons of water (as indicated by the flowmeter) may be drained from the DSC back into the pool or other suitable location to meet the weight limit on the crane. Use 1 to 3 psig of helium to backfill the DSC with helium per ISG-22 [8.2] guidance as water is being removed from the DSC cavity.
17. Lift the TC from the fuel pool. As the cask is raised from the pool, continue to spray the cask with water and decon as directed. Provisions shall be made to assure that air will not enter the DSC cavity. One way to achieve this is by replenishing the helium in the DSC cavity during cask movement from the fuel pool to the decon area in case of malfunction of equipment used for cask movement.
18. Move the TC with loaded DSC to the cask decon area.
- 18a. Replace the water removed from the DSC cavity in Step 16 with water from the fuel pool or an equivalent source which meets the requirements of Technical Specifications 1.2.15d.
19. If applicable to keep the occupational exposure ALARA, temporary shielding may be installed as necessary to minimize personnel exposure. Install cask seismic restraints if required by Technical Specification 1.2.16 (required only on plant specific basis).
20. Verify that the transfer cask dose rates are compliant with limits specified in Technical Specification 1.2.11e.

U.8.1.3 DSC Drying and Backfilling

CAUTION: During performance of steps listed in Section U.8.1.3, monitor the TC/DSC annulus water level and replenish if necessary until drained.

1. Check the radiation levels along the perimeter of the cask. The cask exterior surface should be decontaminated as necessary in accordance with the limits specified in Technical Specification 1.2.12. Temporary shielding may be installed as necessary to minimize personnel exposure.

CAUTION: Continuously monitor the hydrogen concentration in the DSC cavity using the arrangement or other alternate methods described in Step 10 during the inner top cover plate cutting/welding operations. Verify that the measured hydrogen concentration does not exceed a safety limit of 2.4% [8.2 and 8.3]. If this limit is exceeded, stop all welding operations and purge the DSC cavity with approximately 2-3 psig helium via the tubing to reduce the hydrogen concentration safely below the 2.4% limit.

13. Perform dye penetrant weld examination of the inner top cover plate weld in accordance with the Technical Specification 1.2.5 requirements.
14. Remove purge lines and connect the VDS to the DSC siphon and vent ports.
15. Install temporary shielding to minimize personnel exposure throughout the subsequent welding operations as required.
16.
 - a. If using blowdown method to remove water, engage helium supply (up to 15 psig) and open the valve on the vent port and allow helium to force the water from the DSC cavity through the siphon port.
 - b. If using water pumps to remove water without blowdown, pump water from DSC.
17. Once the water stops flowing from the DSC, close the DSC siphon port and disengage the helium source or turn off the section pump, as applicable.
18. Connect the hose from the vent port and the siphon port to the intake of the vacuum pump. Connect a hose from the discharge side of the VDS to the plant's radioactive waste system or spent fuel pool. Connect the VDS to a helium source.

Note: Proceed cautiously when evacuating the DSC to avoid freezing consequences.

19. Open the valve on the suction side of the pump, start the VDS and draw a vacuum on the DSC cavity. The cavity pressure should be reduced in steps of approximately 100 mm Hg, 50 mm Hg, 25 mm Hg, 15 mm Hg, 10 mm Hg, 5 mm Hg, and 3 mm Hg. After pumping down to each level (these levels are optional), the pump is valved off and the cavity pressure monitored. The cavity pressure will rise as water and other volatiles in the cavity evaporate. When the cavity pressure stabilizes, the pump is valved in to complete the vacuum drying process. It may be necessary to repeat some steps, depending on the rate and extent of the pressure increase. Vacuum drying is complete when the pressure stabilizes for a minimum of 30 minutes at 3 mm Hg or less as specified in Technical Specification 1.2.2.

Note: The user shall ensure that the vacuum pump is isolated from the DSC cavity when demonstrating compliance with TS 1.2.2 requirements. Simply closing the valve between the DSC and the vacuum pump is not sufficient, as a faulty valve allows the vacuum pump to continue to draw a vacuum on the DSC. Turning off the pump, or opening the suction side of the pump to atmosphere are examples of ways to assure that the pump is not continuing to draw a vacuum on the DSC.

CAUTION: Radiation dose rates are expected to be high at the vent and siphon port locations. Use proper ALARA practices (e.g., use of temporary shielding, appropriate positioning of personnel, etc.) to minimize personnel exposure.

20. Open the valve to the vent port and allow the helium to flow into the DSC cavity.
21. Pressurize the DSC with helium up to 15 psig.
22. Helium leak test the inner top cover plate weld for a leak rate of 1×10^{-4} atm cm³/sec. This test is optional.
23. If a leak is found, repair the weld, repressurize the DSC and repeat the helium leak test.
24. Once no leaks are detected, depressurize the DSC cavity by releasing the helium through the VDS to the plant's spent fuel pool or radioactive waste system.
25. Re-evacuate the DSC cavity using the VDS. The cavity pressure should be reduced in steps of approximately 10 mm Hg, 5 mm Hg, and 3 mm Hg. After pumping down to each level, the pump is valved off and the cavity pressure is monitored level (these levels are optional). When the cavity pressure stabilizes, the pump is valved in to continue the vacuum drying process. Vacuum drying is complete when the pressure stabilizes for a minimum of 30 minutes at 3 mm Hg or less in accordance with Technical Specification 1.2.2 limits.

Note: The user shall ensure that the vacuum pump is isolated from the DSC cavity when demonstrating compliance with TS 1.2.2 requirements. Simply closing the valve between the DSC and the vacuum pump is not sufficient, as a faulty valve allows the vacuum pump to continue to draw a vacuum on the DSC. Turning off the pump, or opening the suction side of the pump to atmosphere are examples of ways to assure that the pump is not continuing to draw a vacuum on the DSC.

26. Open the valve on the vent port and allow helium to flow into the DSC cavity to pressurize the DSC between 21.5 to 23.0 psig and hold for 10 min. Depressurize the DSC cavity by releasing the helium through the VDS to the plant spent fuel pool or radioactive waste system to about 2.5 psig in accordance with Technical Specification 1.2.3a limits.

CAUTION: Radiation dose rates are expected to be high at the vent and siphon port locations. Use proper ALARA practices (e.g., use of temporary shielding, appropriate positioning of personnel, etc.) to minimize personnel exposure.

27. Close the valves on the helium source.

U.8.1.4 DSC Sealing Operations

CAUTION: During performance of steps listed in Section U.8.1.4, monitor the Cask/DSC annulus water level and replenish as necessary to maintain cooling.

1. Disconnect the VDS from the DSC. Seal weld the prefabricated plugs over the vent and siphon ports. Inject helium into blind space just prior to completing welding, and perform a dye penetrant weld examination in accordance with the Technical Specification 1.2.5 requirements.
2. Temporary shielding may be installed as necessary to minimize personnel exposure. Install the automatic welding machine onto the outer top cover plate and place the outer top cover plate with the automatic welding system onto the DSC. Optionally, outer top cover plate may be installed separately from the welding machine. Verify proper fit up of the outer top cover plate with the DSC shell.
3. Tack weld the outer top cover plate to the DSC shell. Place the outer top cover plate weld root pass.
4. Helium leak test the inner top cover plate and vent/siphon port plate welds using the leak test port in the outer top cover plate in accordance with Technical Specification 1.2.4a limits. Verify that the personnel performing the leak test are qualified in accordance with SNT-TC-1A [8.4]. Alternatively this can be done with a test head in step 1 of Section U.8.1.4.
5. If a leak is found, remove the outer cover plate root pass (if not using test head), the vent and siphon port plugs and repair the inner cover plate welds. Repeat procedure steps from U.8.1.3 Step 19.
6. Perform dye penetrant examination of the root pass weld. Weld out the outer top cover plate to the DSC shell and perform dye penetrant examination on the weld surface in accordance with the Technical Specification 1.2.5 requirements.
7. Install and seal weld the prefabricated plug, if applicable, over the outer cover plate test port and perform dye penetrant weld examinations in accordance with Technical Specification 1.2.5 requirement.
8. Remove the automatic welding machine from the DSC.
9. Open the cask drain port valve and drain the water from the cask/DSC annulus.
10. Rig the cask top cover plate and lower the cover plate onto the TC.
11. Bolt the cask cover plate into place, tightening the bolts to the required torque in a star pattern.

CAUTION: Monitor the applicable time limits of Technical Specification 1.2.18b until the completion of DSC transfer Step 6 of Section U.8.1.6.

12. Verify that the transfer cask dose rates are compliant with limits specified in Technical Specification 1.2.11e.

U.8.1.5 TC Downending and Transfer to ISFSI

Note: Alternate Procedure for Downending of Transfer Cask: Some plants have limited floor hatch openings above the cask/trailer/skid, which limit crane travel (within the hatch opening) that would be needed in order to downend the TC with the trailer/skid in a stationary position. For these situations, alternate procedures are to be developed on a plant-specific basis, with detailed steps for downending.

1. Re-attach the TC lifting yoke to the crane hook, as necessary. Ready the transport trailer and cask support skid for service.
2. Move the scaffolding away from the cask as necessary. Engage the lifting yoke and lift the cask over the cask support skid on the transport trailer.
3. The transport trailer should be positioned so that cask support skid is accessible to the crane with the trailer supported on the vertical jacks.
4. Position the cask lower trunnions onto the transfer trailer support skid pillow blocks.
5. Move the crane forward while simultaneously lowering the cask until the cask upper trunnions are just above the support skid upper trunnion pillow blocks.
6. Inspect the positioning of the cask to insure that the cask and trunnion pillow blocks are properly aligned.
7. Lower the cask onto the skid until the weight of the cask is distributed to the trunnion pillow blocks.
8. Inspect the trunnions to ensure that they are properly seated onto the skid and install the trunnion tower closure plates, if required.
9. Remove the bottom ram access cover plate from the cask if integral ram/trailer is not used. Install the two-piece temporary neutron/gamma shield plug to cover the bottom ram access. Install the ram trunnion support frame on the bottom of the TC. (The temporary shield plug and ram trunnion support frame are not required with integral ram/trailer.)

U.8.1.6 DSC Transfer to the HSM

1. Prior to transporting the cask to the ISFSI or prior to positioning the transfer cask at the HSM designated for storage, remove the HSM door using a porta-crane, inspect the cavity of the HSM, removing any debris and ready the HSM to receive a DSC. The doors on adjacent HSMs should remain in place.

CAUTION: Very high dose rates in the empty HSM are expected if adjacent to a loaded HSM due to high heat loads in 32PTH1 DSC. Proper ALARA practices should be followed during these operations.

2. Inspect the HSM air inlet and outlets to ensure that they are clear of debris. Inspect the screens on the air inlet and outlets for damage.

CAUTION: Verify that the requirements of Technical Specification 1.2.14a "TC/DSC Transfer Operations at High Ambient Temperatures (32PTH1 DSC only)" are met prior to next step.

3. Using a suitable vehicle, transport the cask from the plant's fuel/reactor building to the ISFSI along the designated transfer route.
4. Once at the ISFSI, position the transport trailer to within several inches of the HSM.
5. Check the position of the trailer to ensure the centerline of the HSM and cask approximately coincide. If the trailer is not properly oriented, reposition the trailer, as necessary.
6. Using crane, unbolt and remove the cask top cover plate.

CAUTION: Verify that the applicable time limits of Technical Specification 1.2.18b are met.

7. Back the cask to within a few inches of the HSM, set the trailer brakes and disengage the tractor. Drive the tractor clear of the trailer. Extend the transfer trailer vertical jacks.
8. Connect the skid positioning system hydraulic power unit to the positioning system via the hose connector panel on the trailer, and power it up. Remove the skid tie-down bracket fasteners and use the skid positioning system to bring the cask into approximate vertical and horizontal alignment with the HSM. Using optical survey equipment and the alignment marks on the cask and the HSM, adjust the position of the cask until it is properly aligned with the HSM.
9. Using the skid positioning system, fully insert the cask into the HSM access opening docking collar.
10. Secure the cask trunnions to the front wall embedments of the HSM using the cask restraints.
11. After the cask is docked with the HSM, verify the alignment of the TC using the optical survey equipment.
12. Position the hydraulic ram behind the cask in approximate horizontal alignment with the cask and level the ram. Remove either the bottom ram access cover plate or the outer plug of the two-piece temporary shield plug if installed. Power up the ram hydraulic power supply and extend the ram through the bottom cask opening into the DSC grapple ring.

13. Activate the hydraulic cylinder on the ram grapple and engage the grapple arms with the DSC grapple ring.
14. Recheck all alignment marks in accordance with the Technical Specification 1.2.9 limits and ready all systems for DSC transfer.
15. Activate the hydraulic ram to initiate insertion of the DSC into the HSM. Stop the ram when the DSC reaches the support rail stops at the back of the module.
16. Disengage the ram grapple mechanism so that the grapple is retracted away from the DSC grapple ring.
17. Retract and disengage the hydraulic ram system from the cask and move it clear of the cask. Remove the cask restraints from the HSM.
18. Using the skid positioning system, disengage the cask from the HSM access opening.
19. Install the DSC axial in retainer through the HSM door opening.
20. Install the HSM door using a portable crane and secure it in place. Door may be welded for security. Verify that the HSM dose rates are compliant with the limits specified in Technical Specification 1.2.7g.
21. Replace the TC top cover plate. Secure the skid to the trailer, retract the vertical jacks and disconnect the skid positioning system.
22. Tow the trailer and cask to the designated equipment storage area. Return the remaining transfer equipment to the storage area.
23. Close and lock the ISFSI access gate and activate the ISFSI security measures.
24. Ensure the HSM-H maximum air exit temperature requirements of Technical Specification 1.2.8c are met.

U.8.1.7 Monitoring Operations

1. Perform routine security surveillance in accordance with the licensee's ISFSI security plan.
2. Perform one of the two alternate daily surveillance activities listed below:
 - a. A daily visual surveillance of the HSM air inlets and outlets to insure that no debris is obstructing the HSM vents in accordance with Technical Specification 1.3.1 requirements.
 - b. A temperature measurement of the thermal performance, for each HSM, on a daily basis in accordance with Technical Specification 1.3.2 requirements.